NASA CR-165557

National Aeronautics and
Space Administration

CF6 JET ENGINE PERFORMANCE IMPROVEMENT — LOW PRESSURE TURBINE ACTIVE CLEARANCE CONTROL

by

B.D. Beck and W.A. Fasching

GENERAL ELECTRIC COMPANY
AIRCRAFT ENGINE BUSINESS GROUP
CINCINNATI, OHIO 45215

June 1982

Prepared for

National Aeronautics and Space Administration
LEWIS RESEARCH CENTER
21000 BROOKPARK ROAD
CLEVELAND, OHIO 44135

NASA Lewis Research Center
Contract NAS3-20629

1. Report No. NASA CR-165557	2. Government Accession No.	3. Recipient's Catalog No.
4. Title and Subtitle CF6 Jet Engine Performance Improvement Program - Low Pressure Turbine Active Clearance Control		5. Report Date June 1982 6. Performing Organization Code
7. Author(s) B.D. Beck and W.A. Fasching		8. Performing Organization Report No. R82AEB462 10. Work Unit No.
9. Performing Organization Name and Address General Electric Company Aircraft Engine Group Cincinnati, Ohio 45215		11. Contract or Grant No. NAS3-20629 13. Type of Report and Period Covered Contractor Report
12. Sponsoring Agency Name and Address National Aeronautics and Space Administration Washington, D.C. 20546		14. Sponsoring Agency Code

15. Supplementary Notes
Project Manager - J. McAulay, Project Engineer - R. Antl
NASA-Lewis Research Center, Cleveland, Ohio

16. Abstract

As part of the NASA-sponsored ECI Program, a low pressure turbine (LPT) active clearance control (ACC) cooling system has been developed to reduce the fuel consumption of current CF6-50 turbofan engines for wide-bodied commercial aircraft.

The program performance improvement goal of 0.3 percent Δsfc was determined to be achievable with an improved impingement cooling system. As a result of the technology demonstrated during this program, it is possible to design an optimized manifold and piping system which is capable of a performance gain of 0.45 percent Δsfc.

17. Key Words (Suggested by Author(s))	18. Distribution Statement
Jet Engine Low Pressure Turbine Turbofan Engine Active Clearance Control Performance	Unclassified - Unlimited

19. Security Classif. (of this report)	20. Security Classif. (of this page)	21. No. of Pages	22. Price*
Unclassified	Unclassified	147	

* For sale by the National Technical Information Service, Springfield, Virginia 22161

FOREWORD

The work was performed by the CF6 Engineering Department of General Electric's Aircraft Engine Group, Aircraft Engine Engineering Division, Cincinnati, Ohio. The program was conducted for the National Aeronautics and Space Administration, Lewis Research Center, Cleveland, Ohio, under Subtask 2.7 of the CF6 Jet Engine Performance Improvement Program, Contract Number NAS3-20629. The Performance Improvement Program is part of the Engine Component Improvement (ECI) Project, which is part of the NASA Aircraft Energy Efficiency (ACEE) Program. The NASA Project Engineer for the Low Pressure Turbine (LPT) Active Clearance Control (ACC) Program was R. Antl. The program was initiated in October, 1978 and completed in June, 1981.

The report was prepared by B.D. Beck, Project Engineer and W.A. Fasching, General Electric Program Manager, with the assistance of T.A. Compton, S. Gau, S.B. Gorrepati, F. Harlin, J.L. Hobbs, A.W. Jorgensen, D.P. Leachman and L.E. McIntosh.

TABLE OF CONTENTS

TABLE OF CONTENTS (Concluded)

LIST OF ILLUSTRATIONS

LIST OF ILLUSTRATIONS (Continued)

LIST OF ILLUSTRATIONS (Continued)

LIST OF ILLUSTRATIONS (Continued)

LIST OF ILLUSTRATIONS (Continued)

LIST OF ILLUSTRATIONS (Concluded)

LIST OF TABLES

1.0 SUMMARY

As part of the NASA-sponsored ECI Program, a low pressure turbine (LPT) active clearance control (ACC) cooling system has been developed to reduce the fuel consumption of current CF6-50 turbofan engines for wide-bodied commercial aircraft. Relative to the current production cooling system, the ACC cooling system reduces the airflow impinging on the LPT case during transient, takeoff and climbout, and descent conditions (creating increased LPT rotor/stator clearances) and it increases the impingement airflow during cruise conditions (creating decreased LPT rotor/stator clearances). The LPT performance improvement program included design, analysis, manufacture, and component and engine testing of the ACC system hardware.

The program performance improvement goal of 0.3 percent Δsfc was determined to be achievable with an improved impingement cooling system. As a result of the technology demonstrated during this program, it is possible to design an optimized manifold and piping system which is capable of a performance gain of 0.45 percent Δsfc.

Application of a low pressure active clearance control system offers annual fuel savings of 78,500 to 175,000 liters (20,740 to 46,253 gals) which is dependent on the specific system design, the type of aircraft utilizing the system, and the aircraft mission range.

2.0 INTRODUCTION

National energy demand has outpaced domestic supply creating an increased U.S. dependence on foreign oil. This increased dependence was dramatized by the OPEC oil embargo in the winter of 1973 to 1974. In addition, the embargo triggered a rapid rise in the cost of fuel which, along with the potential of further increases, brought about changes in economic circumstances with regard to the use of energy. These events, of course, were felt in the air transport industry as well as other forms of transportation. As a result of these experiences, the Government, with the support of the aviation industry, initiated programs aimed at both the supply and demand aspects of the problem. The supply problem is being investigated by looking at increasing fuel availability from such sources as coal and oil shale. Efforts are currently underway to develop engine combustor and fuel systems that will accept fuels with broader specifications.

Reduced fuel consumption is the other approach to deal with the overall problem. A long-range effort to reduce fuel consumption is to evolve new technology which will permit development of a more energy efficient turbofan or the use of a different propulsive cycle, such as a turboprop. Although studies have indicated large reductions in fuel usage are possible (e.g., 15 percent to 40 percent), any significant impact of this approach is approximately 15 years away. In the near term, the only practical propulsion approach is to improve the fuel efficiency of current engines. Examination of this approach has indicated that a 5 percent fuel reduction goal starting in the 1980 to 1982 time period is feasible for current commercial engines. These engines will continue to be significant fuel users for the next 15 to 20 years.

Accordingly, NASA sponsored the Aircraft Energy Efficiency (ACEE) Program (based on a congressional request) which was directed at reduced fuel consumption of commercial air transports. The Engine Component Improvement (ECI) Program was the element of the ACEE Program directed at reducing fuel consumption of current commercial aircraft engines. The ECI Program consisted of two parts: engine diagnostics and performance improvement. The engine diagnostics effort

was to provide information to identify the sources and causes of engine deterioration. The performance improvement effort was directed at developing engine components having performance improvement and retention characteristics which could be incorporated into new production and existing engines.

The performance improvement effort was initiated with a feasibility analysis which identified performance improvement concepts and then assessed the technical and economic merits of these concepts. This assessment included a determination of airline acceptability, the probability of introducing the concepts into production by the 1980 to 1982 time period, and their retrofit potential. The study was conducted in cooperation with Boeing and Douglas aircraft companies and American and United Airlines, and is reported in Reference 1.

In the feasibility analysis, the Low Pressure Turbine Active Clearance Control Performance Improvement Program was selected for development and evaluation because of its fuel savings potential and attractive airline payback period. The objective of the program was to develop technology and to verify the predicted fuel savings by engine tests.

The Low Pressure Turbine Active Clearance Control Program was a 33-month effort that included design analysis, hardware manufacture, and component and engine testing.

3.0 DESCRIPTION OF LPT ACTIVE CLEARANCE CONTROL (ACC) CONCEPT

3.1 CURRENT CF6-50 PRODUCTION LPT COOLING SYSTEM

The current CF6-50 low pressure turbine case is cooled by an externally mounted impingement manifold. Air is bled from the fan discharge flowpath via a flush inlet in the fan reverser wall and is piped to a plenum where the reverser interfaces with the radial fire seal.

Downstream of the plenum, the air enters another pipe (inside the core cowling) which mates with an engine pipe via a spring-loaded compression seal commonly referred to as the "kiss" seal. The engine pipe is plumbed to an inlet in the bottom half of the LPT cooling manifold with the top and bottom halves interconnected via pipes mating in a slip joint.

The manifold consists of a network of axial and circumferential tubes. The axial tubes distribute the air to the circumferential tubes (total of 7) which are axially spaced to impinge air on the exterior of the LPT case nozzle and shroud support hooks.

The major elements of the cooling system are shown schematically on the CF6-50 engine cross section in Figure 1, and the LPT manifold is illustrated in Figure 2.

The current LPT cooling manifold was designed to ensure adequate case life by reducing thermal gradients between the hooks and casing skin during transient engine operation, maintain an overall casing temperature at takeoff consistent with the design life requirements of the part, and provide a nominal amount of performance improvement due to the reduction of casing temperatures relative to those which would exist with no cooling flow. It should be noted that the current system is passive in that no attempt is made to alter the percentage of the fan flow supplied at various operating conditions through the use of a flow control device such as a valve. The flow area is constant at all engine operating conditions.

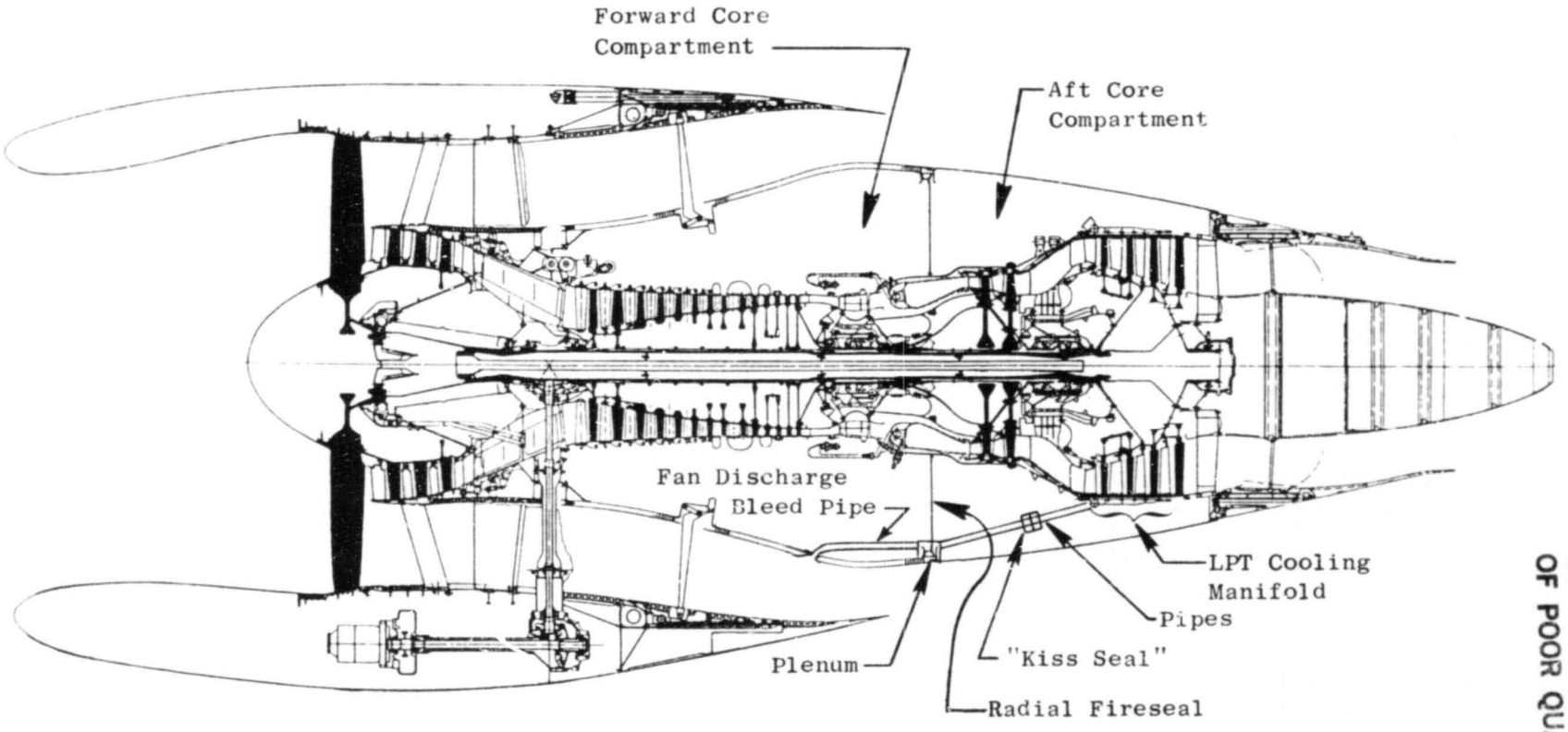

Figure 1. The General Electric CF6-50 Full Engine Cross Section.

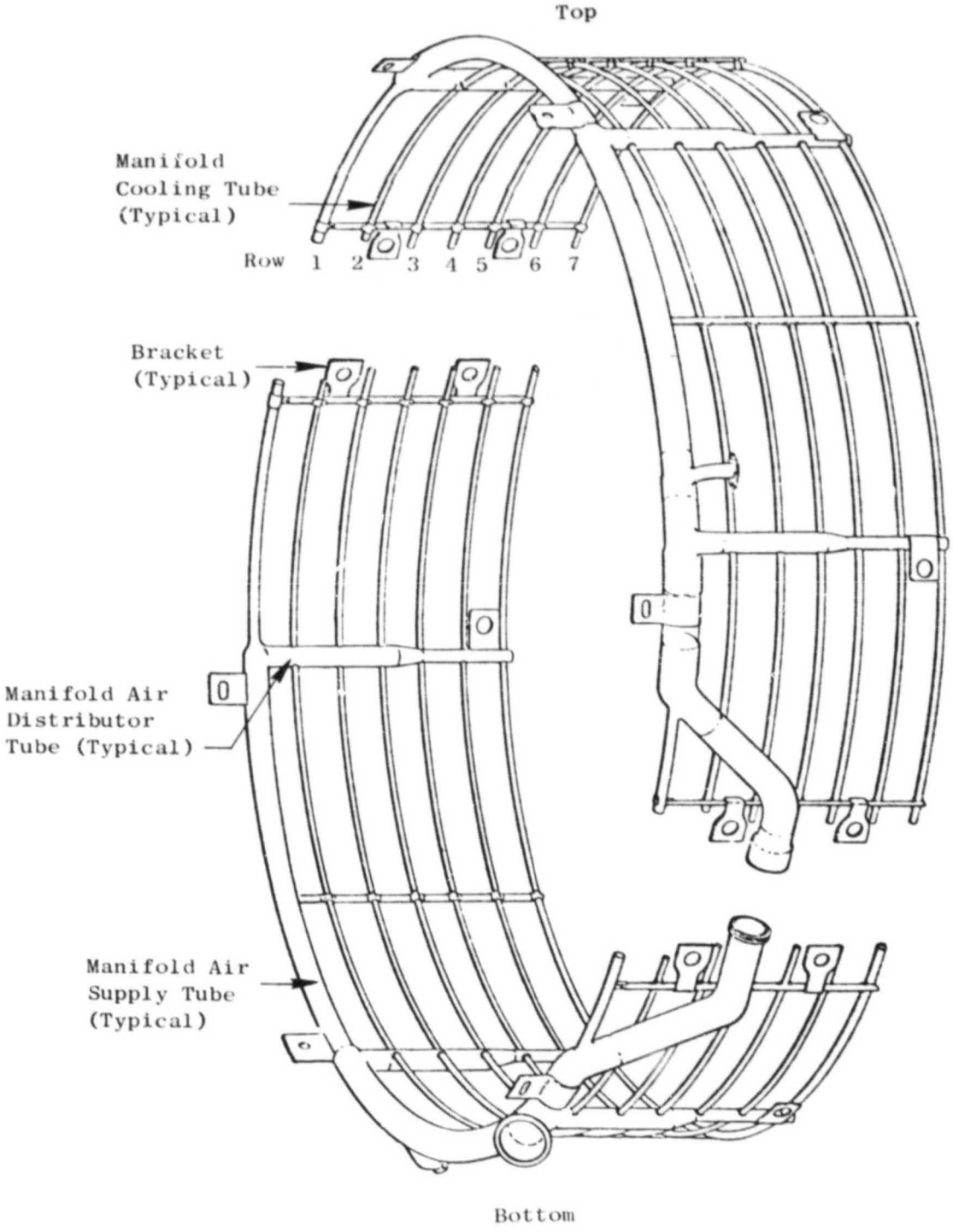

Figure 2. Current Production LPT Cooling Manifold.

3.2 PERFORMANCE IMPROVEMENT AND ACC CONCEPT

The basic goal of this program was to develop an LPT cooling system which would improve LPT efficiency, thereby reducing specific fuel consumption (sfc) by reducing the radial rotor/stator clearances at cruise conditions. The location of these clearances are shown on the LPT cross section presented in Figure 3. The concept for achieving this reduction in cruise clearances consists of two parts: (1) the case cooling flow is intentionally reduced during transient, takeoff and climbout, and descent conditions which allows the case to get hotter and "grow" away from the rotor tips, thereby reducing transient rubs in the stator honeycomb; and (2) the case cooling flow is significantly increased at cruise conditions, causing the case to be cooler and "shrink in" toward the rotor, reducing the operational clearances.

To further illustrate this concept, a typical stator shroud honeycomb wear (rubout) pattern will be examined (interstage seal honeycomb patterns would be similar). Figure 4 illustrates a typical LPT stator shroud wear pattern resulting from the relative motion of rotor and stator components during a transient operation (throttle burst) from ground idle to takeoff. During this transient operation, the difference in the thermal responses of the rotor and stator and the growth of the rotor due to centrifugal loading create relative motion between the rotor and stator in both the radial and axial directions. The arrows indicate the direction of the blade tip motion relative to the shroud. Time is nonlinear along the path. Figure 4 also depicts the estimated cruise clearance reductions due to the reduced flow during the takeoff and climbout transient and the increased flow at cruise operation. It was estimated that the achievable reduction in clearance per stage due to increased flow at cruise was 0.50 mm (0.020 inch) with an additional 0.25 mm (0.010 inch) gained due to the reduced flow during takeoff. This level of clearance reduction, when applied to the stage 1-4 blade tip/stator shrouds and the stage 2-4 rotor/stator interstage seals, was estimated to result in a cruise sfc reduction of approximately 0.3 percent.

3.3 UNIQUE FEATURES OF LPT ACC COOLING SYSTEMS

A new LPT manifold was designed with more than twice the flow capacity of the present system. The manifold sizing, consistent with the case temperature

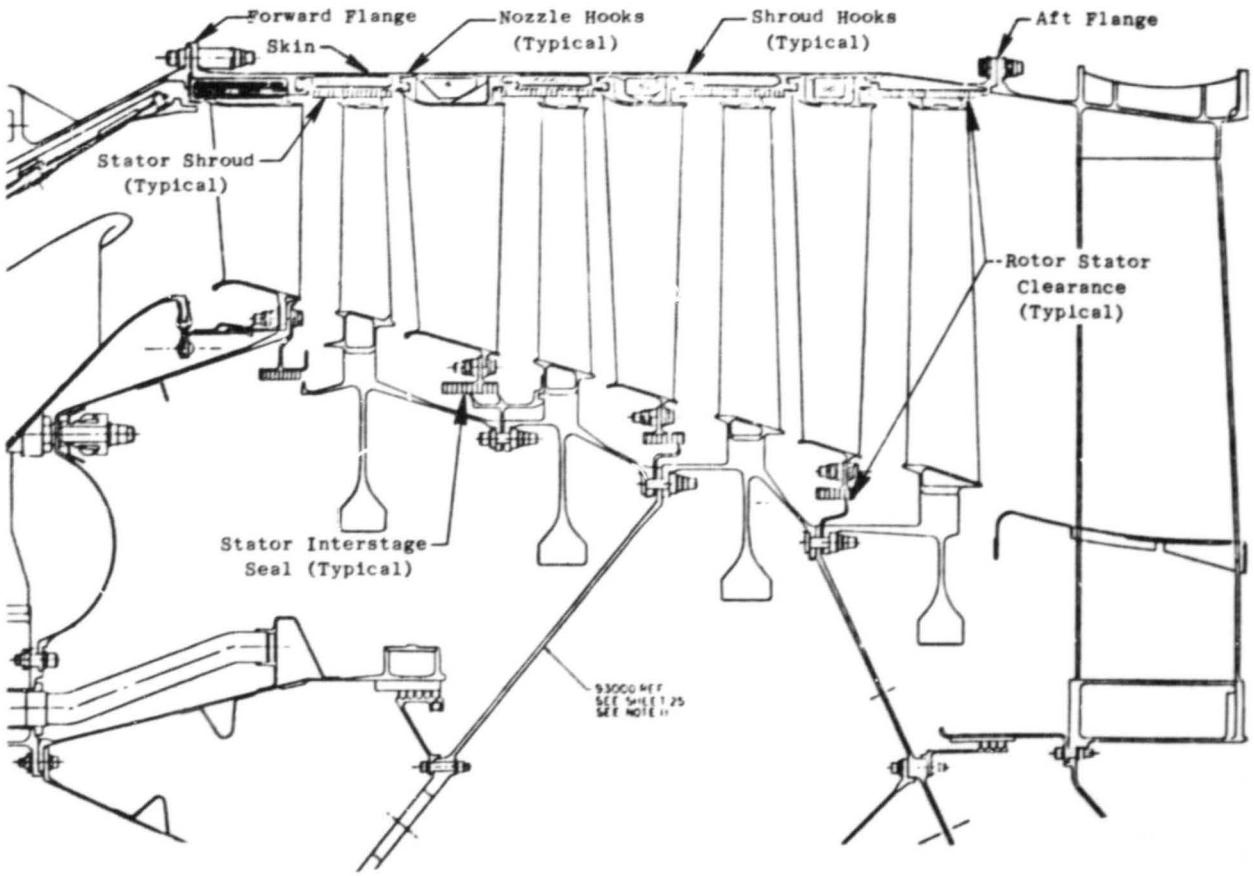

Figure 3. LPT Cross Section.

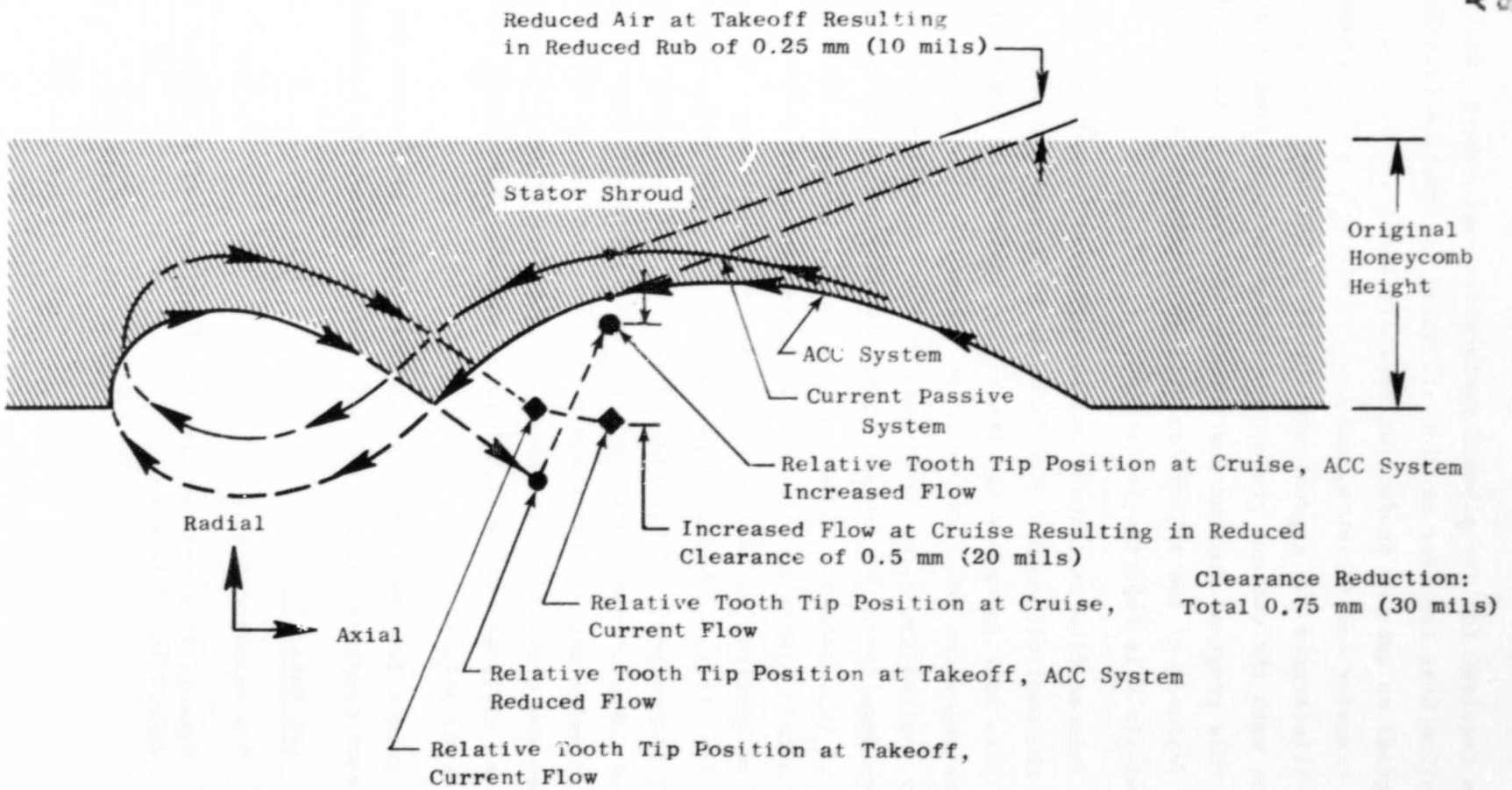

Figure 4. LPT Stator Shroud Honeycomb Wear Pattern.

reduction required for the planned performance improvement, was accomplished with detailed heat transfer studies utilizing information (available prior to this program) on current production manifold airflow rates, case temperatures and heat transfer coefficients, and General Electric's THTD computer program. Figure 5 illustrates the approximate levels of LPT case average surface temperatures for both the current production system (as predicted prior to the initiation of this program) and the goal of the ACC system. Further details on the specific features of the ACC system will be presented later in this section. The ACC manifold is depicted in Figure 6.

The reduced flow at takeoff was accomplished by adding a flow control valve in the manifold supply pipe from the kiss seal interface. It was decided that the kiss seal interface and the piping upstream of the kiss seal would remain unchanged for the convenience of prospective customers. Figure 7 schematically depicts the major components of the ACC system downstream of the kiss seal. The development of the ACC valve and its associated controls logic was not part of this program. However, a description of the anticipated valve to be used in this system and its mode of operation is as follows. The valve would be pneumatically operated and spring loaded closed. During takeoff and climbout (at altitudes below 6,688 m/22,000 feet) the valve would remain in the nominally closed position but would permit a "low" flow equivalent to the flow desired at takeoff conditions. After achieving an altitude of 22,000 feet, a barometric valve would actuate and port actuation air to the ACC valve causing it to open and provide the increased cooling flow at cruise conditions. During descent, at altitudes below 22,000 feet, the ACC valve would move to the low flow (closed) position.

The unique features, relative to the current production LPT cooling system, of each component of the LPT ACC cooling system are enumerated below:

LPT Manifold

- New hardware design.
- Takeoff flow reduced from 0.152 kg/sec (0.335 lb/sec) to 0.045 kg/sec (0.10 lb/sec).

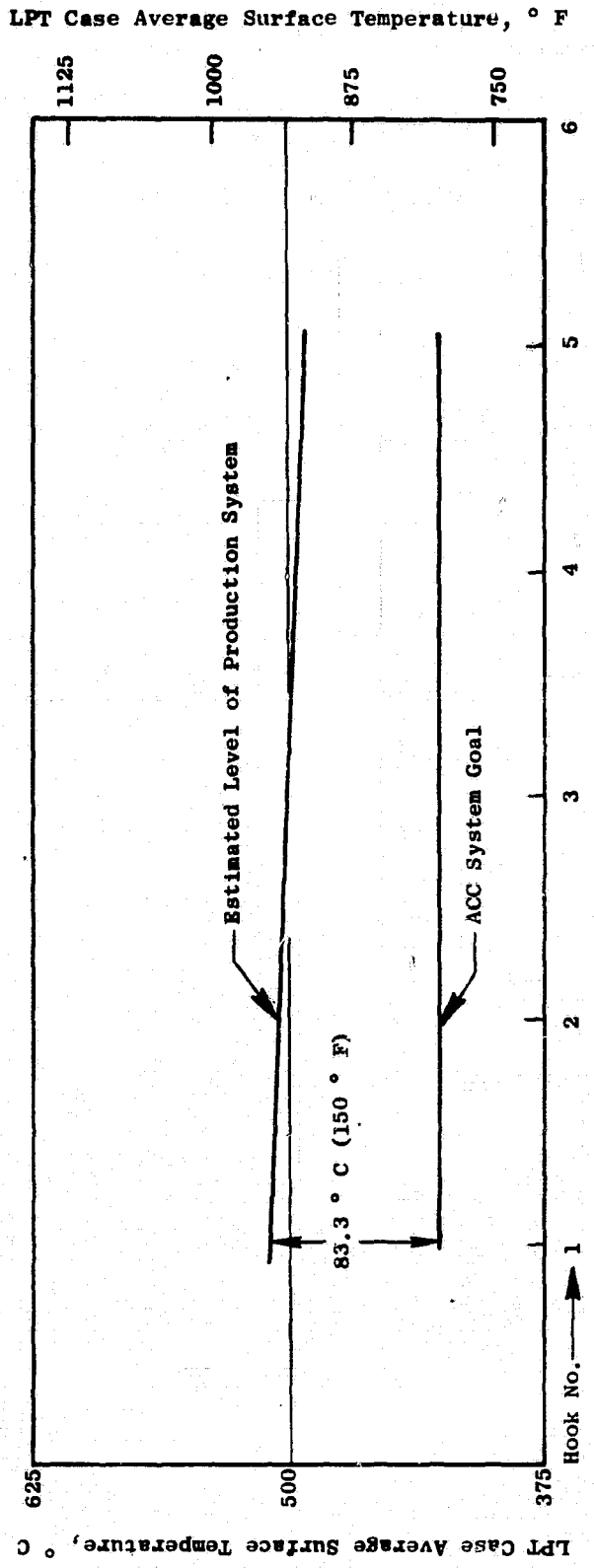

Figure 5. Comparison of LPT Case Temperature Levels: Estimated Production System and ACC System Goal at Program Inception.

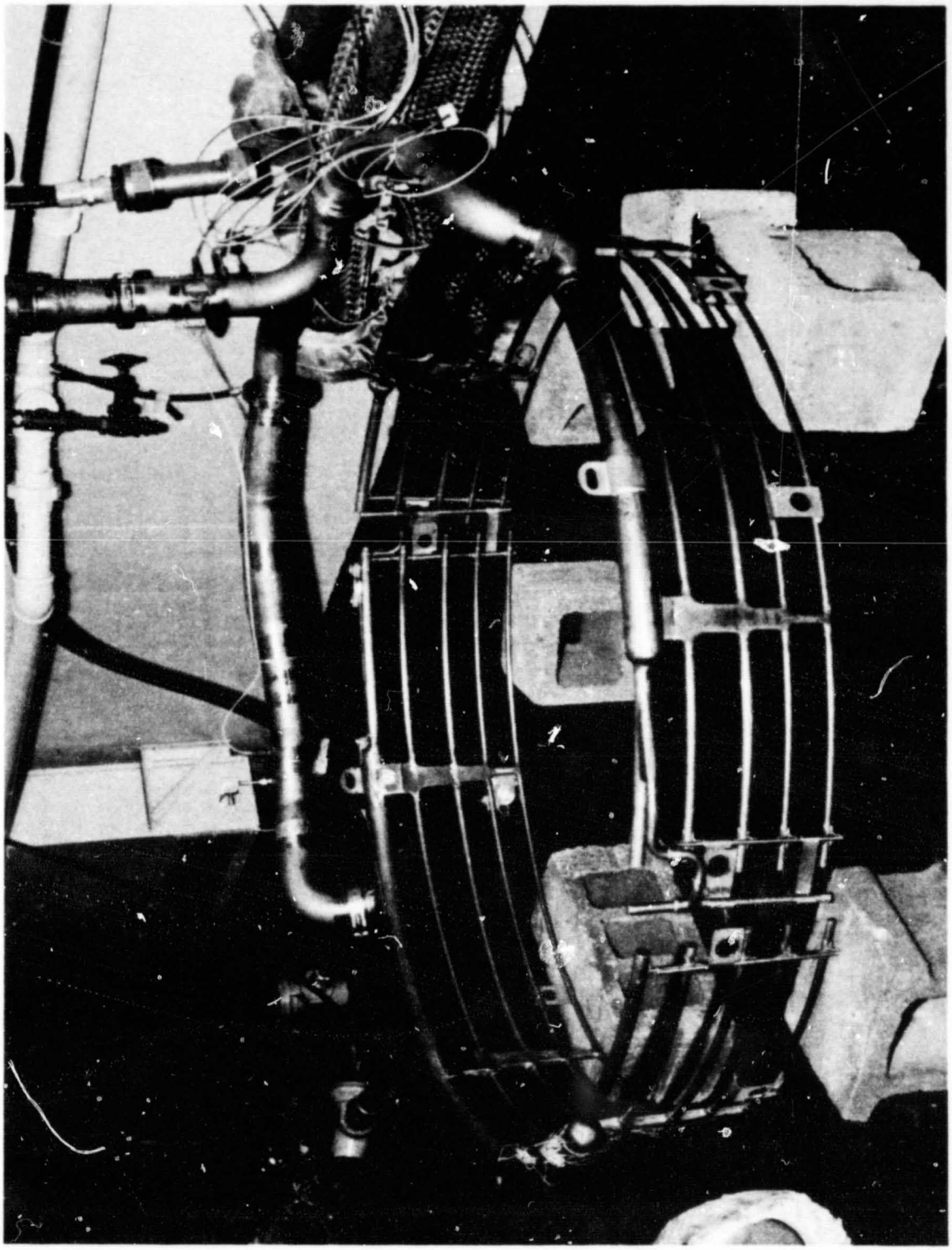

Figure 6. ACC LPT Cooling Manifold.

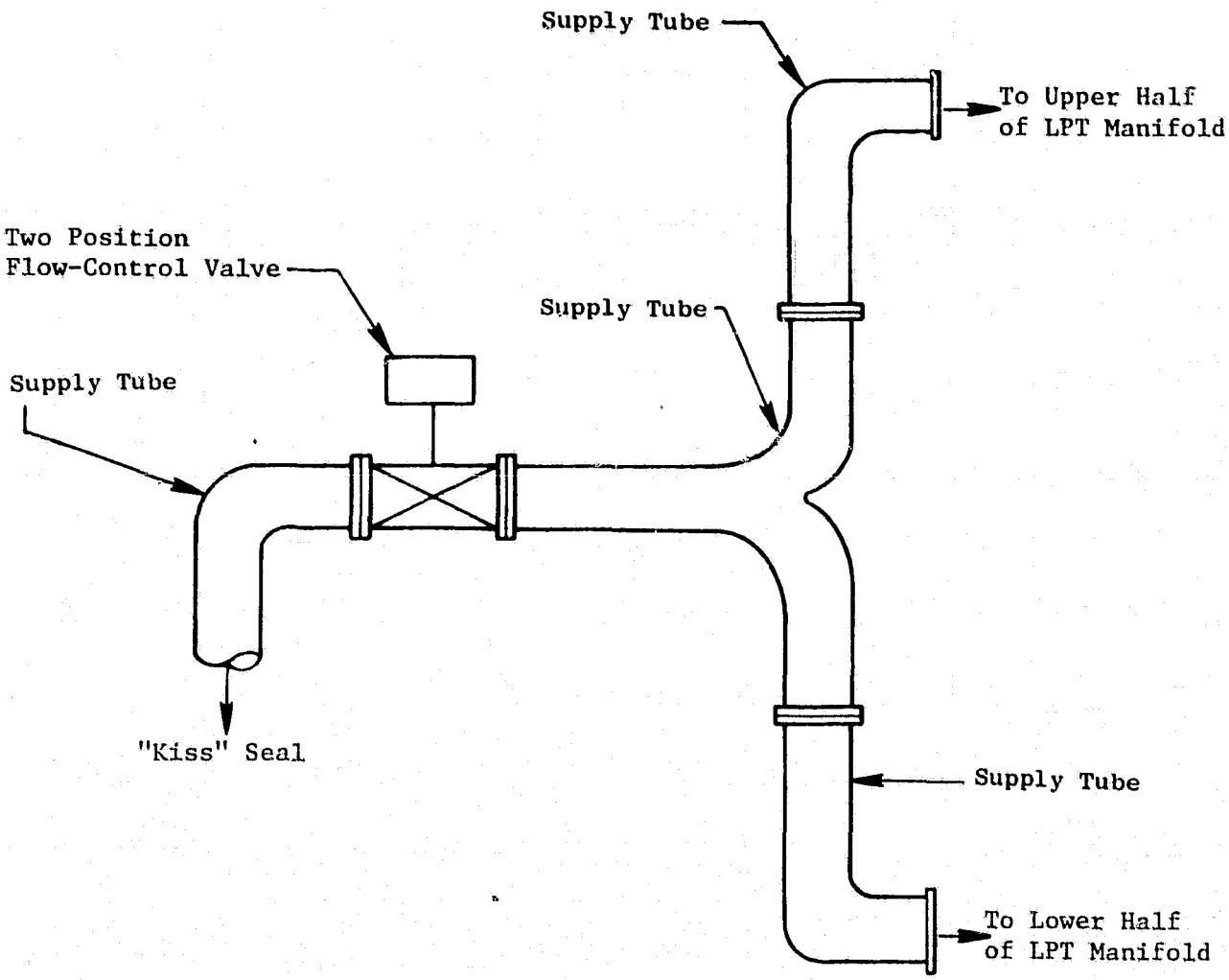

Figure 7. ACC Manifold Supply Tubing Downstream of Kiss Seal.

- Cruise flow increased from 0.074 kg/sec (0.164 lb/sec) to 0.174 kg/sec (0.385 lb/sec).

- Last two (stage 4) circumferential tubes eliminated to concentrate flow on forward hooks.

- Separate air supplies for each half to provide more even flow distribution.

- Horizontal flange cooling tubes added.

- Size of circumferential tubes increased and size and spacing of impingement holes changed to accommodate increased flow.

Air Supply Piping: Kiss Seal to Manifold

- New hardware design to accommodate the ACC valve and separate air supplies to each manifold half.

Air Supply Piping: Reverser Interface to Kiss Seal

- No change.

Fan Air Scoop

- Scoop added over air supply port in cowling wall to provide additional supply pressure and, therefore, assist in achieving additional flow required.

ACC Valve

- Valve added in manifold supply piping to modulate flow at takeoff conditions.

4.0 COMPONENT TESTING

4.1 MANIFOLD FLOW TEST

The overall objectives of this test was to obtain data which would define the airflow characteristics of the LPT ACC cooling system: LPT cooling manifold and associated supply tubing. Specific objectives were:

1. Define flow function versus pressure ratio for each half of the system separately and for the entire system as an assembly.

2. Define the cooling manifold flow split; i.e., determine the flow through each manifold flow segment separately. A flow segment is defined as a circumferential cooling tube or horizontal flange cooling tube in either manifold half.

3. Define the circumferential and axial static pressure distribution of both manifold halves.

4.1.1 Test Setup

The test was conducted in the Component Mechanical Laboratory, and the test setup is shown in Figure 8. The manifold supply tubing was plumbed to the facility line supplying ambient temperature air. Two separate facility systems were employed during the course of the test which had maximum airflow capacities of 1.814 and 3.175 kg/sec (4 and 7 lb/sec), respectively.

Facility airflow was measured usi both orifices and venturis for different portions of the test. Facility airflows and pressures were controlled with pneumatically operated regulators and valves, and were monitored in the cell control room.

The hardware tested included the LPT ACC cooling manifold (top and bottom halves) and portions of the LPT ACC cooling manifold supply tubing. The supply tubes used are illustrated schematicaly in Figure 9. These tubes were included in the component test in order to duplicate system flow characteristics which would exist in an engine application and also to provide satisfactory locations for installation of total pressure/total temperature probes.

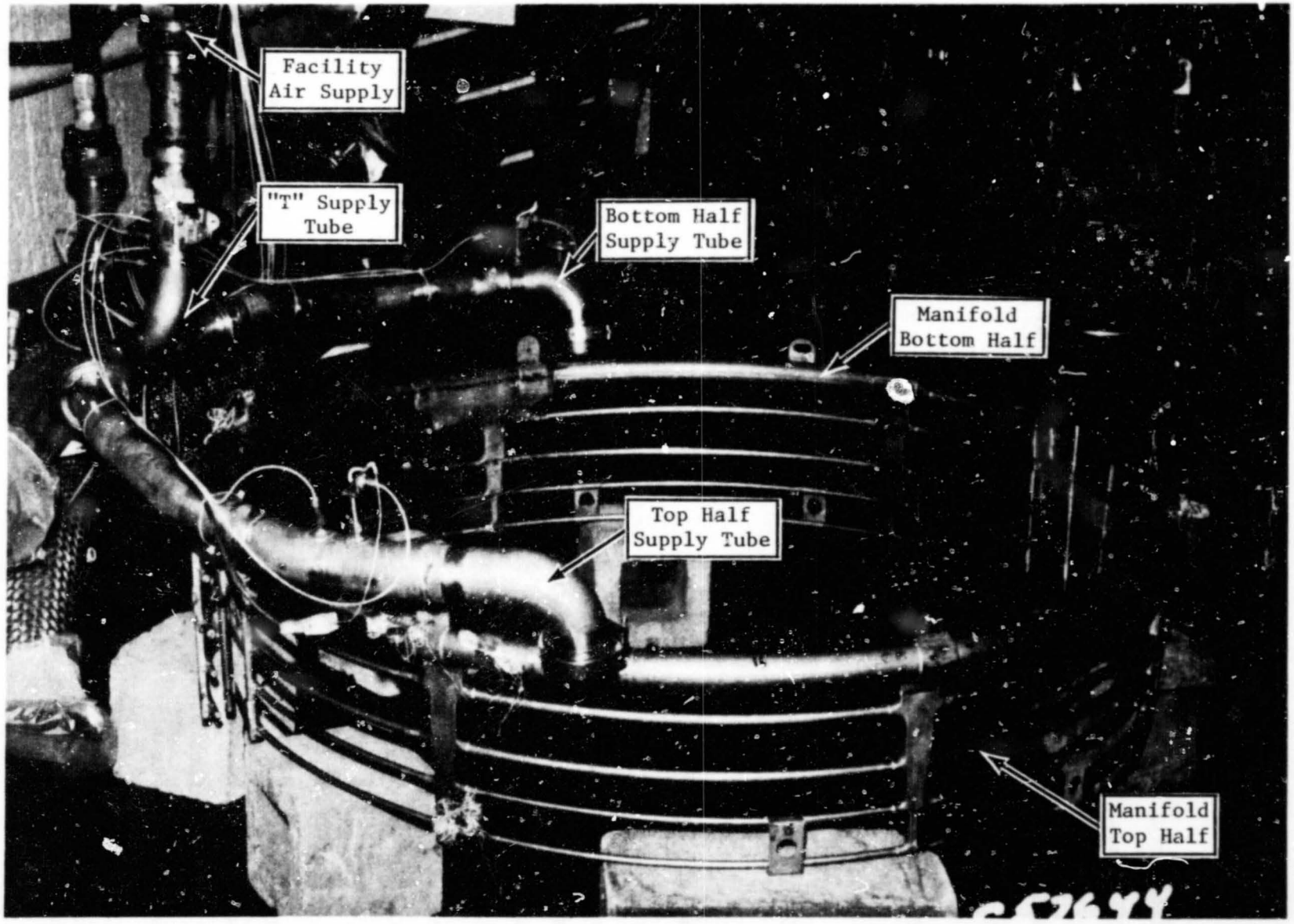

Figure 8. Airflow Component Test Setup.

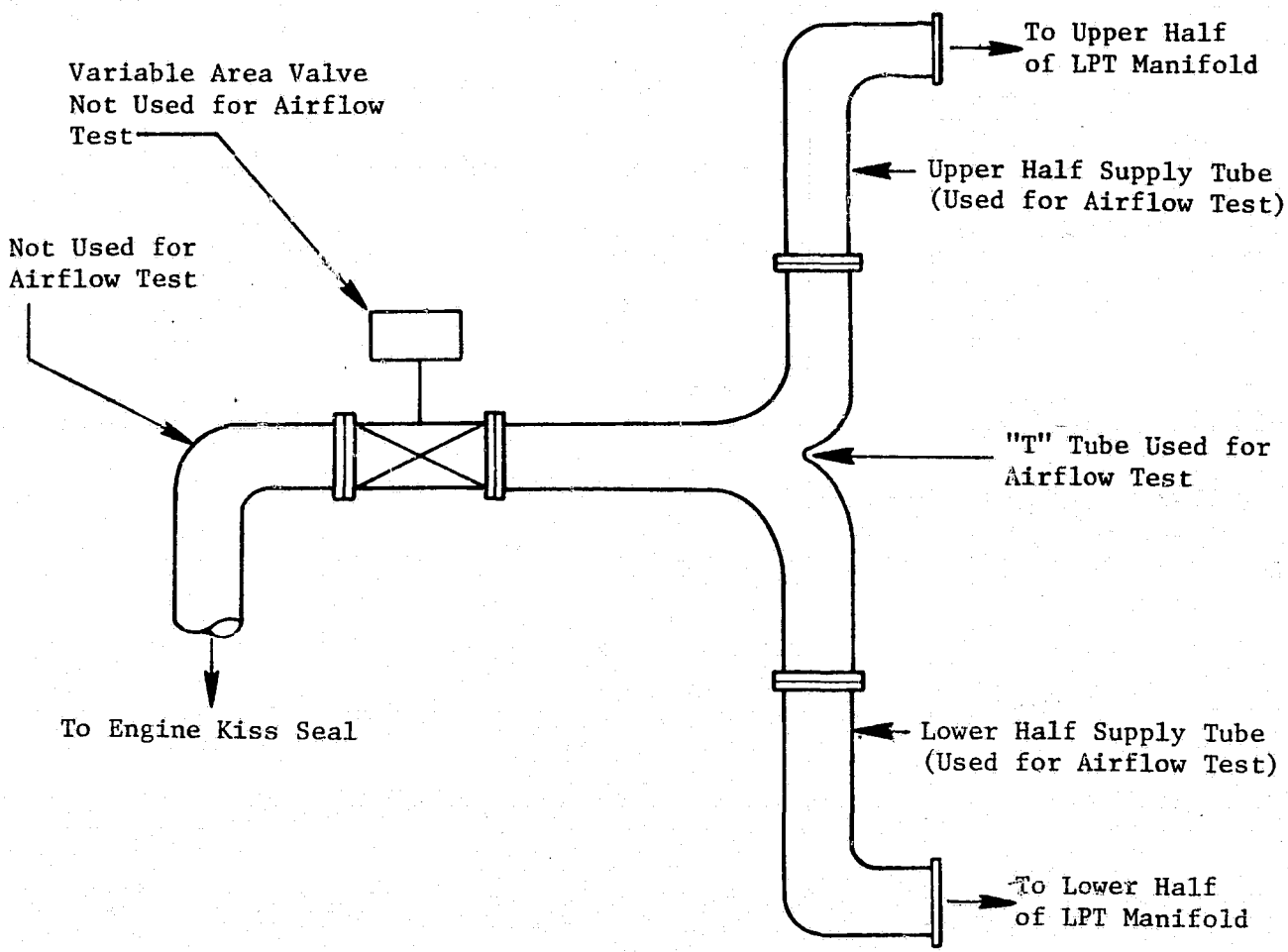

Figure 9. Manifold Supply Tubing: Airflow Component Test.

The ACC valve and the supply tube from the valve to the engine kiss seal were not used in order to simplify the test operation and because it was felt that any changes in system characteristics (such as internal velocity profile) induced by these components would be attenuated upstream of the locations of pressure/temperature probes located in each manifold half supply tube.

4.1.2 Instrumentation

The three manifold supply pipes were instrumented as shown in Figure 10. Combination total pressure/total temperature probes and static pressure taps were installed in each pipe. The total pressure/total temperature probes were located downstream of the static taps to prevent erroneous static readings.

Mercury manometers were used to measure all manifold pressures except those obtained from a hand-held static pressure fitting, employed during the static pressure survey, which were monitored on a digital pressure readout. Manifold temperatures were indicated on digital temperature readouts. Facility pressures and temperatures required to measure airflow rates were routed to gages and digital temperature readouts located inside the control room.

4.1.3 Test Procedure

Definitions

Prior to delineating the specific procedure which was followed, it is pertinent to define various parameters.

$$\text{Flow Function} = \frac{W\sqrt{T_T}}{P_T}$$

where, W = airflow to manifold kg/sec (lb/sec)

T_T = total temperature in K (° R) in one of the manifold supply pipes

P_T = total pressure in N/cm^2 (psia) in one of the manifold supply pipes.

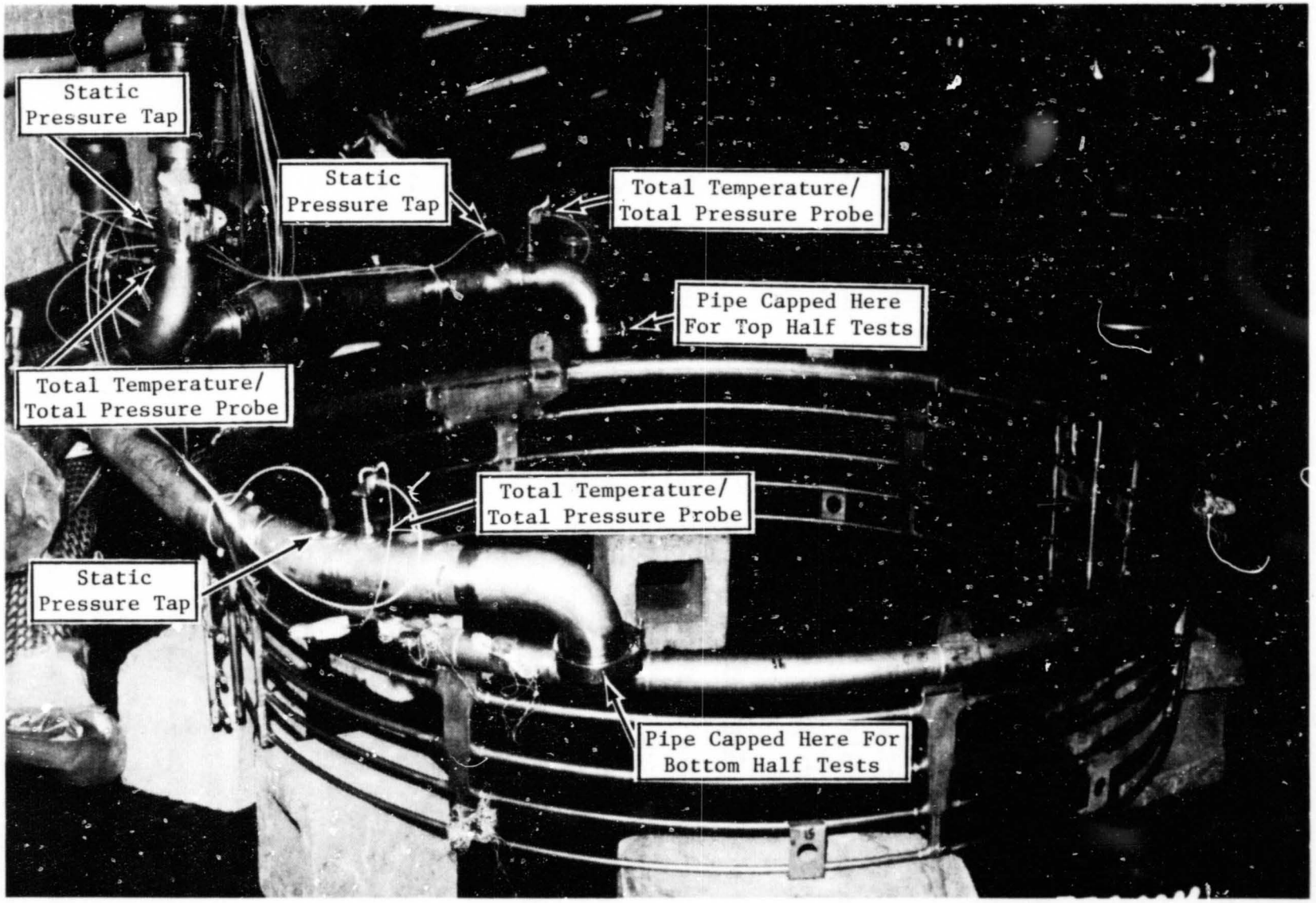

Figure 10. ACC Manifold Supply Piping Airflow Instrumentation.

Pressure Ratio - P_T/P_S

where, P_T = total pressure in N/cm^2 (psia) in one of the manifold supply pipes

P_S = test cell static (barometric) pressure in N/cm^2 (psia)

Flow Segment - A single circumferential cooling tube or horizontal flange cooling tube in either manifold half.

4.1.3.1 Top-Half Flow Function

The manifold and supply pipes were plumbed as shown in Figure 10, except that the bottom-half supply tube was capped at the manifold end. Airflow was varied to the manifold and the flow function was defined over a pressure ratio range of 1.0 to 2.3.

4.1.3.2 Top-Half Flow Split

The manifold and supply pipes were plumbed as defined in Section 4.1.3.1. The flow through each individual segment was obtained by covering all but one segment with aluminum tape while maintaining a pressure ratio of 1.8 (based on P_T in the "T" supply tube). A pressure ratio of 1.8 was chosen since it is approximately equal to the pressure ratio which exists at altitude cruise.

4.1.3.3 Bottom-Half Flow Function

The procedure for defining the bottom-half flow function was the same as that specified in Section 4.1.3.1 except that the top-half supply tube was capped at the manifold end.

4.1.3.4 Bottom-Half Flow Split

The procedure for defining the bottom-half flow split was the same as that specified in Section 4.1.3.2 except that the top-half supply tube was capped.

4.1.3.5 Manifold Assembly Flow Function

The manifold halves and supply pipes were plumbed as shown in Figure 10 with air flowing to both halves. Airflow was varied to the manifold assembly and flow function was defined over the pressure ratio range of 1.0 to 2.4.

4.1.3.6 Manifold Assembly Static Pressure Survey

The manifold setup was the same as in Section 4.1.3.5.. Air was supplied to the manifold at a pressure ratio of 1.8 based on the "T" tube total pressure. This pressure ratio was selected because it is representative of cruise conditions and because it would magnify any circumferential or row-to-row pressure variance due to the much greater airflow provided during the test as compared to that which will actually be used during sea level takeoff conditions.

The static pressure survey was conducted by manually placing a special rubber fitting over one manifold hole at a time. The fitting was flexible enough to provide a good seal and, therefore, yield an accurate reading. Static pressure readings were obtained in this manner at approximately 300 different locations, yielding a very good circumferential and axial mapping of the manifold assembly static pressures.

Figure 11 illustrates the locations of initial readings and direction of subsequent readings for each segment in both halves.

4.1.4 Test Results

4.1.4.1 Flow Function

Figures 12 through 15 are representative of the flow function versus pressure ratio data obtained from each of the supply pipe probes for the top and bottom manifold halves flowing separately and for both halves flowing simultaneously as an assembly. These calibration curves were used to compute the airflow to each manifold half as well as the total flow to the manifold assembly during the instrumented engine test.

Flow function versus pressure ratio curves were generated with data from different probes under the same test conditions. This was done to provide a redundancy of data to be used in flow calculations from the engine test data.

Figure 15 also provides a comparison between the flow function curves for the ACC manifold assembly and a current production CF6-50 manifold assembly which was flow tested in 1978. This comparison demonstrates the greater flow potential throughout the pressure ratio range of the ACC manifold which was the design intent. Flow function comparisons for each half flowing separately

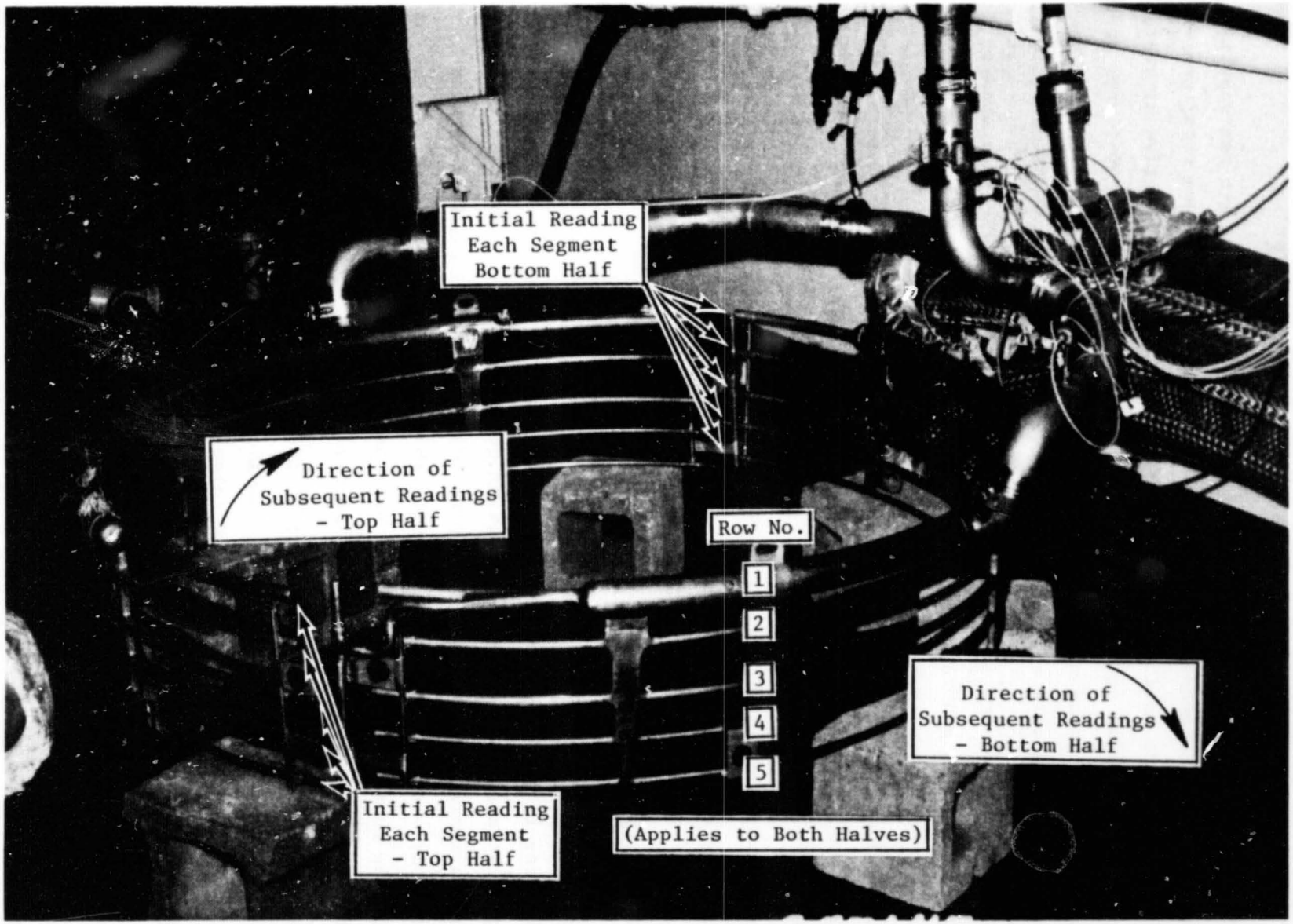

Figure 11. ACC Manifold Static Pressure Survey Nomenclature.

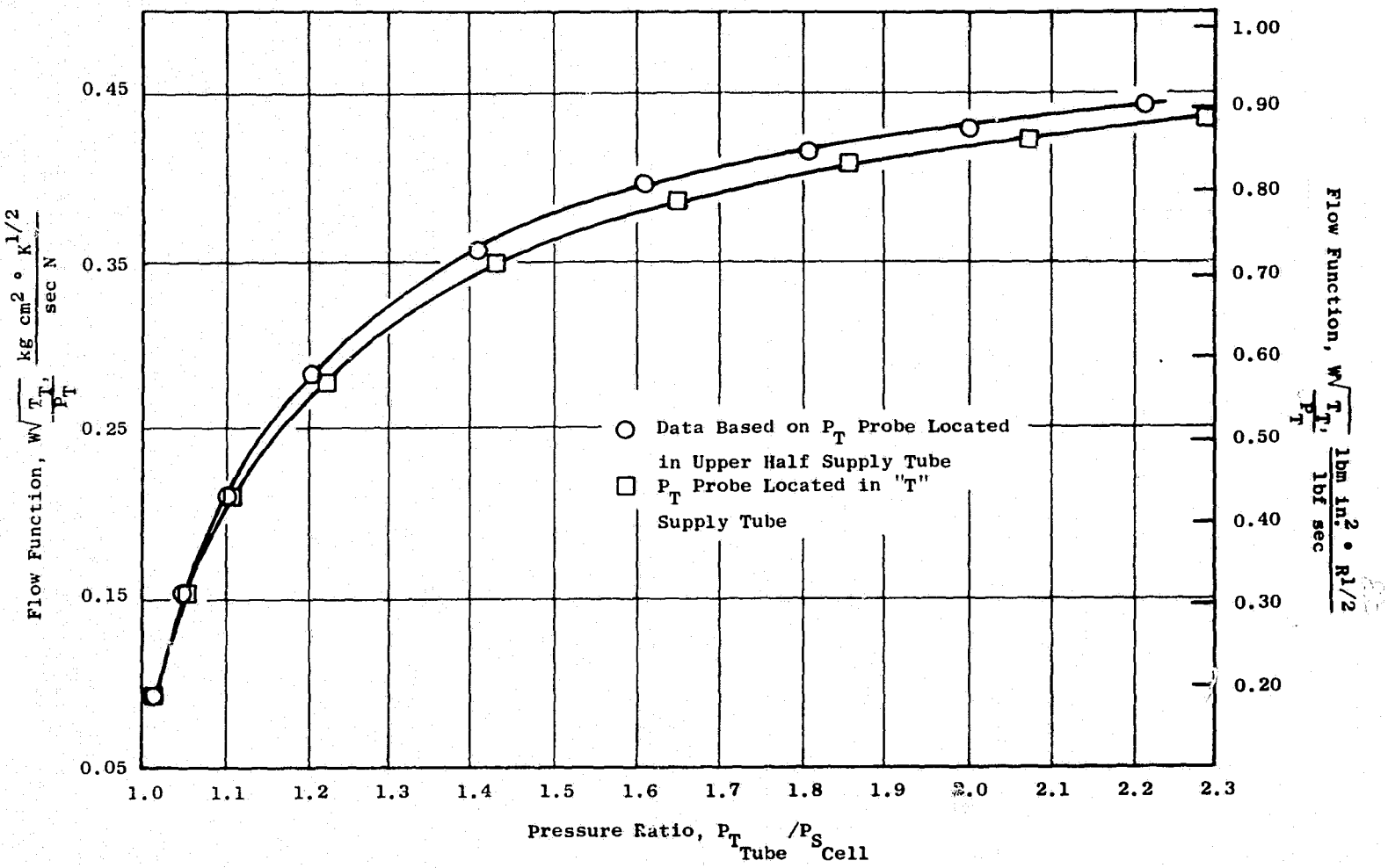

Figure 12. Flow Function Versus Pressure Ratio: Top Half Flowing, ACC Manifold.

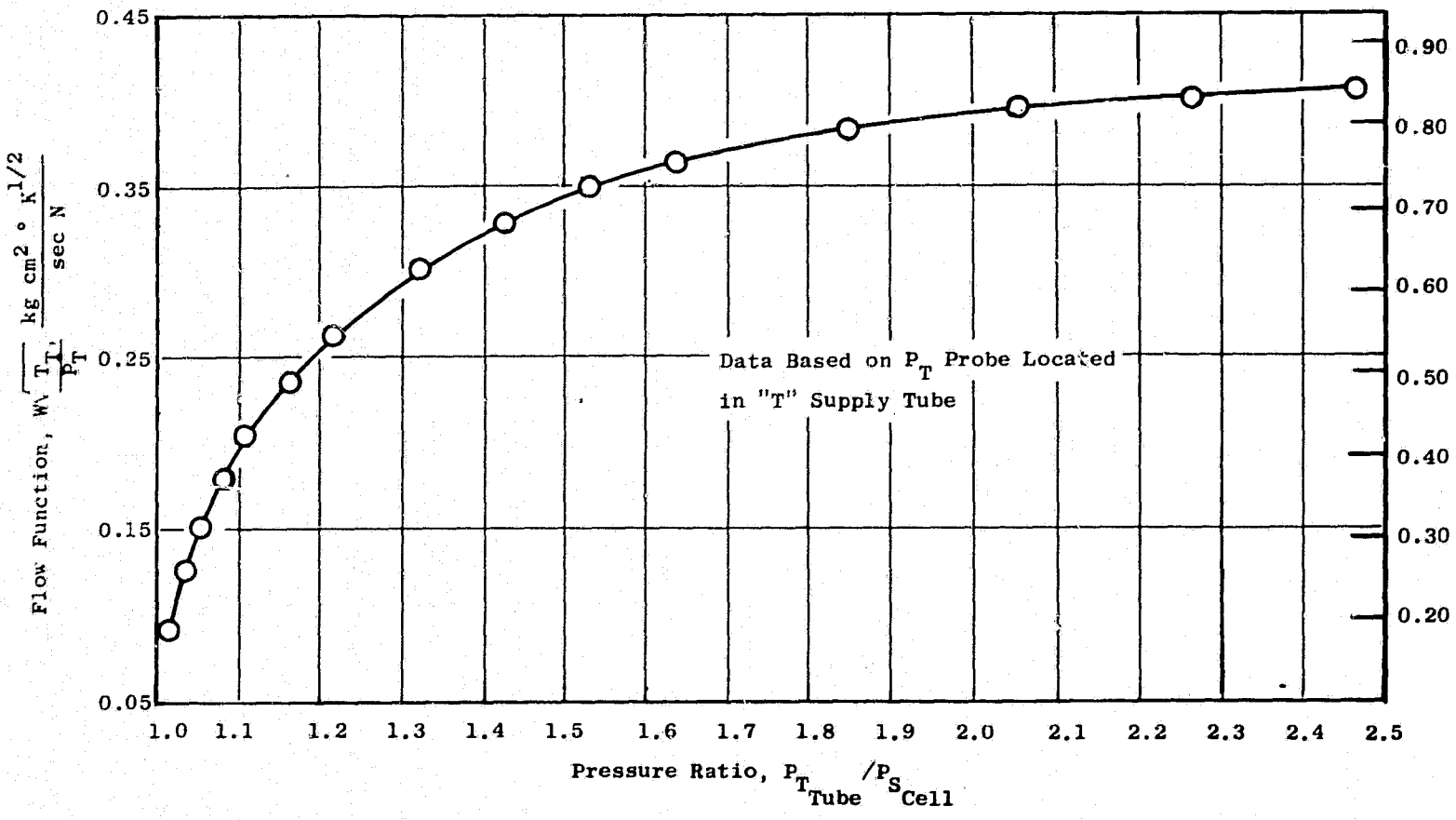

Figure 13. Flow Function Versus Pressure Ratio: Bottom Half Flowing, ACC Manifold.

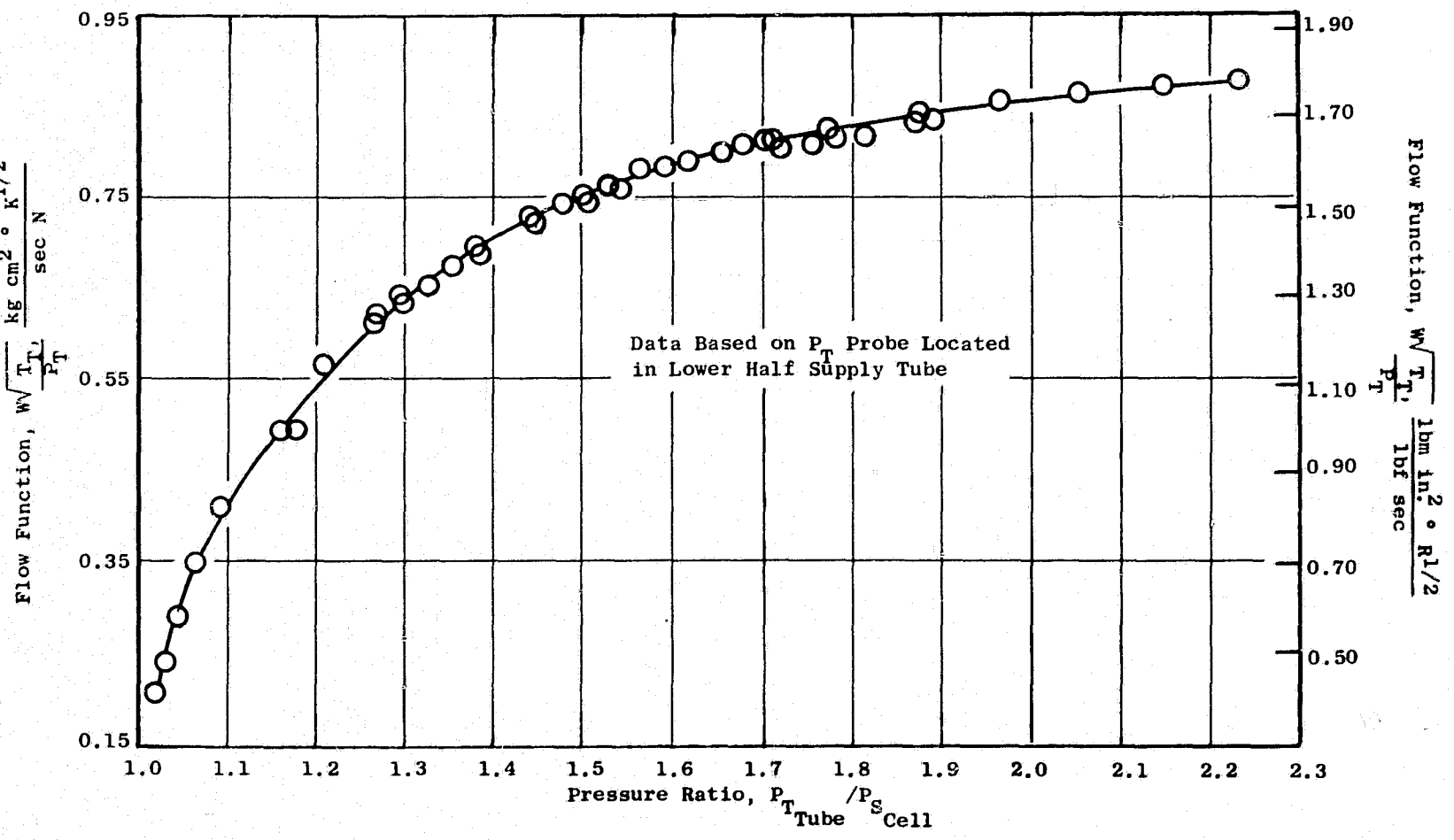

Figure 14. Flow Function Versus Pressure Ratio: Both Halves Flowing, ACC Manifold.

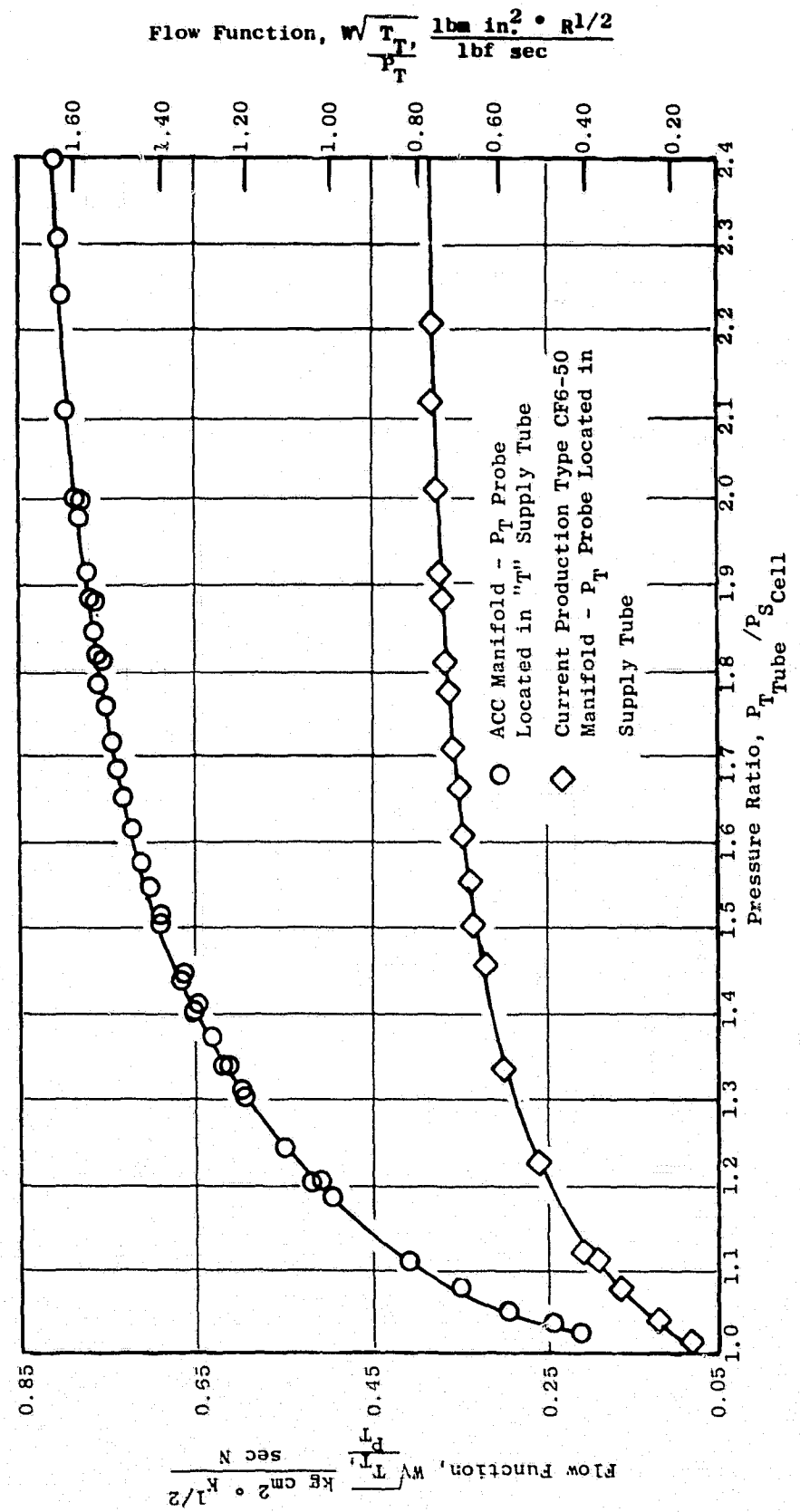

Figure 15. Flow Function Versus Pressure Ratio: Both Halves Flowing, ACC Manifold.

are not possible because the current production manifold configuration does not have separate supply pipes for each half.

4.1.4.2 Static Pressure Survey

Figures 16 through 18 present the static pressure surveys conducted on each of the circumferential flow segments in the manifold top half and are typical of the results obtained for the corresponding flow segments in the bottom half. Static pressure is plotted versus hole number which is equivalent to circumferential distance.

It is interesting to compare the results shown in Figures 16 through 18 to the static pressure surveys conducted on a current production-type CF6-50 manifold in 1978. Figure 19 depicts that manifold and identifies the flow segments. Figures 20 through 22 depict the static surveys conducted on the top half of the manifold.

Examination of Figures 16, 17, 18, and 20 through 22 reveal sharp local peaks in static pressure. These peaks are coincident with the intersections of axial flow distributors and circumferential tubes for both manifolds, and appear to be inherent with this type of design. On the ACC manifold, peaks also exist in the first tube where the supply pipe joins the manifold.

Although approximately the same magnitude of peaks exist in both manifolds, it is important to note that the ACC manifold was flowing approximately twice as much as the current production manifold, and some of the individual tubes were flowing four times as much as comparable ones in the current production manifold. If these two manifolds were flowing the same amount, the peak-to-peak variations would be less in the ACC manifold.

Also, there appears to be less variation in the mean pressure levels with the ACC manifold. The design goal is a uniform pressure distribution.

Additionally, it is important to reiterate the fact that the surveys for both manifolds were conducted at a pressure ratio of 1.8 in order to magnify any circumferential differences. Under actual engine operating conditions, the static pressure variations will be much less for both manifolds than those indicated in Figures 16, 17, 18, and 20 through 22, since, at sea level, the

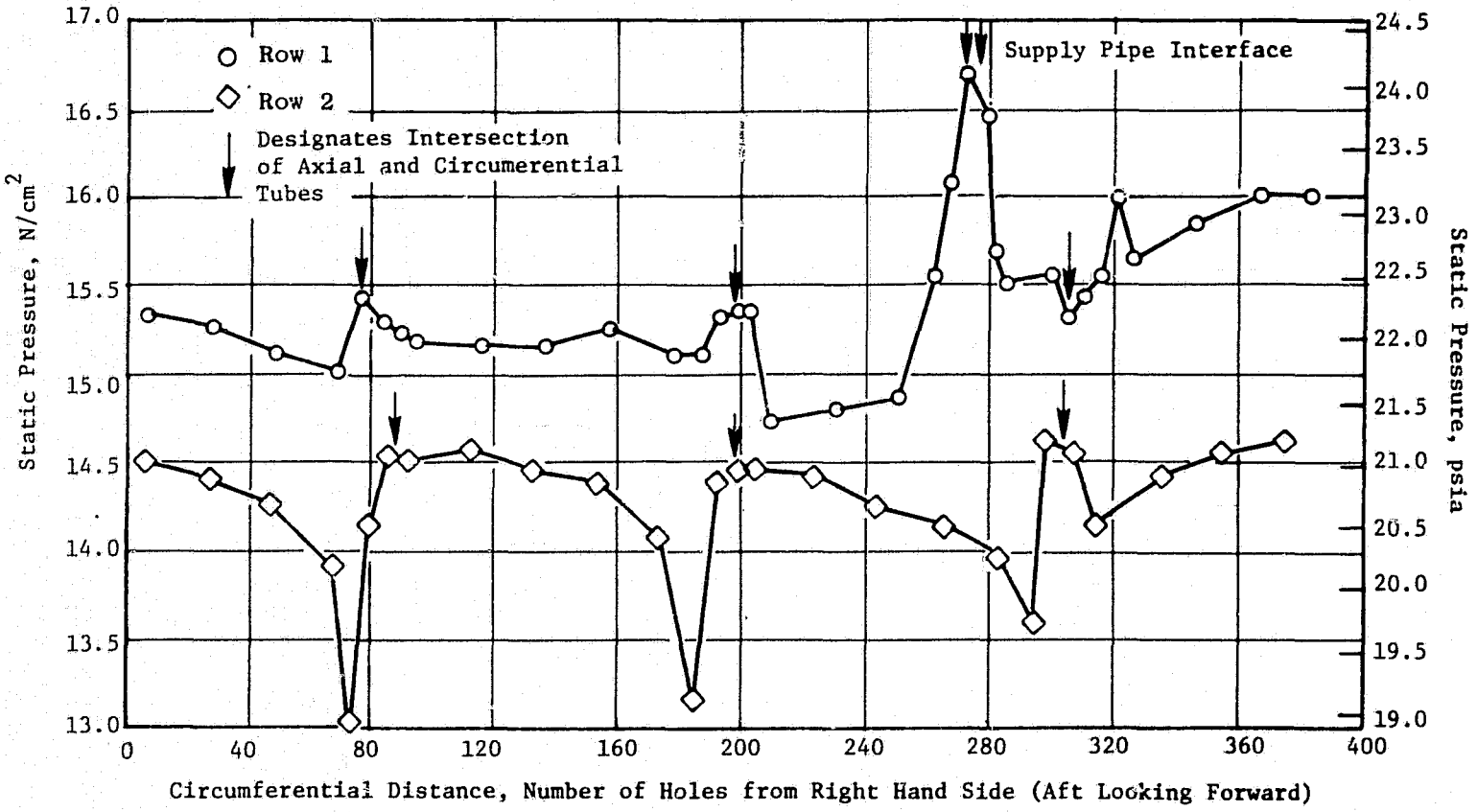

Figure 16. Static Pressure Versus Circumferential Distance: Top Half, Tube Rows 1 and 2, ACC Manifold.

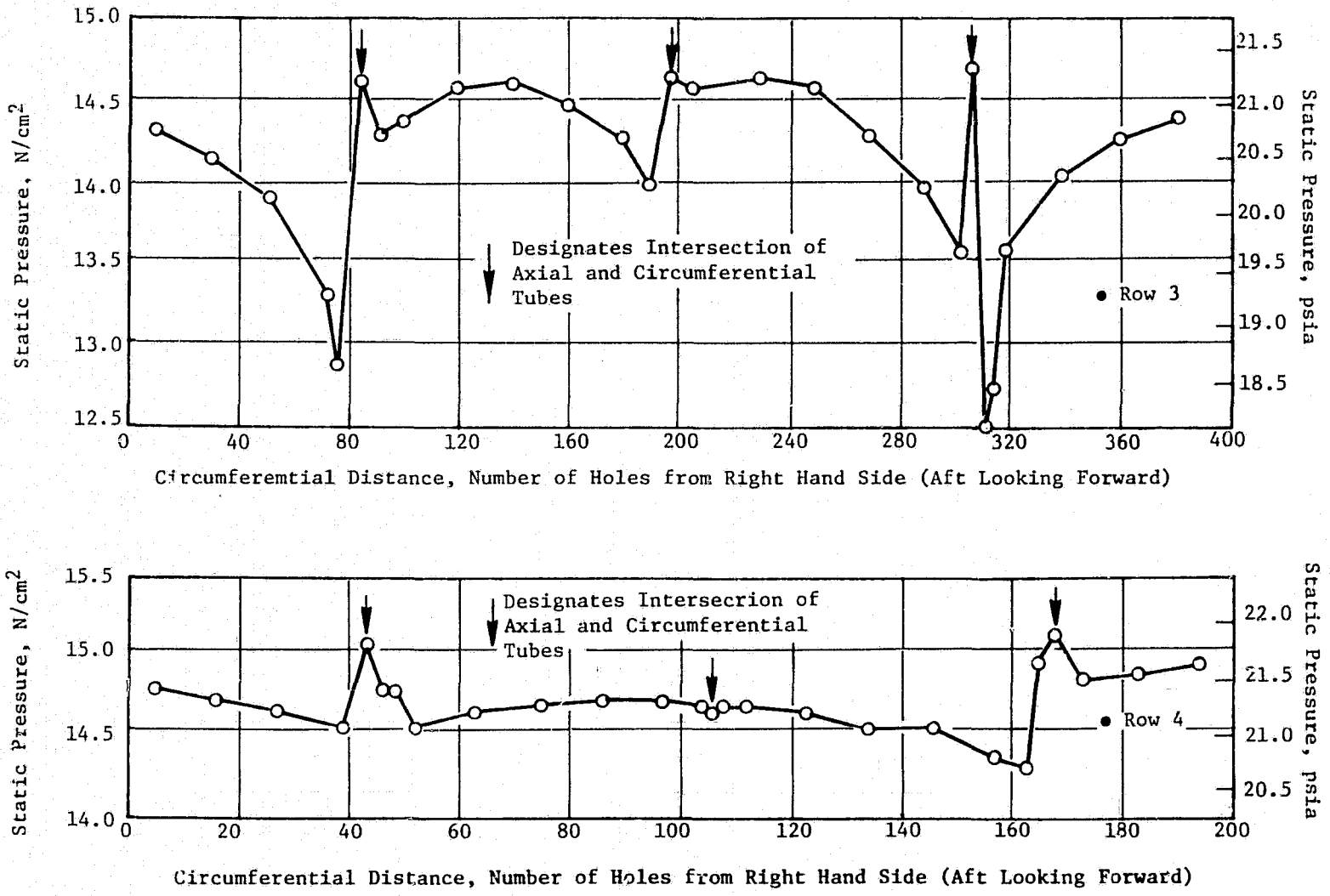

Figure 17. Static Pressure Versus Circumferential Distance: Top Half, Tube Rows 3 and 4, ACC Manifold.

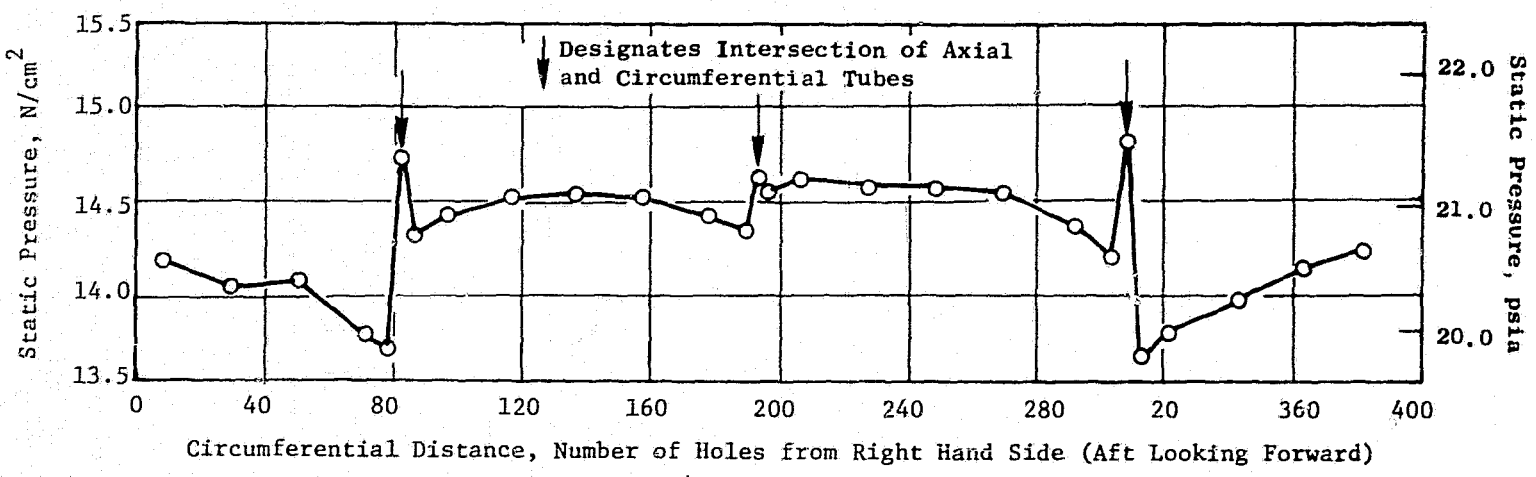

Figure 18. Static Pressure Versus Circumferential Distance: Top Half, Tube Row 5, ACC Manifold.

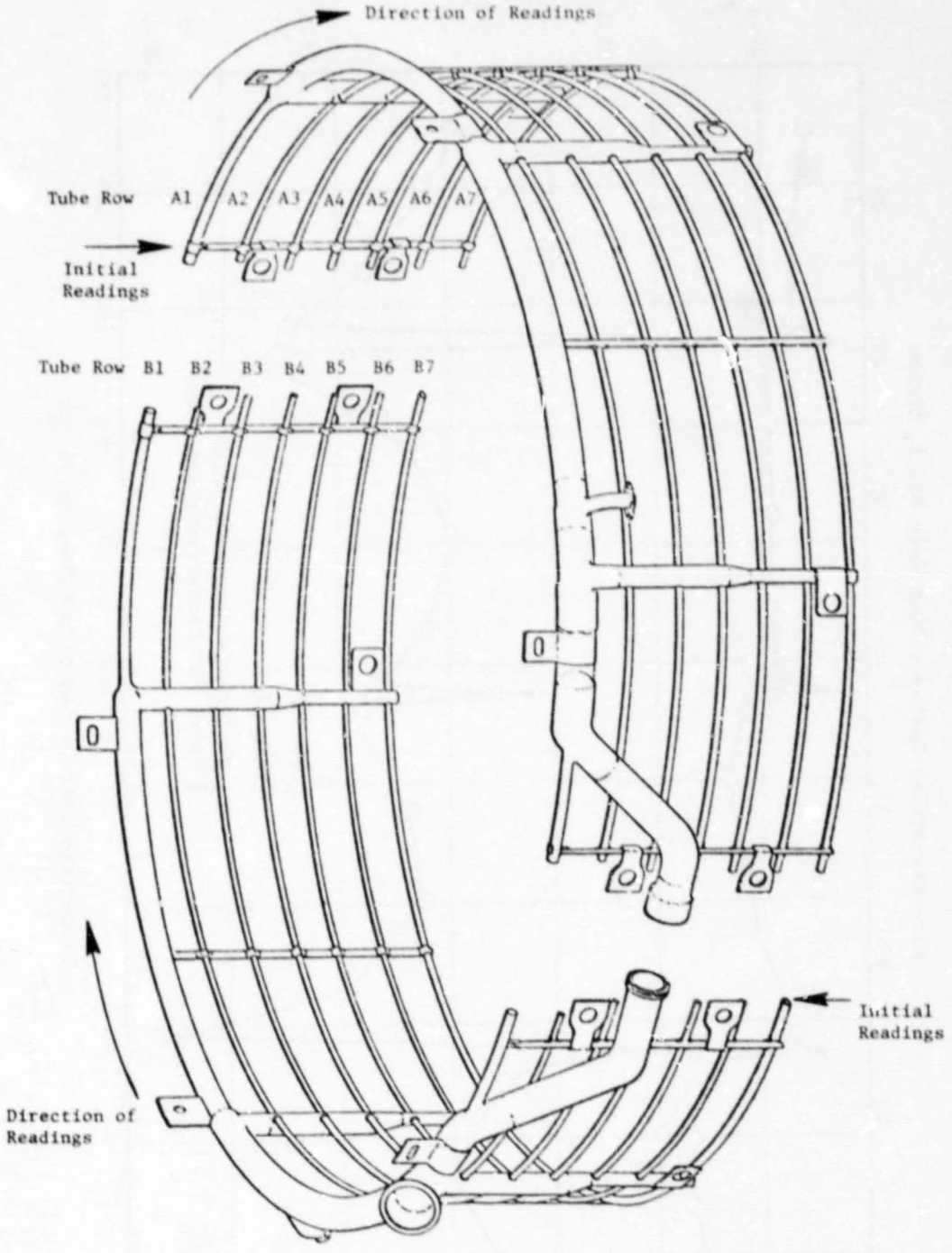

Figure 19. Current Production Manifold Static Pressure Survey Nomenclature.

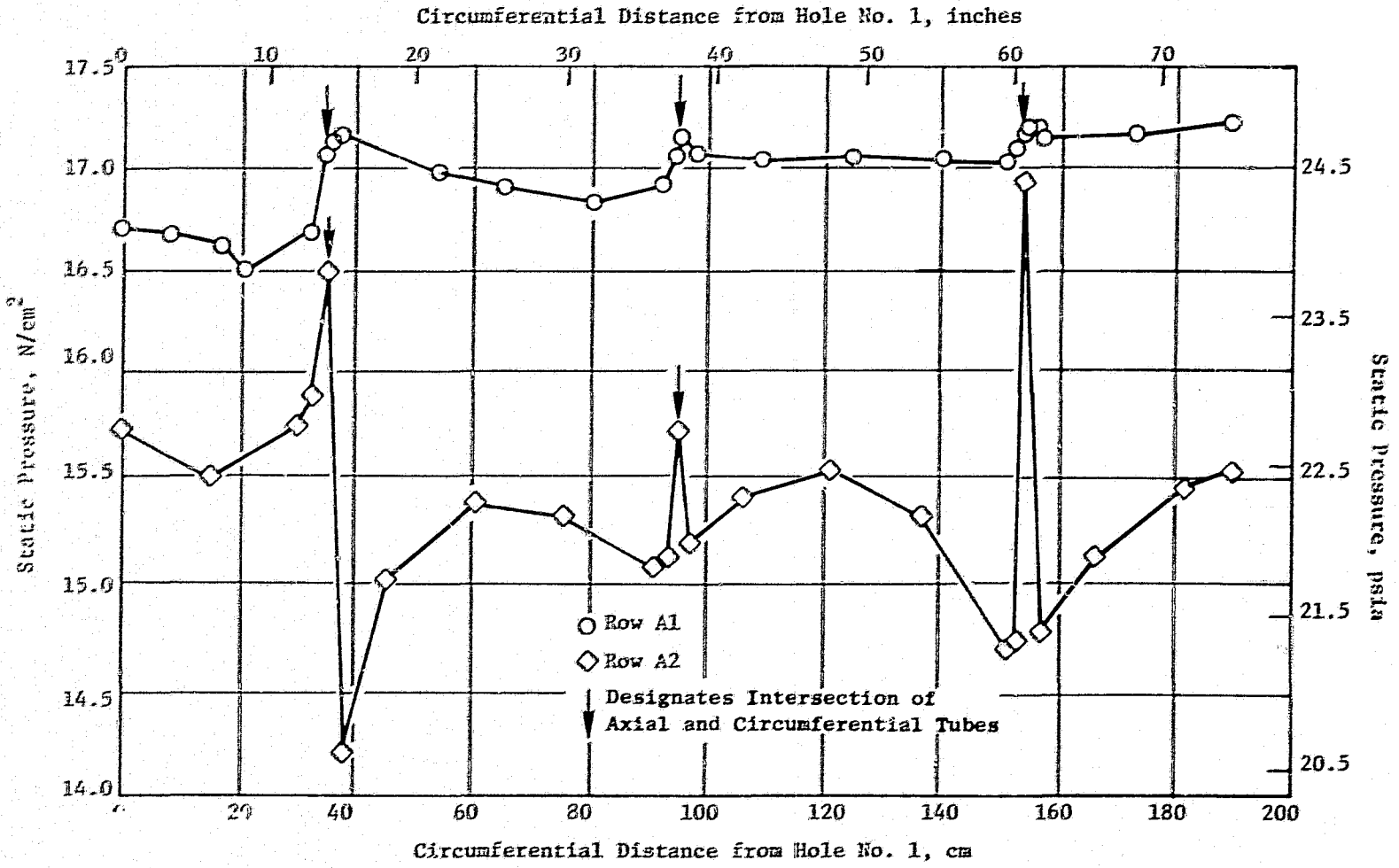

Figure 20. Static Pressure Versus Circumferential Distance: Tube Rows A1 and A2, Current Production Manifold.

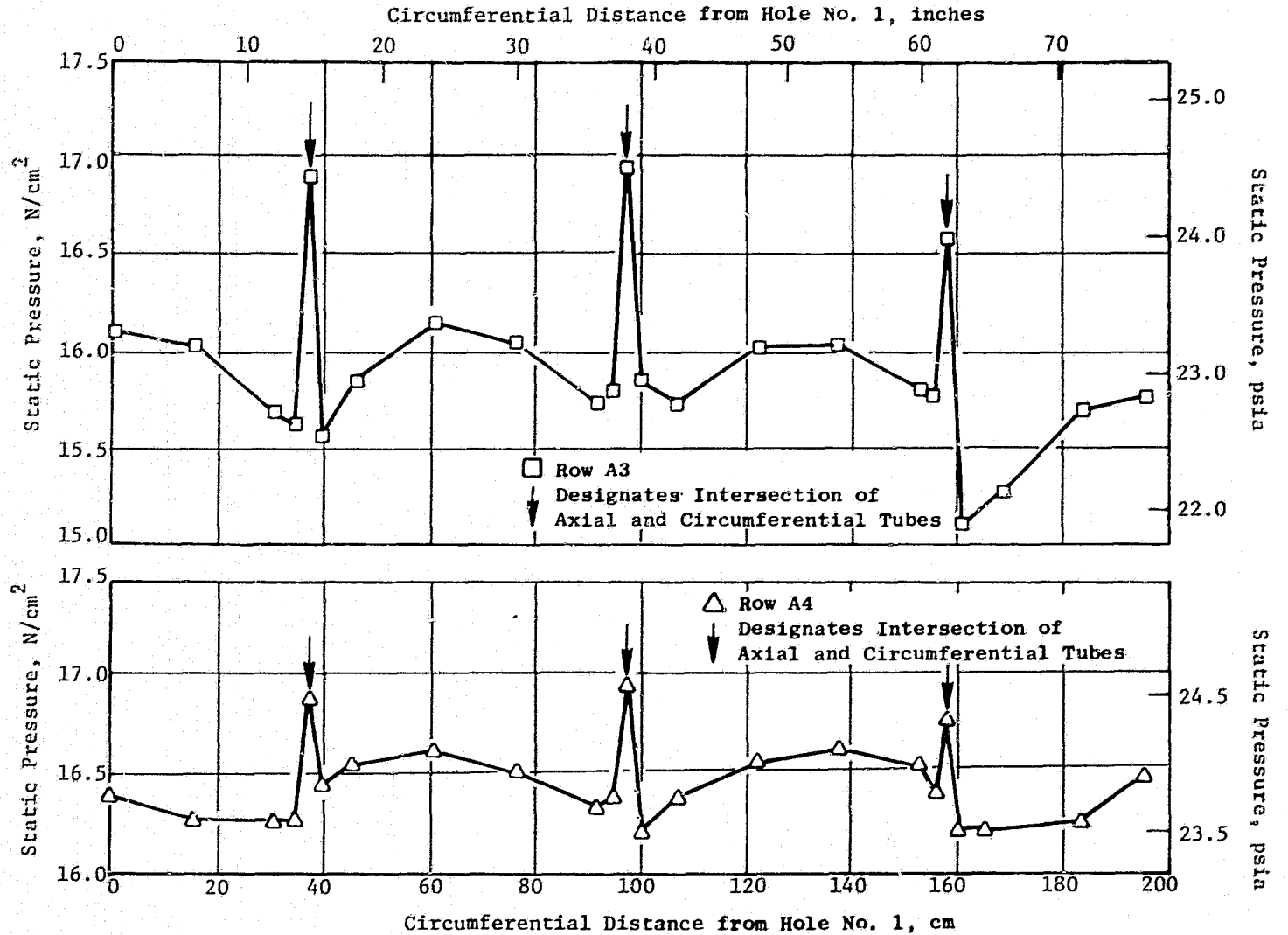

Figure 21. Static Pressure Versus Circumferential Distance: Tube Rows A3 and A4, Current Production Manifold.

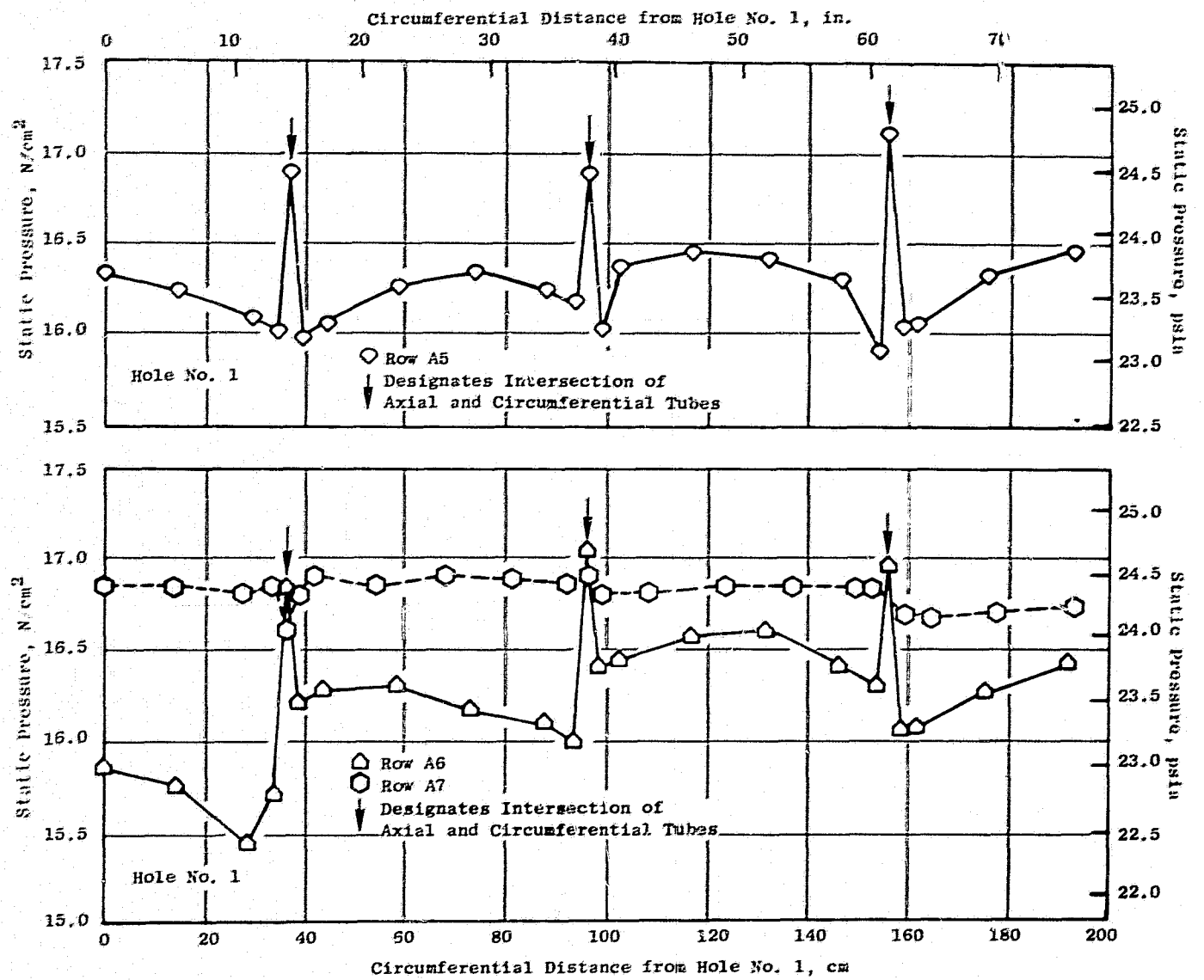

Figure 22. Static Pressure Versus Circumferential Distance: Tube Rows A5, A6, and A7, Current Production Manifold.

actual flow rates will be much less than the test flow rates and, at cruise, the flow rate and actual pressure levels will be less than the component test values. If the component test results for both manifolds were prorated through their respective cruise flow rates, the ACC manifold would exhibit lower magnitudes of pressure variations except in the first (most forward) cooling row, which would be greater.

The static pressure surveys were available as diagnostic tools to be used in conjunction with the circumferential variations in casing skin temperature to assist in understanding the results of the instrumented engine test.

4.1.4.3 Flow Splits

Table I delineates the results of the flow split test where the flow through each segment was determined separately as described in Section 4.1.3.

Varying amounts of cooling flow were required through each manifold segment in order to produce the desired temperatures at each axial location on the case skin and on the case horizontal flanges. The purpose of the flow split test was to determine if the actual flow splits matched the design intent. The measured flow percentages agree well with the intended design flow splits, particularly for the forward three tubes, as indicated in Table I.

4.2 MANIFOLD VIBRATION TEST

The objectives of this test were as follows:

1. Determine natural frequencies and associated mode shapes of responsive LPT cooling manifold components and of the manifold as an assembly throughout the frequency range of 20 to 300 Hz. This range exceeds the maximum engine one/rev operating frequency. Engine out-of-balance forces, at engine one/rev frequencies, were expected to be the principal driving forces for LPT manifold vibrations.

2. Identify areas of maximum stress on the LPT manifold, for primary modes of vibration, based on the results of preliminary vibration explorations employing the use of a strobe light tuned to the shake table, and then apply strain gages to the manifold at these locations. Record strain gage outputs as the manifold is excited in each of two radial planes throughout the frequency range of 20 to 300 Hz.

3. Extrapolate laboratory strain gage data to conditions imposed by actual engine operation and analyze with respect to manifold structural integrity.

Table I. Flow Split Results.

Flow Segment	Top Half Flow			Bottom Half Flow			Intended Design Flow
	kg/sec	lb/sec	% of Total	kg/sec	lb/sec	% of Total	% of Total
Row 1	0.176	0.3882	38.0	0.194	0.4275	39.2	41.2
Row 2	0.084	0.186	18.2	0.091	0.2011	18.4	18.3
Row 3	0.111	0.244	23.9	0.117	0.2580	23.6	25.3
Row 4	0.034	0.075	7.3	0.034	0.0749	6.9	4.9
Row 5	0.055	0.122	11.9	0.054	0.1193	10.9	9.9
Horizontal Cooling Tube	0.003	0.0074	0.7	0.005	0.0114	1.0	0.4

4.2.1 Test Setup

The test was conducted in the Component Mechanical Laboratory, and the test setup is shown in Figures 23 and 24. The LPT ACC manifold and the supply tubing, as defined in Figure 25, were mounted to a CF6-50 LPT casing and turbine midframe. This assembly was then fastened to the adapter plate of a 88,964 N (20,000 lb) rated electrodynamic shake table. The shake table adapter plate was attached to a slider plate coupled to the shaker armature and floated on an oil film on top of a granite slab rigidly connected to the facility floor. A control accelerometer mounted on the slider plate in the direction of excitation provided the feedback control of the shaker. The assembly was excited by the shaker in each of the two radial directions shown in Figure 26.

The hardware that was tested included the LPT ACC manifold (top and bottom halves), LPT manifold mount brackets and associated mount hardware, a portion of the LPT ACC manifold supply piping and supply piping mount brackets and associated mount hardware. In addition, CF6-50 turbine midframe (TMF) and LPT cases were used as vehicles to mount the LPT manifold and associated supply tubing. Although the LPT manifold was the object of testing, a portion of the manifold supply tubing was used to create appropriate boundary conditions at the two manifold inlets (one in each half). The supply tubing is illustrated schematically in Figure 25.

4.2.2 Instrumentation

The manifold hardware was instrumented with 21 accelerometers and 20 strain gages as delineated in Table II and depicted in Figures 27 through 35.

4.2.3 Test Procedure

The component test was conducted as follows:

1. The manifold assembly was oriented as shown in Figure 23, and preliminary vibration scans were conducted with the assembly excited in a radial direction parallel to the case horizontal centerline from 20 to 300 Hz (direction C-C, Figure 26). During these scans the manifold assembly movement was observed using a strobe light tuned to the excitation frequency. Based on these observations, 20 locations were selected for accelerometer mounting in order to measure the most significant manifold response.

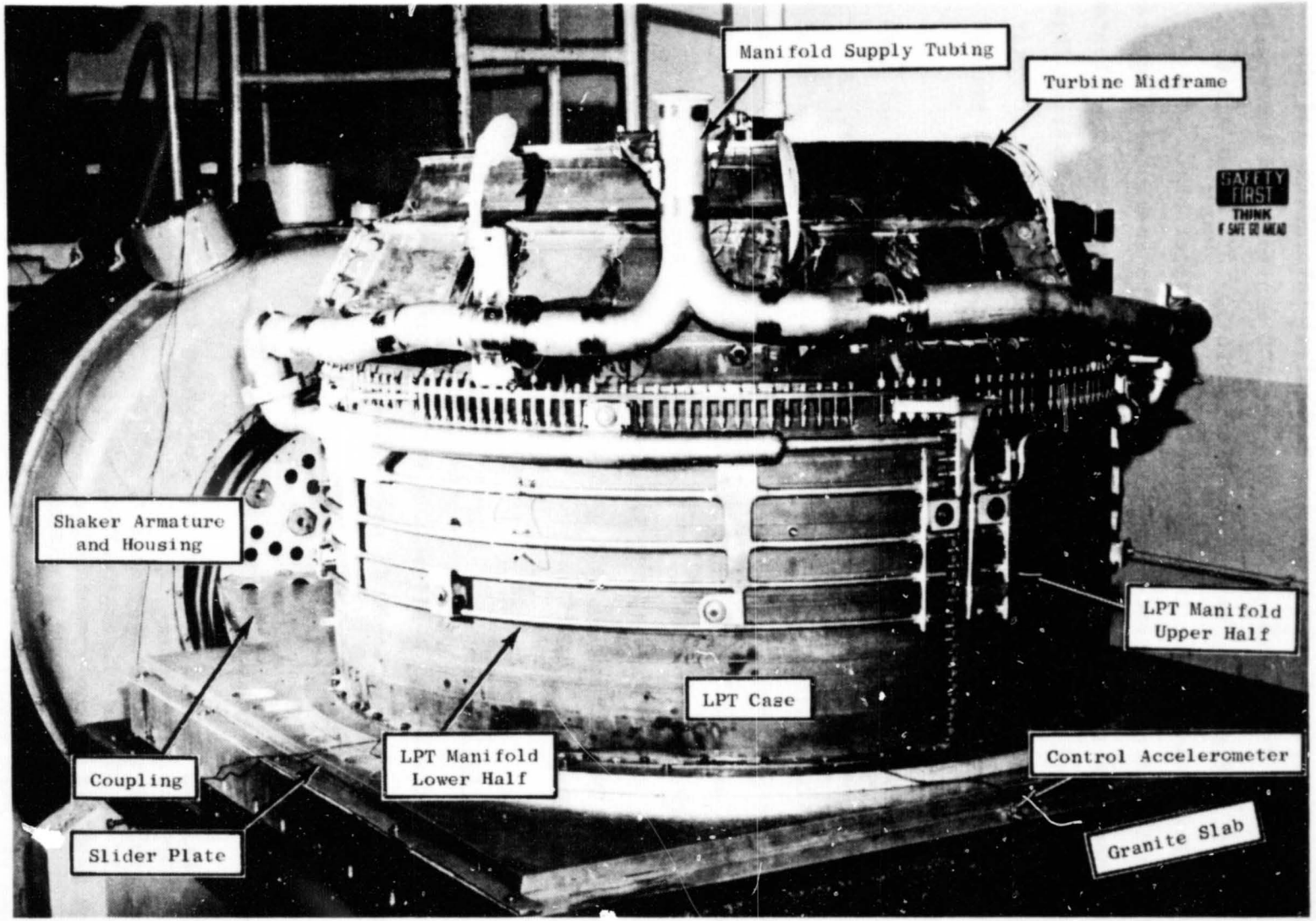

Figure 23. Test Facility and Setup: Vibration Component Test.

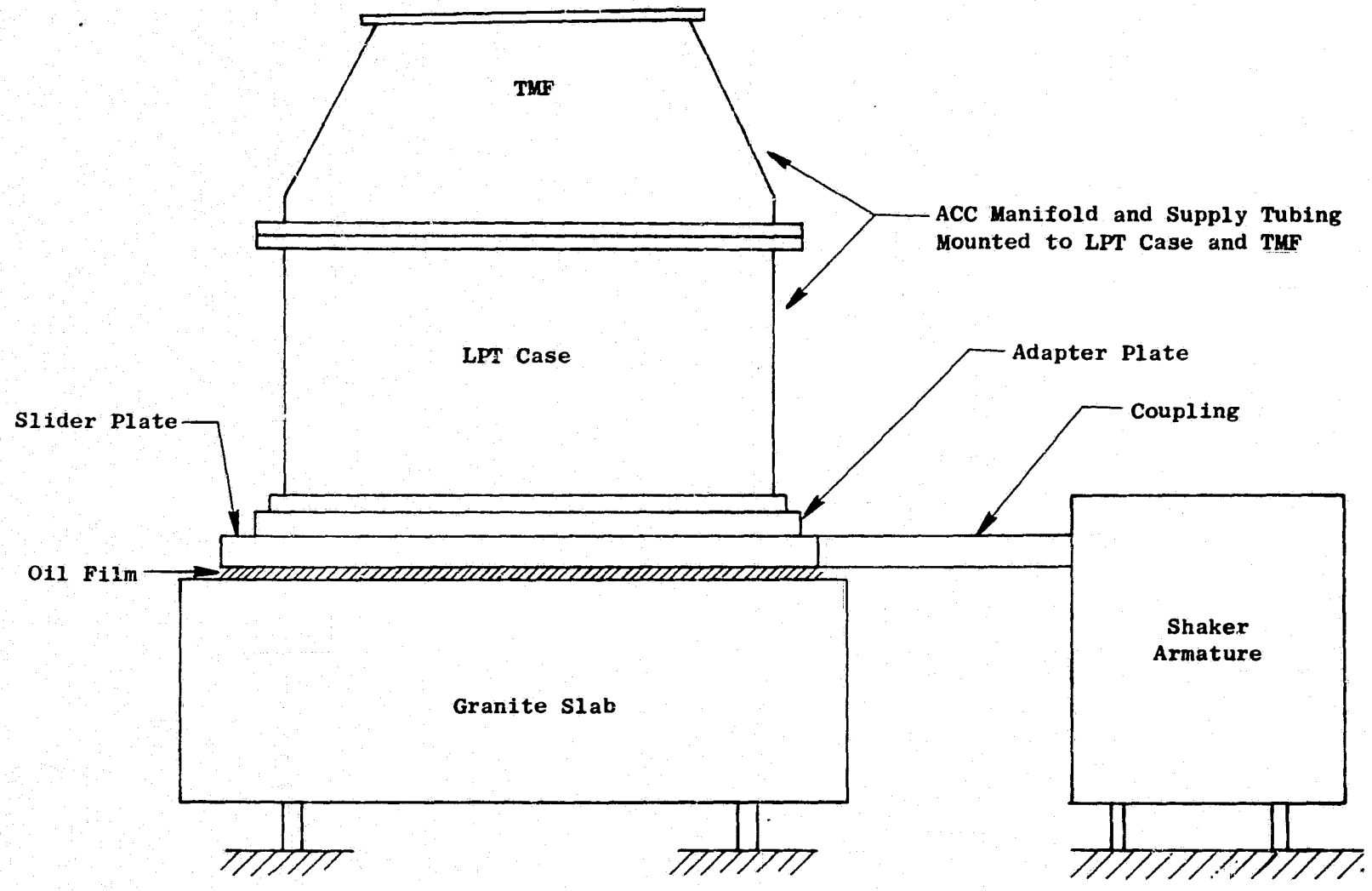

Figure 24. Test Facilities and Hardware Configuration: Vibration Component Test.

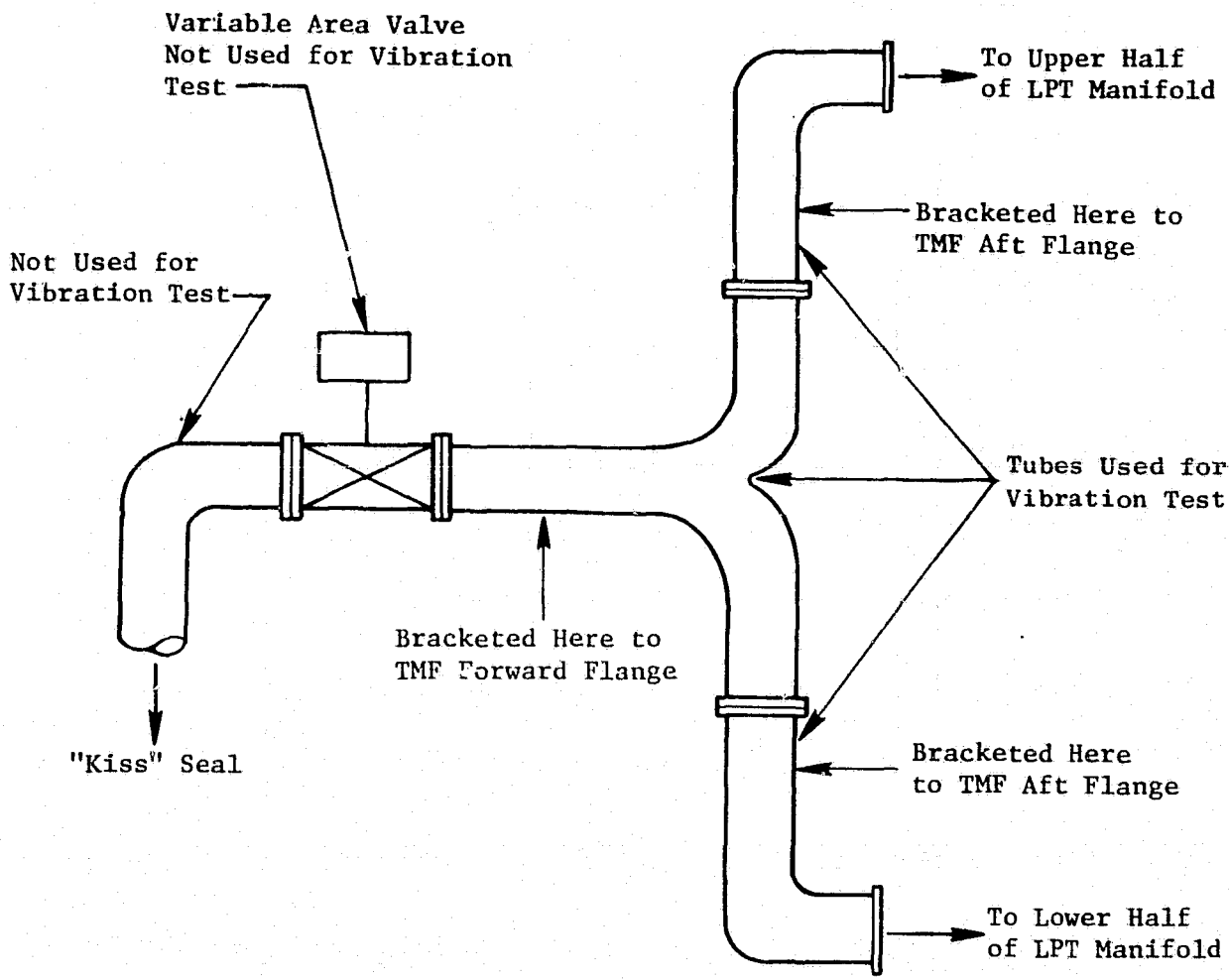

Figure 25. ACC Manifold Supply Tubing: Vibration Component Test.

Section AA

BB and CC are Radial Directions of Manifold Excitation

Figure 26. Radial Directions of Excitation.

Table II. Accelerometer and Strain Gage Locations.

A. Accelerometers

Location No.	Description of Location	* Approximate Circumferential Location, degrees	Direction of Orientation
1	Lower Manifold Half Supply Tube	170	Axial
2	Upper Manifold Half Supply Tube	318	Axial
3	Upper Manifold Half Supply Tube	318	Radial
4	Lower Manifold Half, 2nd Tube	210	Axial
5	Lower Manifold Half, 2nd Tube	210	Radial
6	Lower Manifold Half, 3rd Tube	220	Axial
7	Lower Manifold Half Horizontal Cooling Tube - Aft End	90	Radial
8	Upper Manifold Half Supply Tube Near Junction with "Y" Tube	---	Radial
9	Upper Manifold Half Supply Tube Near Junction with Tee Tube	---	Axial
10	"Y" Supply Tube - Forward End	---	Tangential
11	Bottom Manifold Half Stiffener, Aft End	264	Radial
12	Top Manifold Half Horizontal Cooling Tube, Aft End	270	Radial
13	Top Manifold Half, Rear Bracket	313	Radial
14	Top Manifold Half, Axial, Over Tube No. 5	0	Radial
15	Top Manifold Half, Rear Bracket	346	Radial
16	Top Manifold Half, Tube No. 1	343	Radial
17	Top Manifold Half, Tube No. 1	25	Radial
18	Top Manifold Half, Tube No. 1	82	Radial
19	Top Half of LPT Casing ≈ 1 in. Aft of Tube No. 5	0	Radial
20	Top Half of TMF, 2 in. Below Forward Flange	0	Radial
21	Lower Manifold Half Supply Tube	170	Radial

*Circumferential locations were not measured but were based on visual observations and given dimensions for various manifold features. The specified angles are measured from top center, moving in a clockwise direction, in an aft looking forward view.

Table II. Accelerometer and Strain Gage Locations (Concluded).

B. Strain Gages

Location No.	Description of Location	* Approximate Circumferential Location, degrees
1	Lower Manifold Half, Tube No. 2, Forward Surface	238
2	Lower Manifold Half, Tube No. 2, OD Surface	238
3	Lower Manifold, Tube No. 3, Forward Surface	238
4	Lower Manifold, Tube No. 3, OD Surface	238
5	"Y" Supply Tube Bracket Gusset	---
6	Upper Manifold Half Inlet	326
7	Lower Manifold Half, Horizontal Flange Bracket	264
8	Upper Manifold Half, Horizontal Flange Bracket	276
9	Upper Manifold Half, Horizontal Flange Bracket	276
10	Upper Manifold Half, Tube No. 5 OD Surface	309
11	Upper Manifold Half, Rear Bracket	309
12	Upper Manifold Half, Rear Bracket	311
13	Casing Forward Flange Bracket	308
14	Upper Manifold Half, Forward Flange Bracket	310
15	Upper Manifold Half, Axial, OD Surface, Forward of Weld Line	52
16	Upper Manifold Half, Axial, OD Surface, Aft of Weld Line	52
17	Upper Manifold Half, Rear Bracket	60
18	Upper Manifold Half, Axial, OD Surface, Forward of Weld Line	308
19	Upper Manifold Half, Tube No. 1 OD Surface	303
20	Rear Casing Bracket, Surface with Nozzle Lock Hole	313

*Circumferential locations were not measured but were based on visual observations and given dimensions for various manifold features. The specified angles are measured from top center, moving in a clockwise direction, in an aft looking forward view.

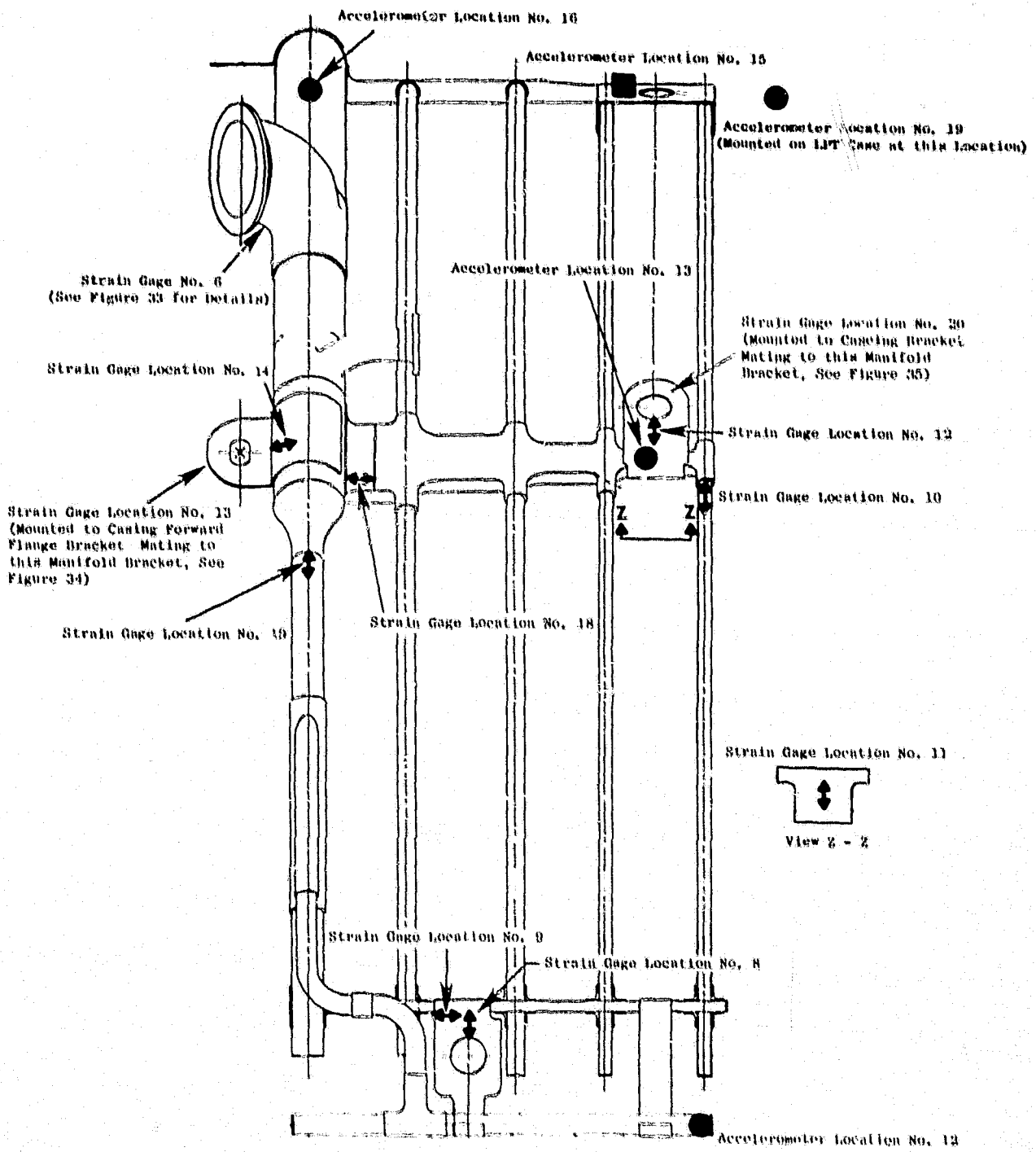

Figure 27. Accelerometer/Strain Gage Locations: ACC Manifold Top Half, Right-Hand Side.

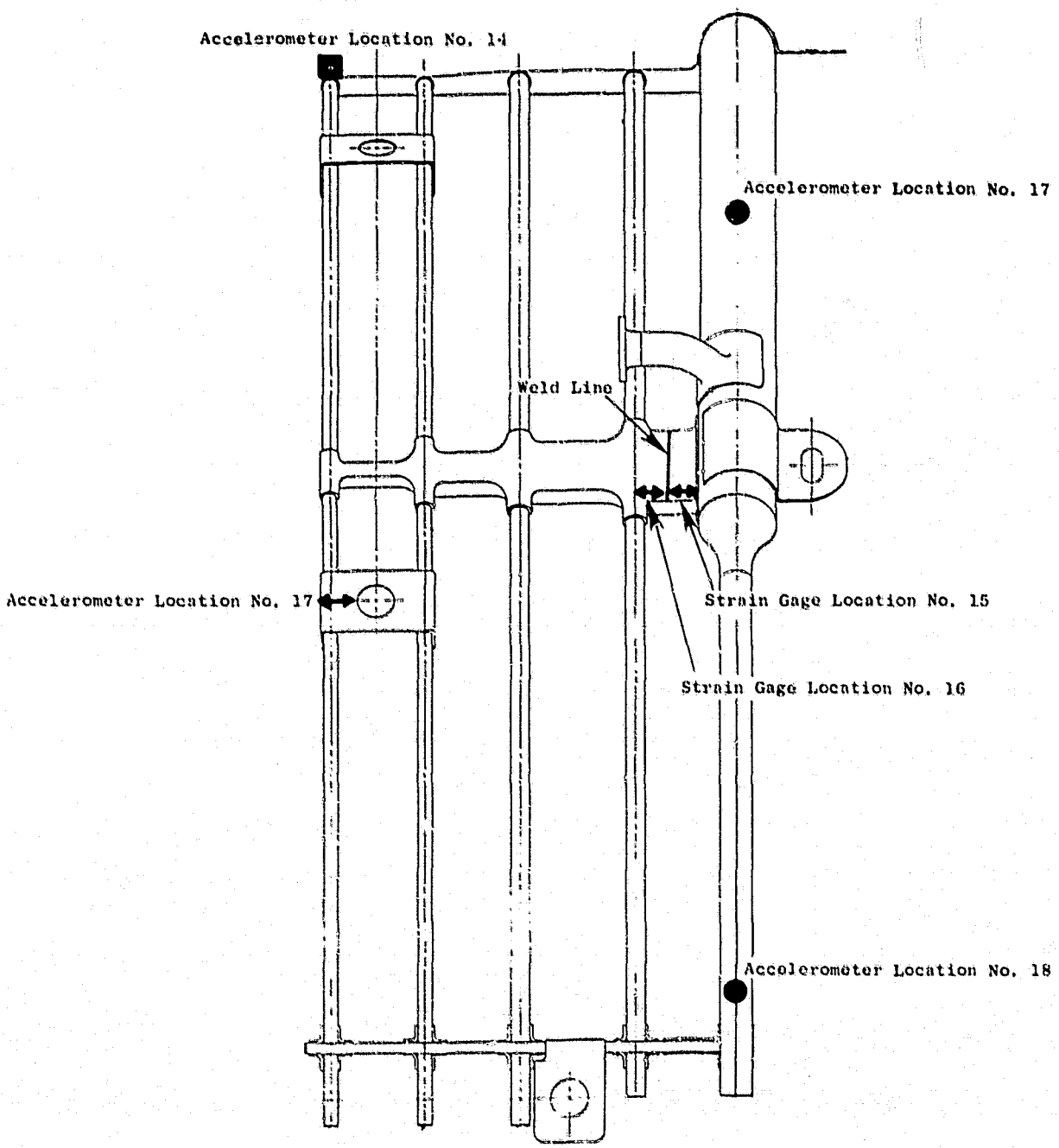

Figure 28. Accelerometer/Strain Gage Locations: ACC Manifold Top Half, Left-Hand Side.

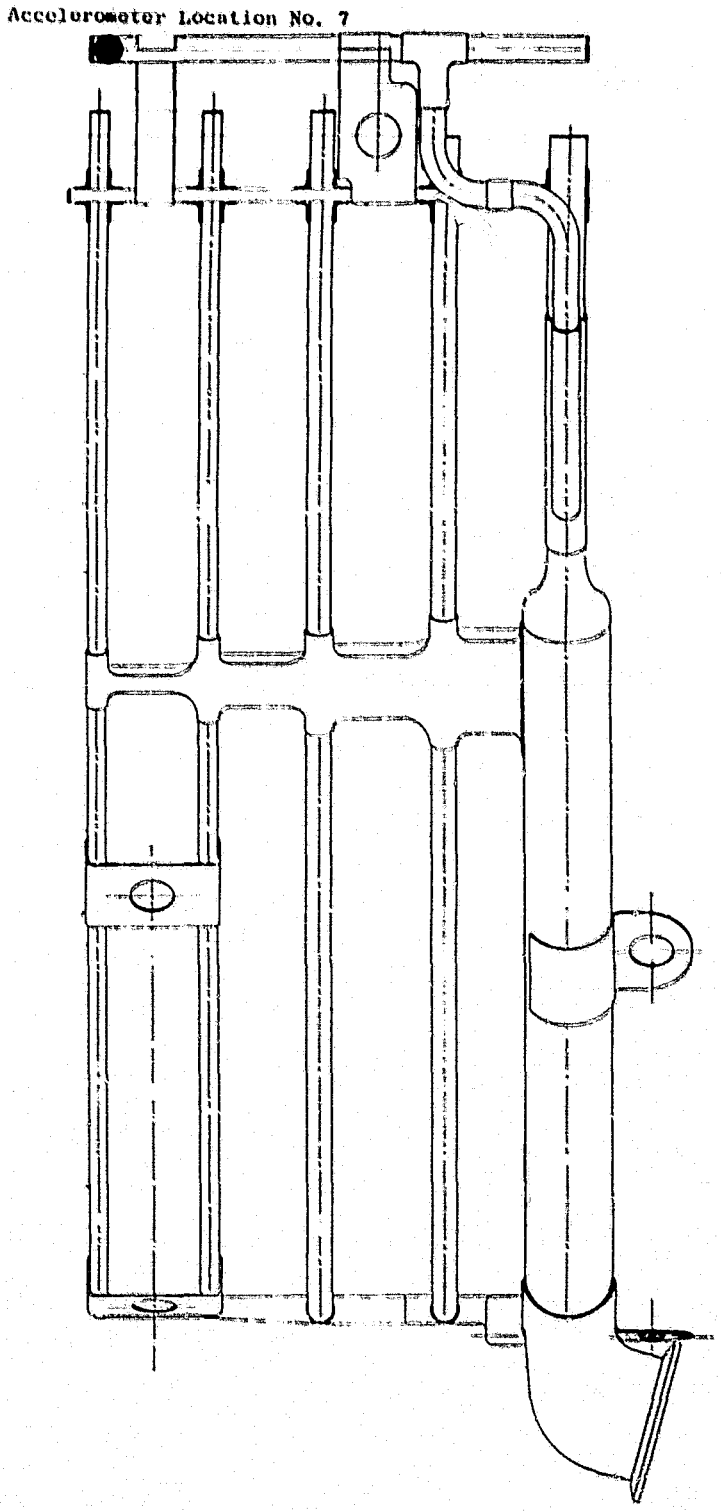

Figure 29. Accelerometer/Strain Gage Locations: ACC Manifold Bottom Half, Right-Hand Side.

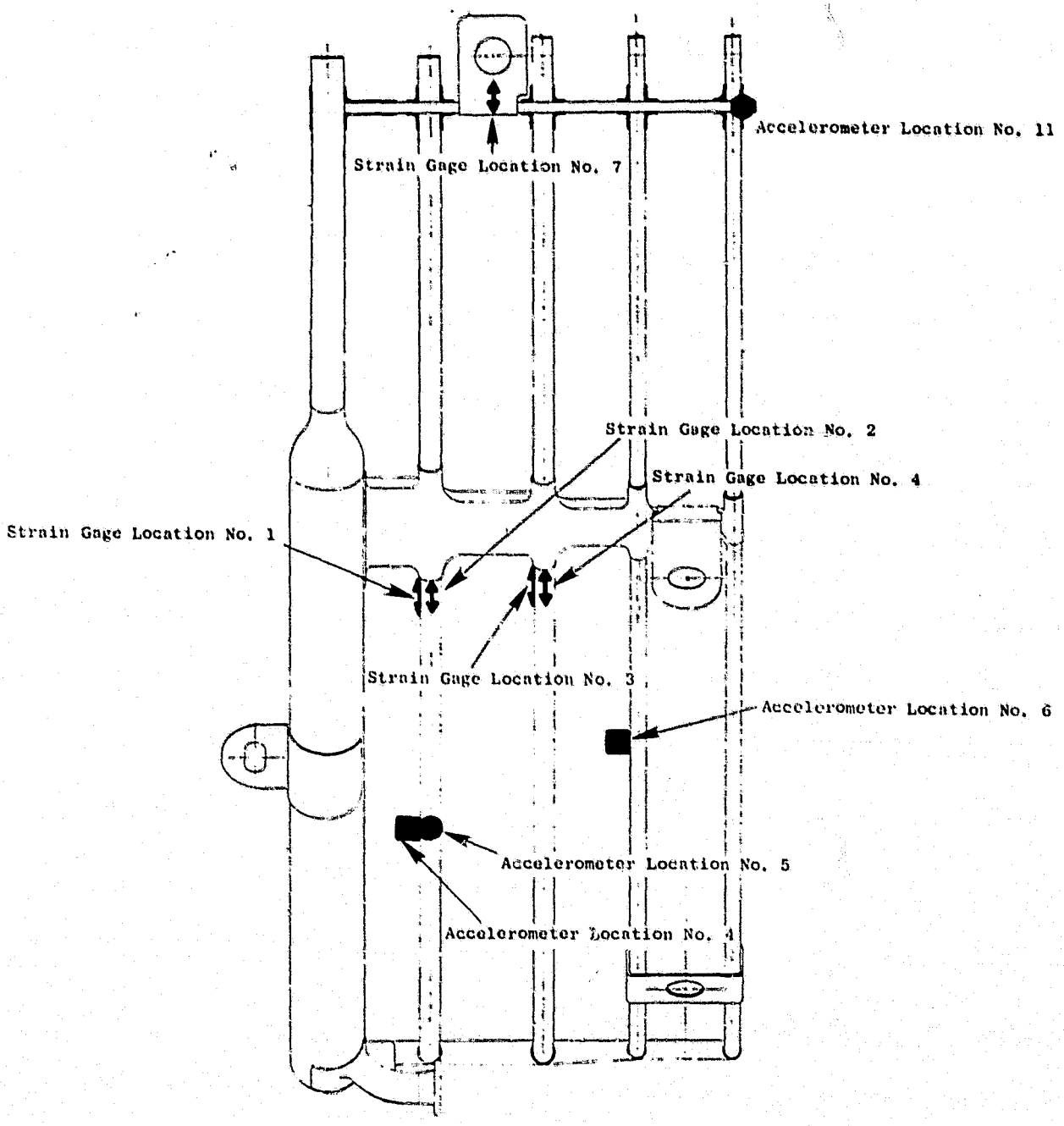

Figure 30. Accelerometer/Strain Gage Locations: ACC Manifold Bottom Half, Left-Hand Side.

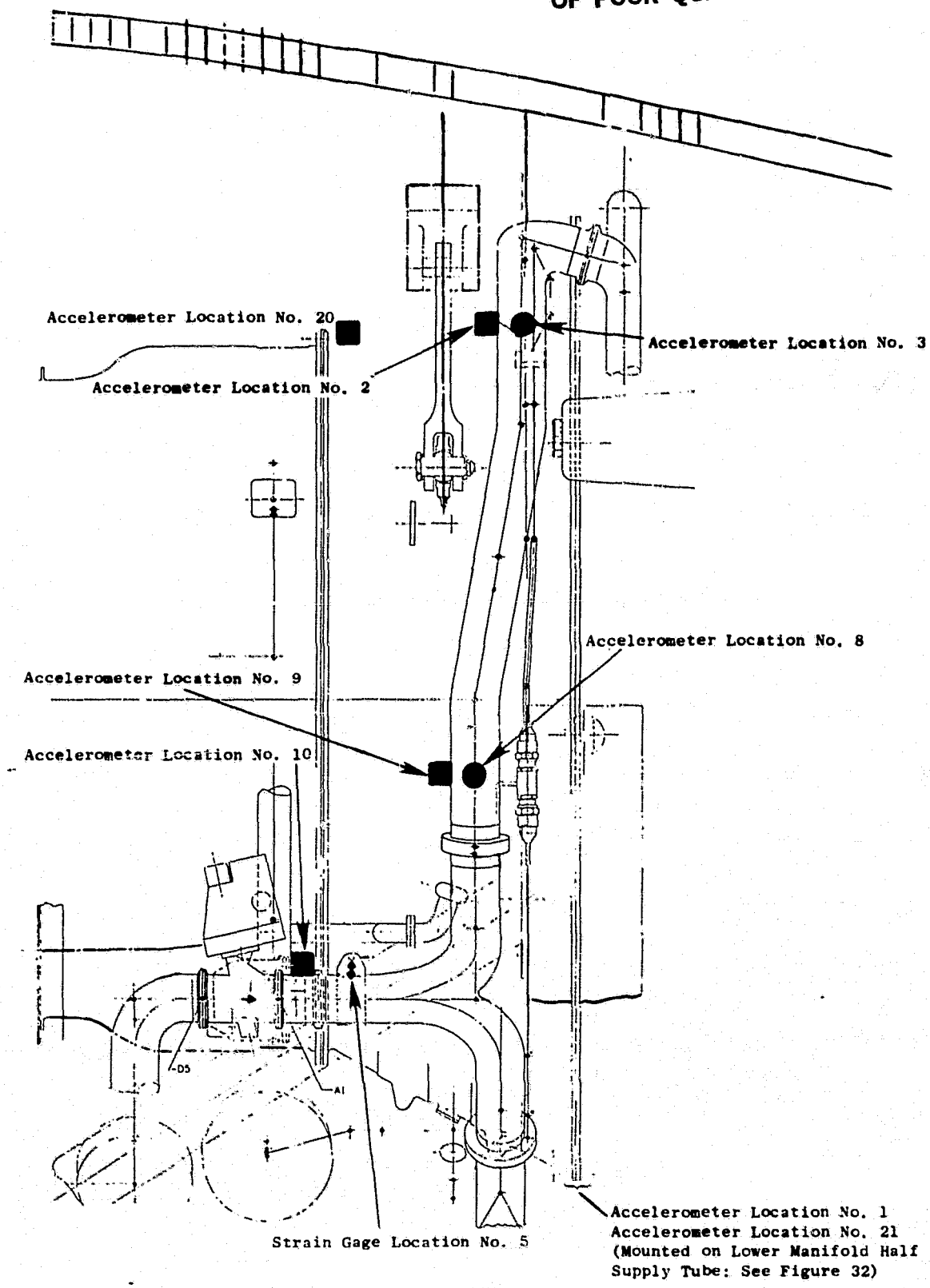

Figure 31. Accelerometer/Strain Gage Locations: ACC Manifold Supply Tubing.

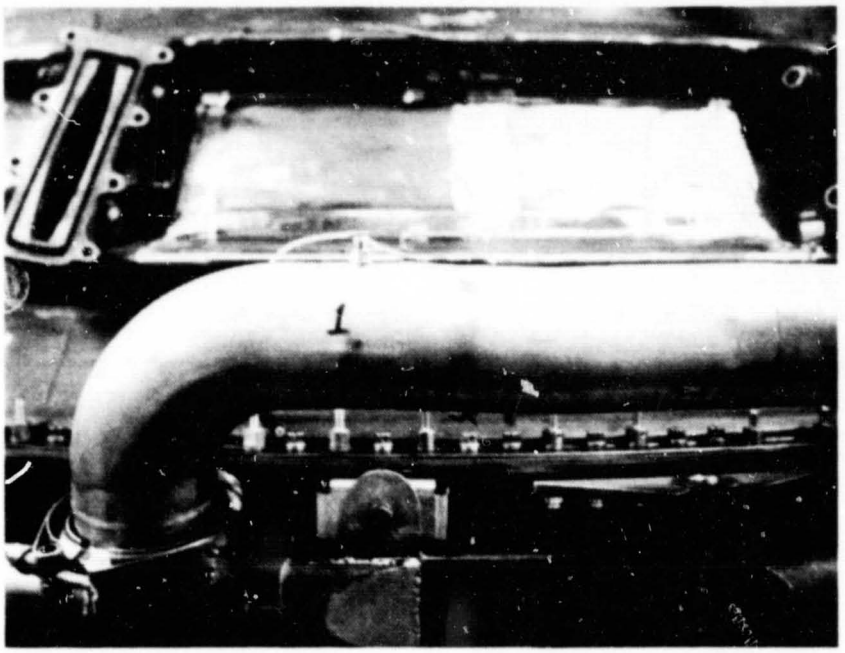

Located on Lower Half Supply Tube

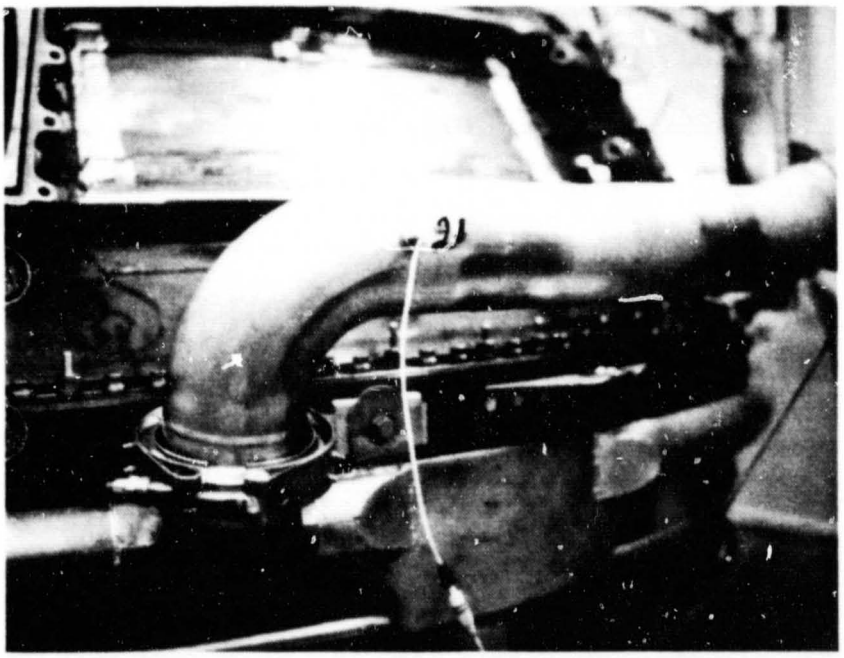

Figure 32. Locations of Accelerometer Nos. 1 and 2.

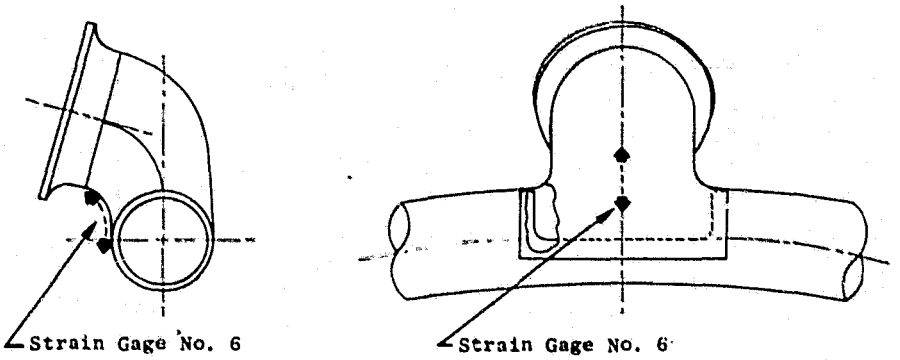

Figure 33. Location of Strain Gage No. 6 on Top Half Manifold Inlet.

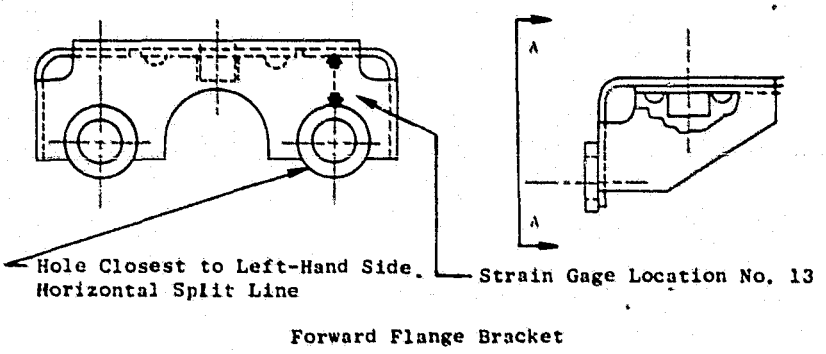

Figure 34. Location of Strain Gage No. 13 on Forward Flange Bracket.

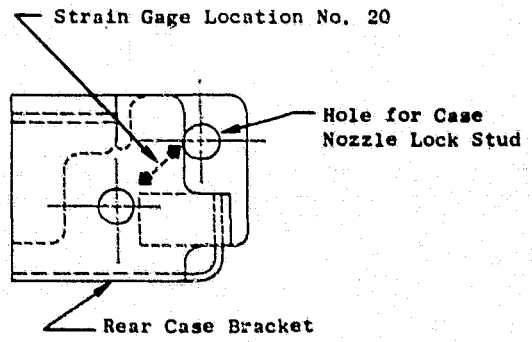

Figure 35. Location of Strain Gage No. 20 on Rear Case Bracket.

2. Output from the 20 accelerometers were recorded as the manifold was excited from 20 to 300 Hz in direction C-C (refer to Figure 26) in the horizontal plane from 20 to 300 Hz.

3. The slider plate and manifold assembly were rotated 90° to allow excitation in a radial direction parallel to the case vertical centerline (direction B-B, Figure 26). Again, preliminary scans were conducted with visual observation of movement via the strobe light. Based on these observations, it was decided to record the output from 13 of the 20 accelerometers plus that from one new location (Accelerometer 21). This output was recorded as the manifold was excited from 20 to 300 Hz.

4. Output plots from all accelerometers (in both directions of excitation) were then reviewed. Based on this review, 11 frequencies were selected as producing the most significant manifold system response. The manifold assembly was then excited in the vertical direction at each of these frequencies for approximately 3 to 5 minutes. During this time the manifold assembly movement was closely observed with the tuned strobe light. This technique was used to identify areas of most likely maximum stress for the purpose of strain gage application. Strain gages were mounted on the manifold assembly at the 20 locations illustrated previously.

5. Output from all strain gages was recorded as the manifold assembly was excited from 20 to 300 Hz.

6. The slider plate and manifold assembly were then rotated 90° to permit excitation in the horizontal direction. Again, the output of all strain gages was recorded as the manifold assembly was excited from 20 to 300 Hz.

   During all component tests the excitation input was limited to a constant 0.05 mm (0.002 inch) from 20 to 140 Hz and a constant 2 g's from 140 to 300 Hz. This was done to prevent damage to the manifold assembly.

7. Strain gages capable of withstanding an engine operating environment were applied to the manifold hardware at location numbers 1, 3, 11, 13, and 14. Additionally, accelerometers were installed on the forward and aft LPT case flanges as shown in Figure 36. The output from these gages and accelerometers was recorded during portions of the instrumented engine testing which included both a 10 second and 2 minute accel/decel from ground idle to takeoff. This was done so that the component test strain data could be extrapolated to actual engine operating conditions for the purpose of manifold structural integrity analysis. The specific gages selected were chosen because they were among the most active during the component tests.

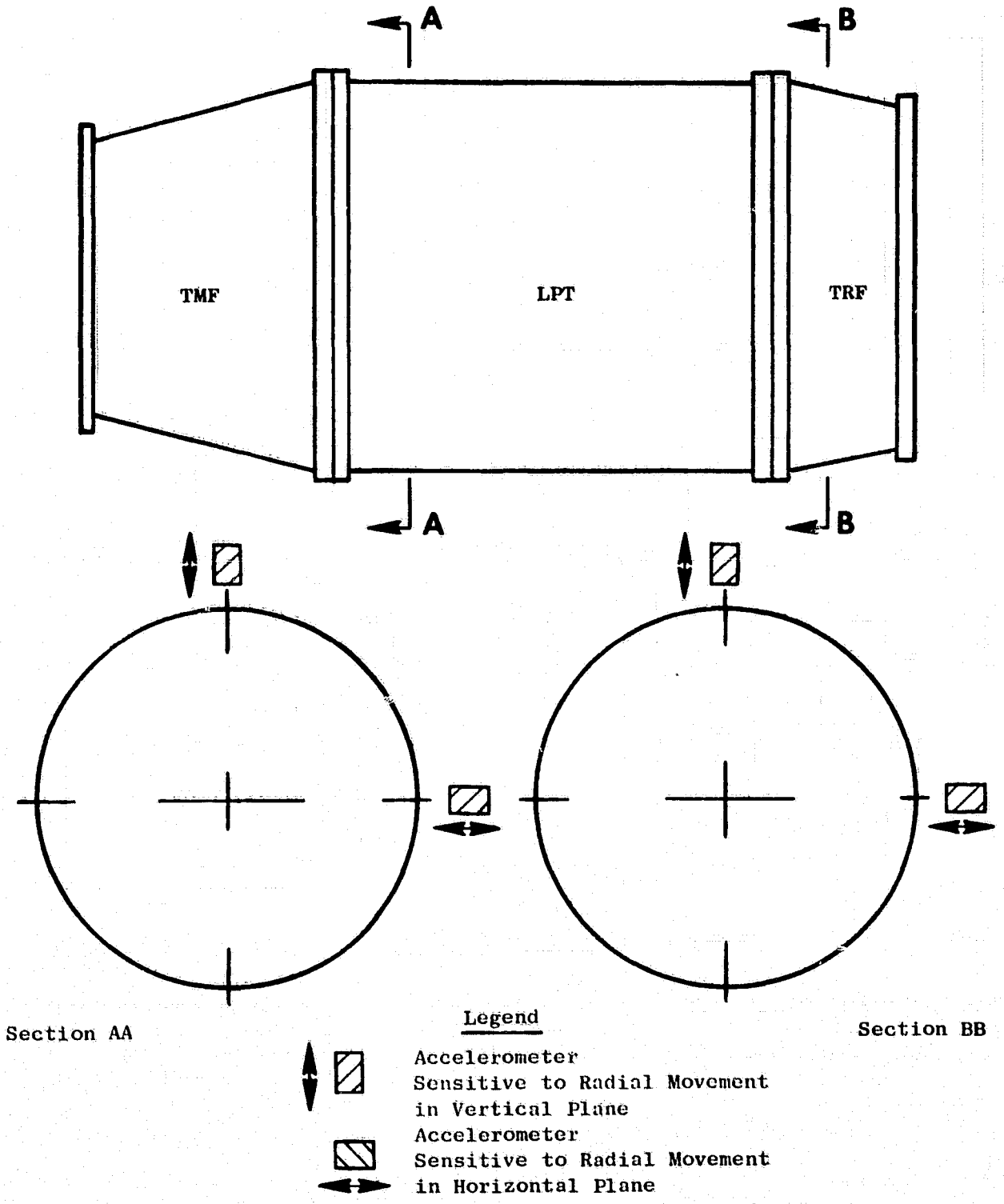

Figure 36. Accelerometer Locations: Instrumented Engine Test.

4.2.4 Test Results

4.2.4.1 Natural Frequencies and Mode Shapes

The natural frequencies of the system, within the excitation range, can be obtained from the instrumentation output plots. Many of the system mode shapes are complex and difficult to describe. Some of the modes producing significant system motion, based on visual observation, are delineated as follows:

1. Axial flexing of the second and third manifold tubes in the longest circumferential span in the bottom half - between axial distributors at 180° and 240° (aft looking forward).

2. Same as Mode 1 except in the longest circumferential spans in the top half.

3. Pivoting and twisting motion of the horizontal flange cooling tube assembly in the top half about the bolt through the top half horizontal flange bracket.

4. Same as Mode 3 on the bottom half horizontal cooling tube assembly. Motion not as pronounced.

5. Flexing of the manifold rear bracket located at 313° (aft looking forward) about the bracket bolt.

6. Flexing of the top half inlet about its horizontal centerline.

7. Radial motion of entire manifold half (both halves).

8. Flexing of casing forward flange brackets about their horizontal centerlines.

Some of these modes are depicted in Figure 37.

4.2.4.2 Accelerometer Data: Component Test

Examples of the accelerometer data obtained during the component test are shown in Figures 38 and 39. These data were instrumental in the process of selecting probable areas of maximum stress for strain gage application.

4.2.4.3 Strain Gage Data: Component Test

Due to the limited number of strain gages employed, it is not possible to definitely state that all areas of maximum strain (stress) have been identified.

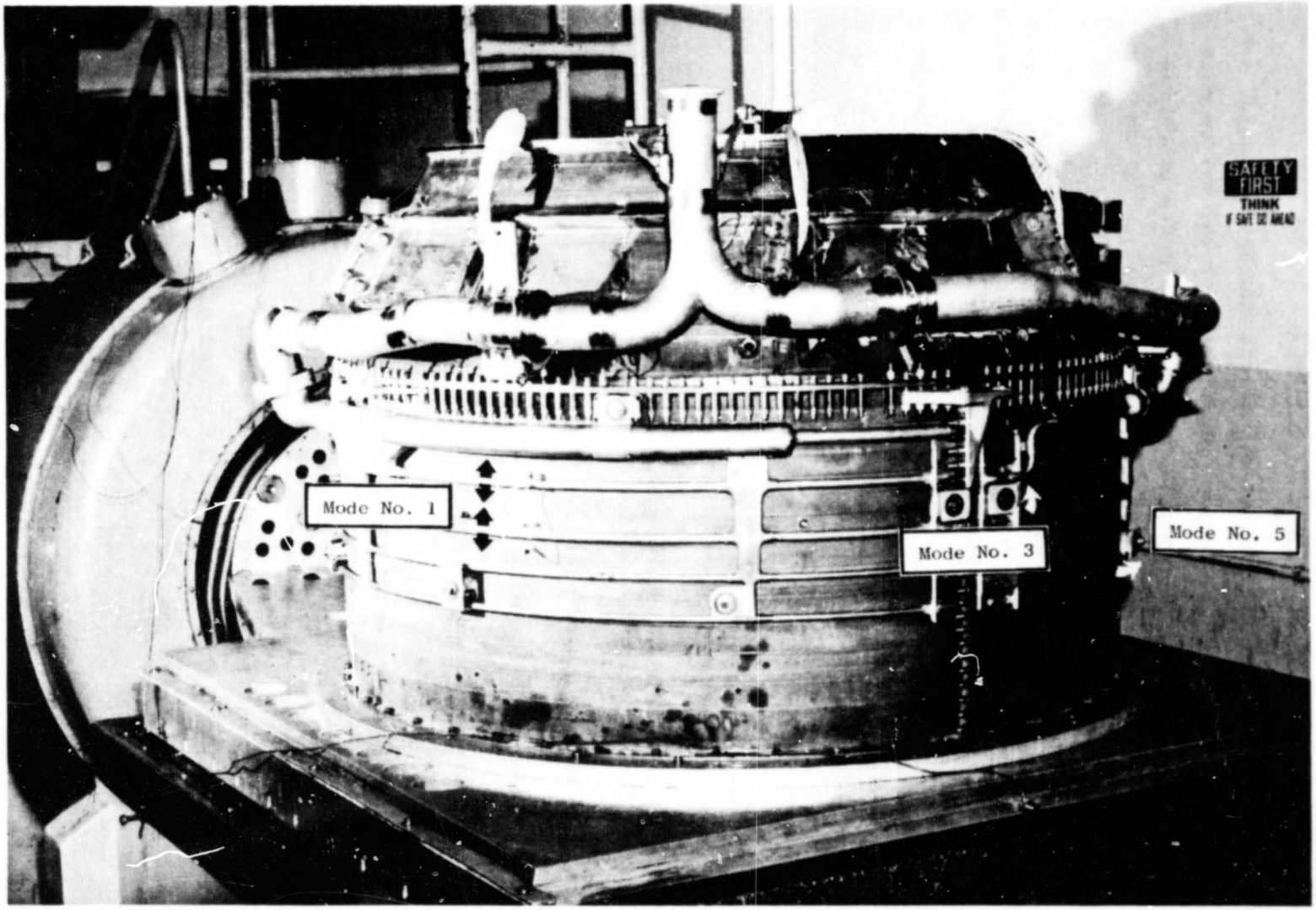

Figure 37. Selected Manifold System Vibration Modes.

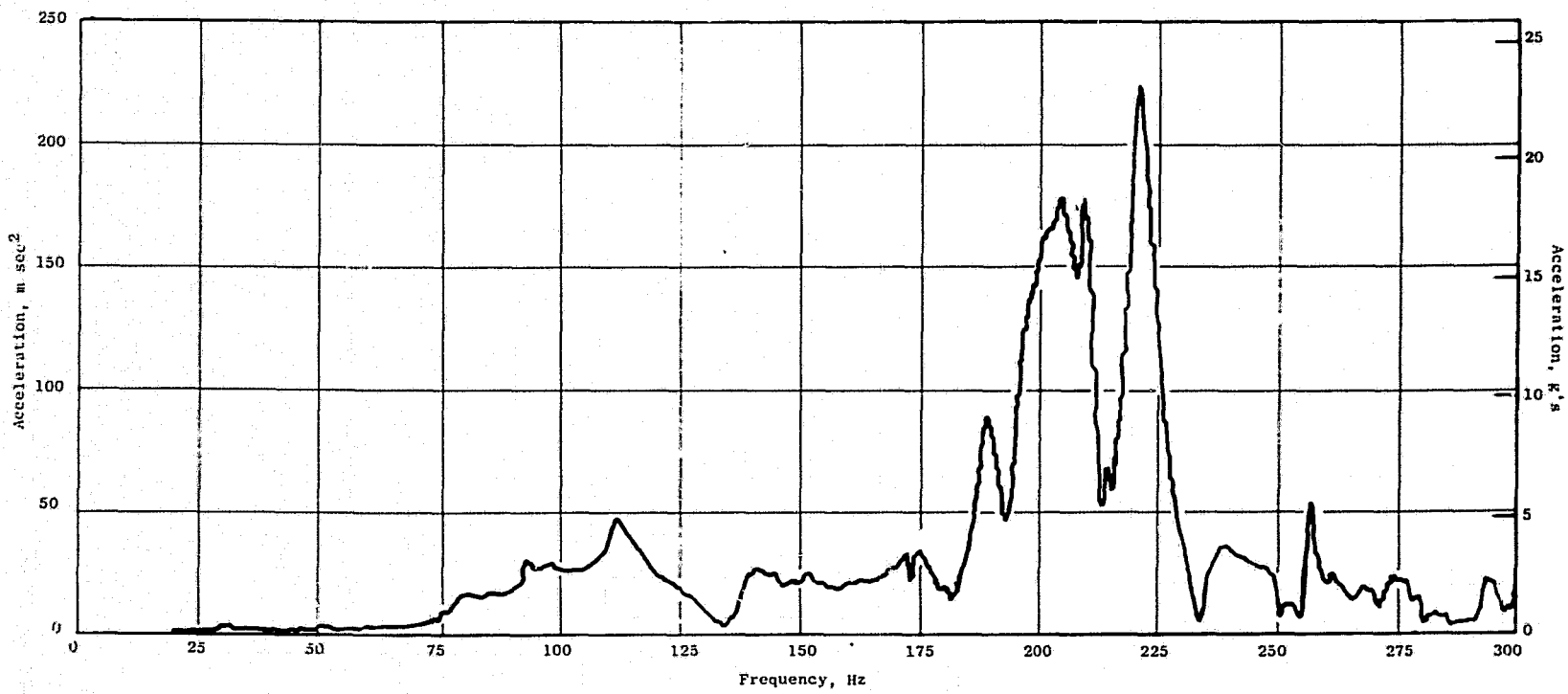

Figure 38. Acceleration Versus Frequency: Accelerometer No. 2, Horizontal Excitation.

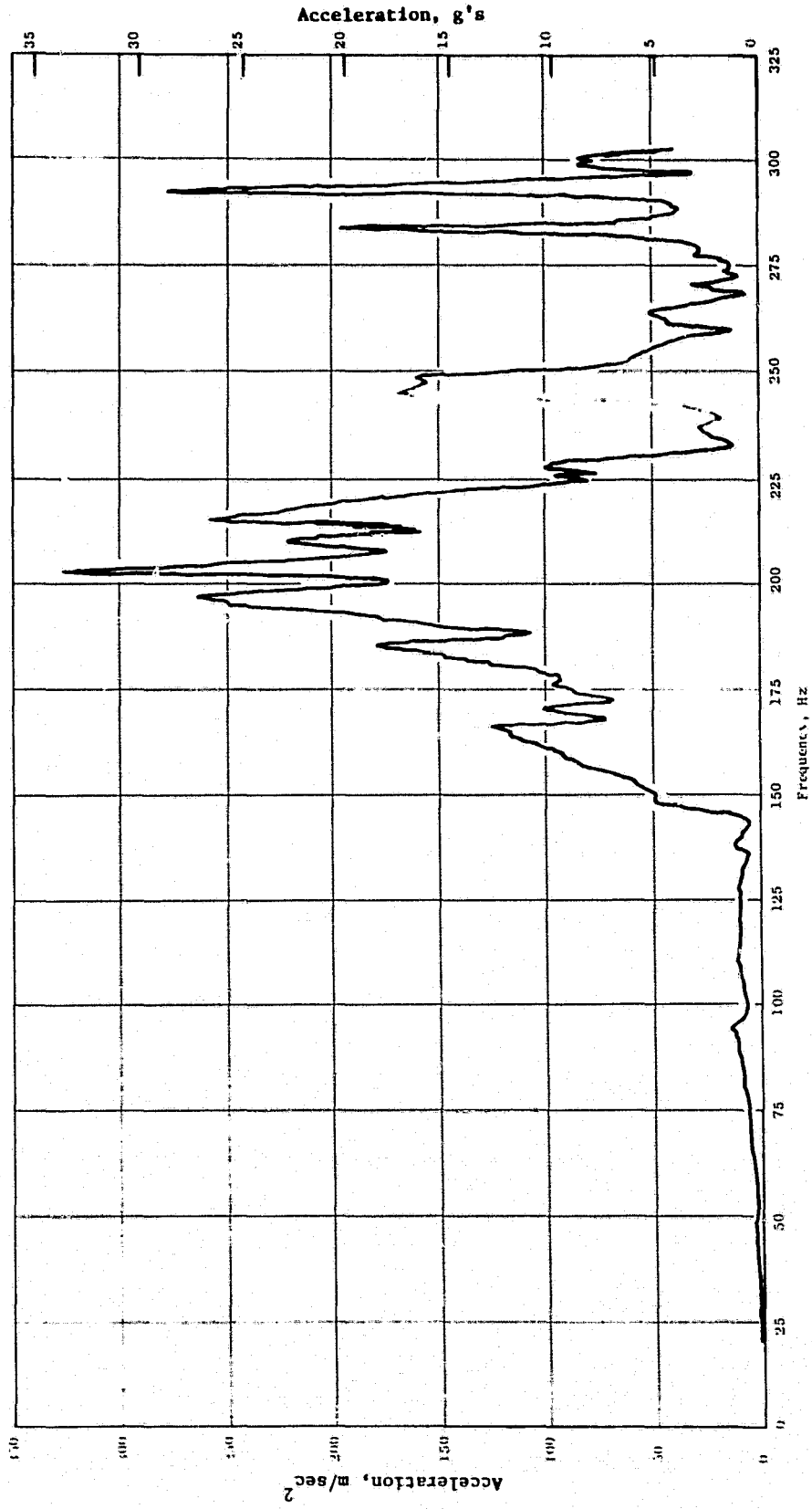

Figure 39. Acceleration Versus Frequency: Accelerometer No. 5, Vertical Excitation.

However, the technique employed (identifying these areas via strobe light/visual observations) was a sound one, and the output from the strain gages should be representative of maximum system stresses.

The measured strains (and subsequent stresses) are presented in Table III as a function of gage number, resonant frequency, and mode of excitation. The strains/stresses presented are in peak-to-peak values and therefore the alternating component is one half of that presented. Resonant frequencies which exhibited measured peak-to-peak strains of less than 100 μ mm/mm (μ in./in.) were disregarded based on the assumption that they were insignificant. This assumption was substantiated by the engine testing discussed in the following section.

The maximum measured strain of all gages was found on gage No. 13 and was equivalent to an alternating stress of approximately 16,548 N/cm^2 (24,000 $lb/in.^2$). However, this was at a frequency of 228 Hz which is above the expected engine excitation range. The maximum recorded strain within the expected range of excitation was also found on gage No. 13 at a frequency of 182 Hz and translated to an alternating stress of approximately 13,790 N/cm^2 (20,000 $lb/in.^2$).

As stated previously, the excitation input during the component test was held to a constant 0.05 mm (0.002 inch) from 20-140 Hz and a constant 2 g's from 140-300 Hz in order to prevent damage to the manifold assembly. Since the excitation levels incurred during actual engine operation would not necessarily match the component test excitation, the strains/stresses presented in Table III cannot be interpreted as the expected magnitude of strains/stresses during engine operation. In order to provide a correlation between engine operation and component test strains, which is required to assess the hardware integrity, gages were installed on the manifold hardware during the instrumented engine test at several locations identified as being among the most active during the component test. The output from these gages and the resulting conclusions relative to the hardware integrity are presented in the following section.

Table III. Manifold Vibration Component Test Strain/Stress Data.

Notes: 1) All strains and stresses given are in peak to peak values
2) Strains less than 100μ in./in. peak to peak were not recorded

Strain Gage	Excitation Mode	Frequency, Hz	Strain, μ in./in.	Stress, psi	Frequency, Hz	Strain, μ in./in.	Stress, psi	Frequency, Hz	Strain, μ in./in.	Stress, psi
1	Vertical	197	100	2,840	208	420	11,928	221	882	25,049
1	Vertical	241	372	10,565	244	250	7,100	275	170	4,828
1	Vertical	293	110	3,124						
1	Horizontal	203	170	4,828	208	200	5,680	221	790	22,436
1	Horizontal	240	540	15,336	248	130	3,692	276	110	3,124
2	Vertical	Nothing above 100μ in./in.								
2	Horizontal	221	105	2,982						
3	Vertical	166	1000	28,400	185	100	2,840	202	200	5,680
3	Vertical	208	275	7,810	221	340	9,656	166	480	13,632
4	Gage Malfunctioned - No Data									
5	Vertical	224	120	3,408						
5	Horizontal	197	170	4,828	218	170	4,828			
6	Vertical	Nothing above 100μ in./in.								
6	Horizontal	197	145	4,118	208	140	3,976			
7	Vertical	186	120	3,408	195	130	3,692	203	250	7,100
7	Vertical	213	100	2,840	221	150	4,260	226	160	4,544
7	Vertical	244	150	4,260	276	120	3,408			
7	Horizontal	185	160	4,544	202	180	5,112	208	145	4,118
7	Horizontal	220	150	4,260	227	100	2,840	275	100	2,840
8	Vertical	118	110	3,124	166	250	7,100	171	215	6,105
8	Vertical	188	350	9,940	203	165	4,686	219	290	8,236
8	Vertical	227	580	16,472	250	160	4,544	258	110	3,124
8	Vertical	275	105	2,982						
8	Horizontal	174	190	5,396	186	333	9,514	198	155	4,402
8	Horizontal	209	370	10,508	223	115	3,266			
9	Vertical	190	120	3,408	228	205	5,822			
9	Horizontal	188	130	3,692	209	120	3,408			
10	Vertical	209	120	3,408	218	195	5,538	258	115	3,266
10	Vertical	291	140	3,976						
10	Horizontal	211	160	4,544	218	205	5,822	291	105	2,982

Table III. Manifold Vibration Component Test Strain/Stress Data (Continued).

Notes: 1) All strains and stresses given are in peak to peak values
2) Strains less than 100μ in./in. peak to peak were not recorded

Strain Gage	Excitation Mode	Frequency, Hz	Strain, μ in./in.	Stress, psi	Frequency, Hz	Strain, μ in./in.	Stress, psi	Frequency, Hz	Strain, μ in./in.	Stress, psi
11	Vertical	150	100	2,840	185	700	19,880	203	410	11,644
11	Vertical	211	240	6,816	221	415	11,786	227	430	12,212
11	Vertical	244	130	3,692	263	140	3,976			
11	Horizontal	183	1000	28,400	192	640	18,176	202	590	16,756
11	Horizontal	205	550	15,620	210	730	20,732	216	430	12,212
11	Horizontal	252	120	3,408	262	130	3,692	266	160	4,544
12	Vertical	185	120	3,408	209	110	3,124	218	110	3,124
12	Vertical	225	130	3,692	227	140	3,976			
12	Horizontal	187	290	8,236	192	260	7,384	202	120	3,408
12	Horizontal	219	110	3,124						
13	Vertical	78	120	3,408	111	530	15,052	138	130	3,692
13	Vertical	149	230	6,532	171	270	7,668	184	700	19,880
13	Vertical	190	195	5,538	198	320	9,088	205	420	11,928
13	Vertical	209	395	11,218	215	230	6,532	221	510	14,484
13	Vertical	228	1700	48,280	264	160	4,544	269	160	4,544
13	Vertical	293	560	15,904						
13	Horizontal	75	120	3,408	109	520	14,768	138	150	4,260
13	Horizontal	148	210	5,964	182	1400	39,760	192	1110	31,524
13	Horizontal	209	900	25,560	230	800	22,720	248	310	8,804
13	Horizontal	255	270	7,668	268	200	5,680	290	410	11,644
14	Vertical	183	100	2,840	191	100	2,840	215	100	2,840
14	Vertical	227	360	10,224	294	260	7,384	249	200	5,680
14	Vertical	255	110	3,124	291	160	4,544			
14	Horizontal	147	130	3,692	181	660	18,744	185	550	15,620
14	Horizontal	199	560	15,904	208	550	15,620	223	305	8,662
14	Horizontal	248	170	4,878	291	140	3,976			
15	Vertical	218	160	4,544	221-226	180	5,112	250	120	3,408
15	Horizontal	192	175	4,970	206	160	4,544	219	150	4,260
16	Vertical	Nothing above 100μ in./in.								
16	Horizontal	192	120	3,408						

Table III. Manifold Vibration Component Test Strain/Stress Data (Concluded).

Notes: 1) All strains and stresses given are in peak to peak values
2) Strains less than 100μ in./in. peak to peak were not recorded

Strain Gage	Excitation Mode	Frequency, Hz	Strain, μ in./in.	Stress, psi	Frequency, Hz	Strain, μ in./in.	Stress, psi	Frequency, Hz	Strain, μ in./in.	Stress, psi
17	Vertical	Nothing above 100μ in./in.								
17	Horizontal	Nothing above 100μ in./in.								
18	Vertical	186	120	3,408	221	220	6,248	225	240	6,816
18	Horizontal	184	160	4,544	202	110	3,124	211	145	4,118
18	Horizontal	220	370	10,508						
19	Vertical	208	100	2,840	217	110	3,124	223	105	2,982
19	Vertical	226	105	2,982	263	100	2,840			
19	Horizontal	185	140	3,976	209	100	2,840	214	100	2,840
19	Horizontal	218	135	3,834	225	125	3,550			
20	Vertical	117	125	3,550	164	185	5,254	185	250	7,100
20	Vertical	203	150	4,260	208	150	4,260	218-233	230	6,532
20	Vertical	226	190	5,396	290	130	3,692			
20	Horizontal	173	110	3,124	185	340	9,656	197	190	5,396
20	Horizontal	208	250	7,100	221	285	8,094			

4.2.4.4 Strain Gage Data: Instrumented Engine Test

Dynamic strain gages capable of withstanding an engine operating environment were applied to the manifold hardware at locations 1, 3, 11, 13, and 14 (see Figures 27 through 35). These locations were selected based on activity exhibited during the component test. As shown in Table IV, 36 system resonant frequencies were identified during the component test as producing peak-to-peak strains greater than 100 μ mm/mm (μ in./in.) and the maximum component test strain found in 29 of those frequencies was produced by one of the five gages selected. The method of obtaining engine test to component test correlation was as follows:

1. Maximum component test strain from one of the five selected gages was recorded for each frequency.

2. Absolute maximum component test strain (selected by examining the output from each of the 21 gages) was recorded for each frequency.

3. Ratio of absolute maximum strain to maximum strain for selected gages was computed (in almost all cases, it was equal to 1.0).

4. The measured engine test strains/stresses were recorded and the maximum expected stress at any of the 21 component test locations was computed using the ratio defined previously. To simplify data reduction and to be conservative, the maximum engine test stress (for each of the five gages) was chosen regardless of frequency instead of identifying stresses at each resonant frequency. This data is shown in Table IV.

5. Due to the use of some special development engine hardware, the mount brackets for the two manifold inlet tubes had to be moved relative to their position during the component test. It is judged that the changes incurred did not have a significant impact on the test results.

The output from the engine gages was recorded during various portions of the test, which included both 10 second and 2 minute accel/decels from ground idle to takeoff. The data from the accel/decels was played back through peak-to-peak detectors (yielding overall stress levels) as well as one and two per rev tracking filters for both fan and core speeds. Figure 40 illustrates a portion of this information from gage No. 3. Additionally, after digitizing the data, a Fast Fourier Processor was used to prepare Campbell Diagrams for each gage output during the 2 minute accel/decel. This data is presented in Figures 41 through 48. (Strain gage No. 1 was inoperable during this test.)

Table IV. Correlation Engine Test Strains/Stresses.

	Component Test Resonant Frequency, Hz	75	78	109 111	117 118	138	147 150	164 166	171	173 174	181	182 183	184 186	188	190 192	195
Component Test	Gage No. 1 Strain ~ Vertical Excitation															
	Gage No. 1 Strain ~ Horizontal Excitation															
	Gage No. 3 Strain ~ Vertical Excitation							1000					100			
	Gage No. 3 Strain ~ Horizontal Excitation							480								
	Gage No. 11 Strain ~ Vertical Excitation						100						700			
	Gage No. 11 Strain ~ Horizontal Excitation											1000			640	
	Gage No. 13 Strain ~ Vertical Excitation		120	530		130	230		270				700		195	
	Gage No. 13 Strain ~ Horizontal Excitation	120		520		150	210					1400			1110	
	Gage No. 14 Strain ~ Vertical Excitation											100			100	
	Gage No. 14 Strain ~ Horizontal Excitation						130				660		550			
	Gage with Maximum Strain (1, 3, 11, 13 & 14)	13	13	13		13	13	3	13		14	13	13		13	
	Maximum Strain - Gages 1, 3, 11, 13 & 14	120	120	530		150	230	1000	270		660	1400	700		1110	
	Maximum Strain - Gages 1-21	120	120	530	125	150	230	1000	270	190	660	1400	700	350	1110	130
	Gage with Maximum Strain (1-21)	13	13	13	20	13	13	3	13	8	14	13	11	8	13	7
	Ratio - Maximum Strain (1-21) to Maximum Strain (1, 3, 11, 13, 14)	1.0	1.0	1.0	---	1.0	1.0	1.0	1.0	---	1.0	1.0	1.0	---	1.0	---
Engine Test	Maximum Engine Test Stress (Any Frequency) - Gages 1, 3, 11, 13 & 14	3600	3600	3600	---	3600	3600	16000	3600	---	3000	3600	3600	---	3600	---
	Maximum Expected Stress - Any Gage (See Note 4)	3600	3600	3600	---	3600	3600	16000	3600	---	3000	3600	3600	---	3600	---

Notes:
1. Gage No. 1 inoperable during test
2. All strains given are in μ in./in. peak to peak
3. All stresses given are in psi peak to peak
4. Designated frequencies for maximum expected stresses correspond to room temperature. Actual frequency of occurrence during engine operation would be shifted downward by approximately 10 percent due to elevated temperatures during engine operation.

Table IV. Correlation Engine Test Strains/Stresses (Continued).

	Component Test Resonant Frequency, Hz	197 199	202 203	205	208 211	213 216	217 219	220 221	223 224	225 228	230	240 241	243 244	248 249	250 252
Component Test	Gage No. 1 Strain ~ Vertical Excitation	100	170		420			882				372	250		
	Gage No. 1 Strain ~ Horizontal Excitation				200			790				540		130	
	Gage No. 3 Strain ~ Vertical Excitation		200		275			340							
	Gage No. 3 Strain ~ Horizontal Excitation														
	Gage No. 11 Strain ~ Vertical Excitation		410		240			415		430			130		120
	Gage No. 11 Strain ~ Horizontal Excitation		590	550	730	430									
	Gage No. 13 Strain ~ Vertical Excitation	320		420	395	230		510		1700					
	Gage No. 13 Strain ~ Horizontal Excitation				900						800			310	
	Gage No. 14 Strain ~ Vertical Excitation					100				360			260	200	
	Gage No. 14 Strain ~ Horizontal Excitation	560			550				305					170	
	Gage with Maximum Strain (1, 3, 11, 13 & 14)	14	11	11	13	11		1	14	13	13	1	14	13	11
	Maximum Strain - Gages 1, 3, 11, 13 & 14	560	590	550	900	430		882	305	1700	800	540	260	310	120
	Maximum Strain - Gages 1-21	560	590	550	900	430	290	882	305	1700	800	540	260	310	160
	Gage with Maximum Strain (1-21)	14	11	11	13	11	8	1	14	13	13	1	14	13	8
	Ratio - Maximum Strain (1-21) to Maximum Strain (1, 3, 11, 13, 14)	1.0	1.0	1.0	1.0	1.0	---	1.0	1.0	1.0	1.0	1.0	1.0	1.0	1.33
Engine Test	Maximum Engine Test Stress (Any Frequency) - Gages 1, 3, 11, 13 & 14	3000	1800	1800	3600	1800	---	---	3000	3600	3600	---	3000	3600	1800
	Maximum Expected Stress - Any Gage (See Note 4)	3000	1800	1800	3600	1800	---	---	3000	3600	3600	---	3000	3600	2400

Table IV. Correlation Engine Test Strains/Stresses (Concluded).

	Component Test Resonant Frequency, Hz	255	258	262 264	266	268 269	275 277	290 293
Component Test	Gage No. 1 Strain ~ Vertical Excitation						170	110
	Gage No. 1 Strain ~ Horizontal Excitation						110	
	Gage No. 3 Strain ~ Vertical Excitation							
	Gage No. 3 Strain ~ Horizontal Excitation							
	Gage No. 11 Strain ~ Vertical Excitation			140				
	Gage No. 11 Strain ~ Horizontal Excitation			130	160			
	Gage No. 13 Strain ~ Vertical Excitation			160		160		560
	Gage No. 13 Strain ~ Horizontal Excitation	270				200		410
	Gage No. 14 Strain ~ Vertical Excitation	110						160
	Gage No. 14 Strain ~ Horizontal Excitation							140
	Gage with Maximum Strain (1, 3, 11, 13 & 14)	13		13	11	13	1	13
	Maximum Strain - Gages 1, 3, 11, 13 & 14	270		160	160	200	170	560
	Maximum Strain - Gages 1-21	270	115	160	160	200	170	560
	Gage with Maximum Strain (1-21)	13	10	13	11	13	1	13
	Ratio - Maximum Strain (1-21) to Maximum Strain (1, 3, 11, 13, 14)	1.0	---	1.0	1.0	1.0	1.0	1.0
Engine Test	Maximum Engine Test Stress (Any Frequency) - Gages 1, 3, 11, 13 & 14	3600	---	3600	1800	3600	---	3600
	Maximum Expected Stress - Any Gage	3600	---	3600	1800	3600	---	3600

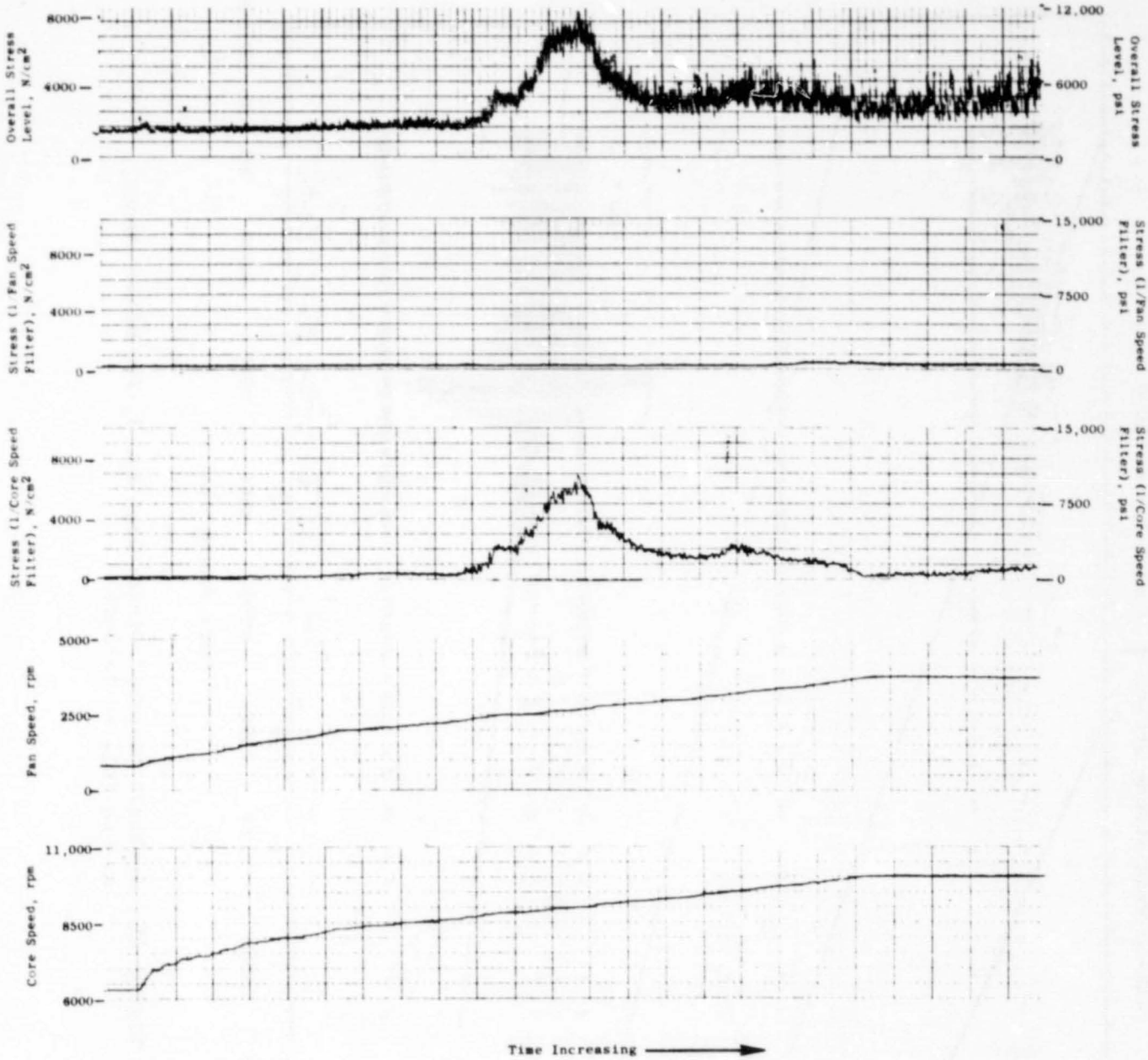

Figure 40. Strain Gage No. 3 Data: Instrumented Engine Test, Two Minute Accel, Ground Idle to Takeoff.

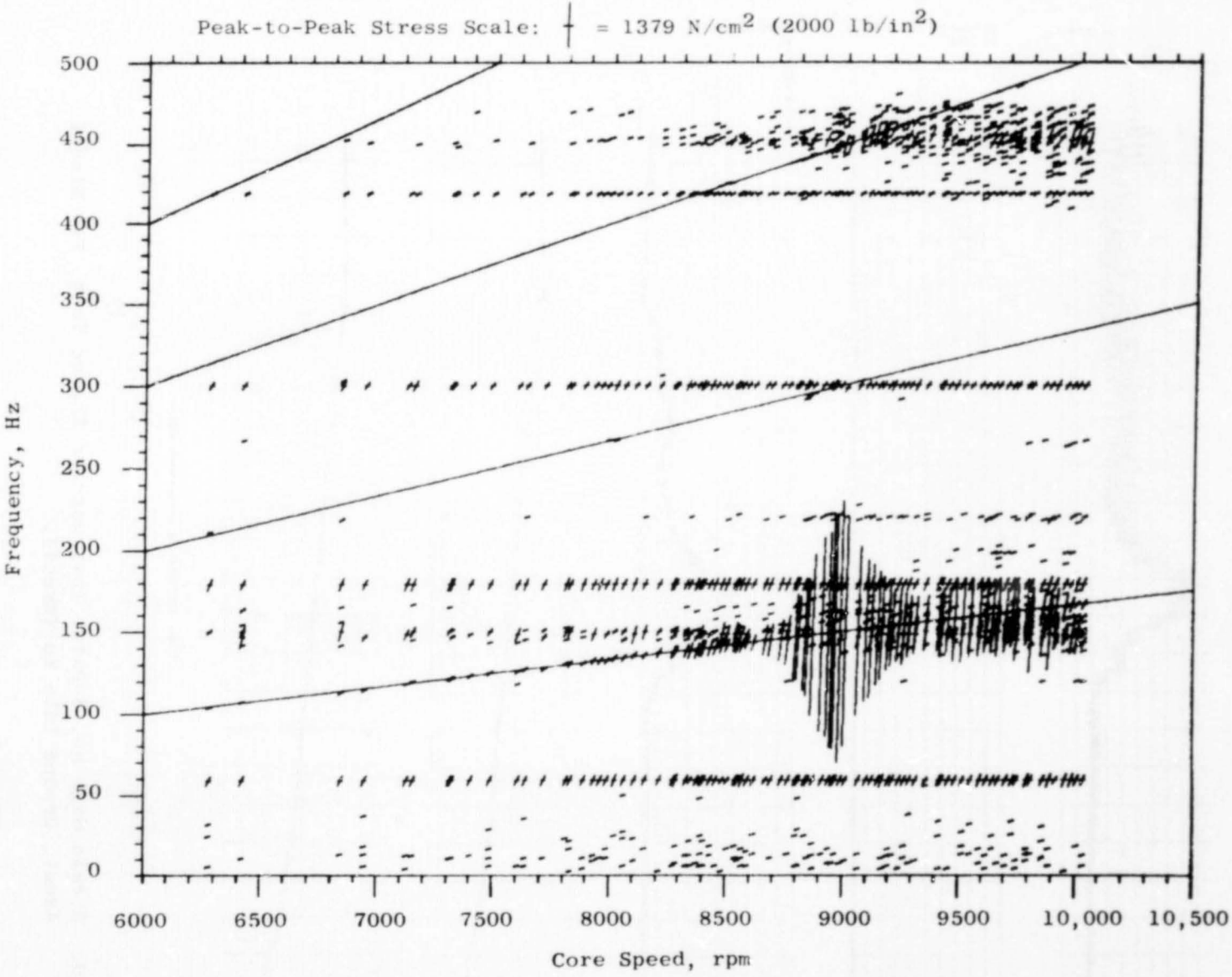

Figure 41. Campbell Diagram: Strain Gage No. 3, Two Minute Accel, Ground Idle to Takeoff.

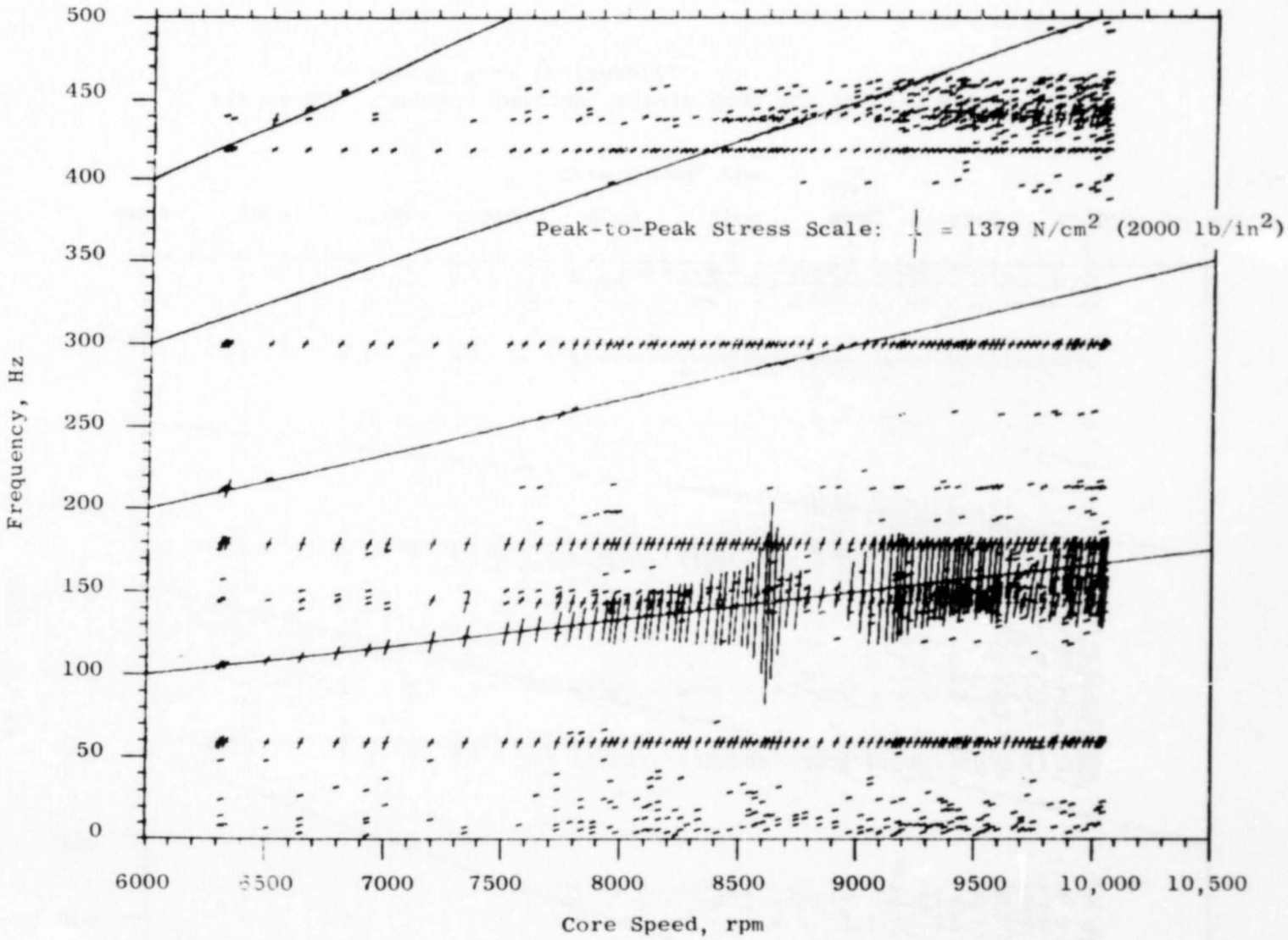

Figure 42. Campbell Diagram: Strain Gage No. 3, Two Minute Decel, Takeoff to Ground Idle.

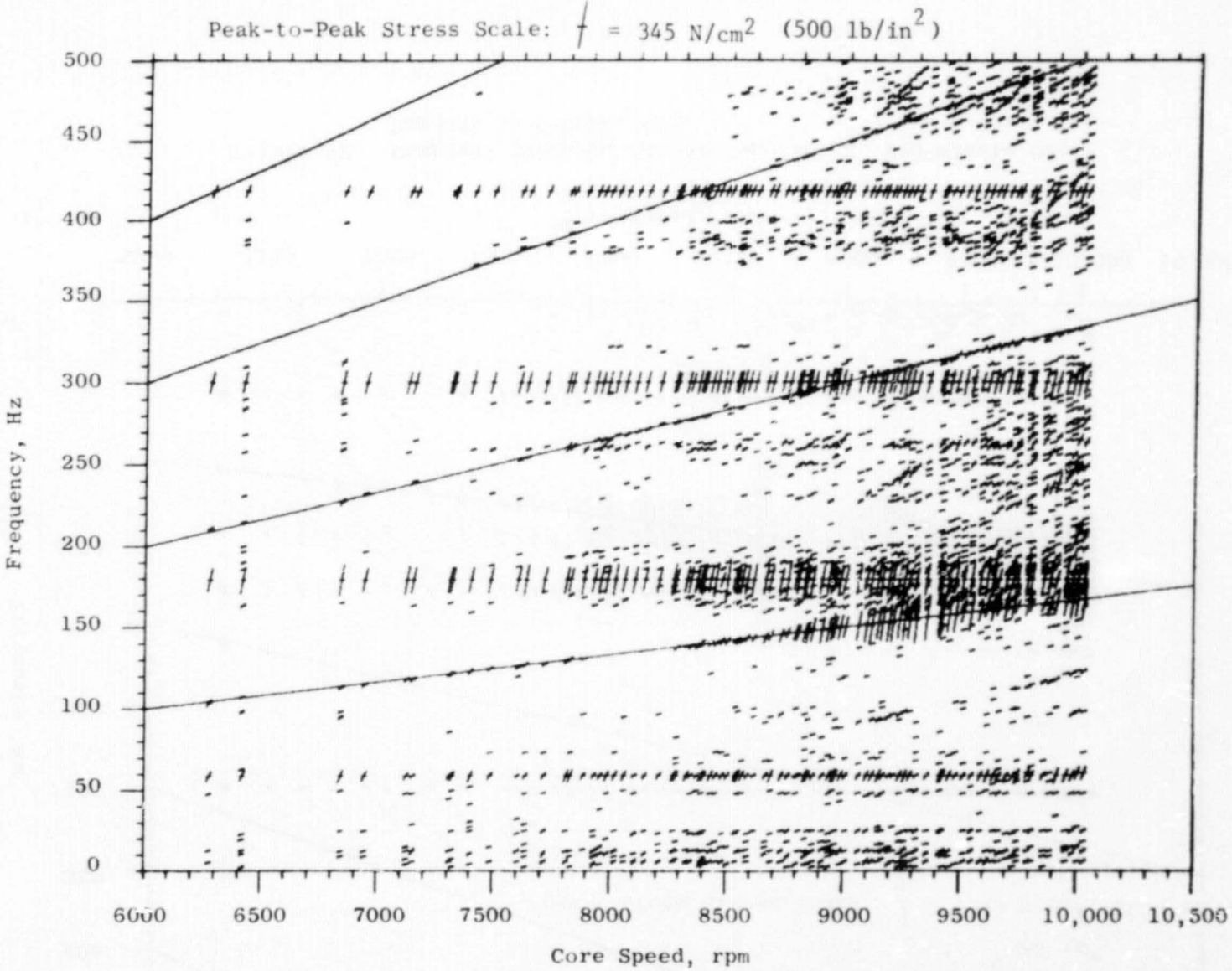

Figure 43. Campbell Diagram: Strain Gage No. 11, Two Minute Accel, Ground Idle to Takeoff.

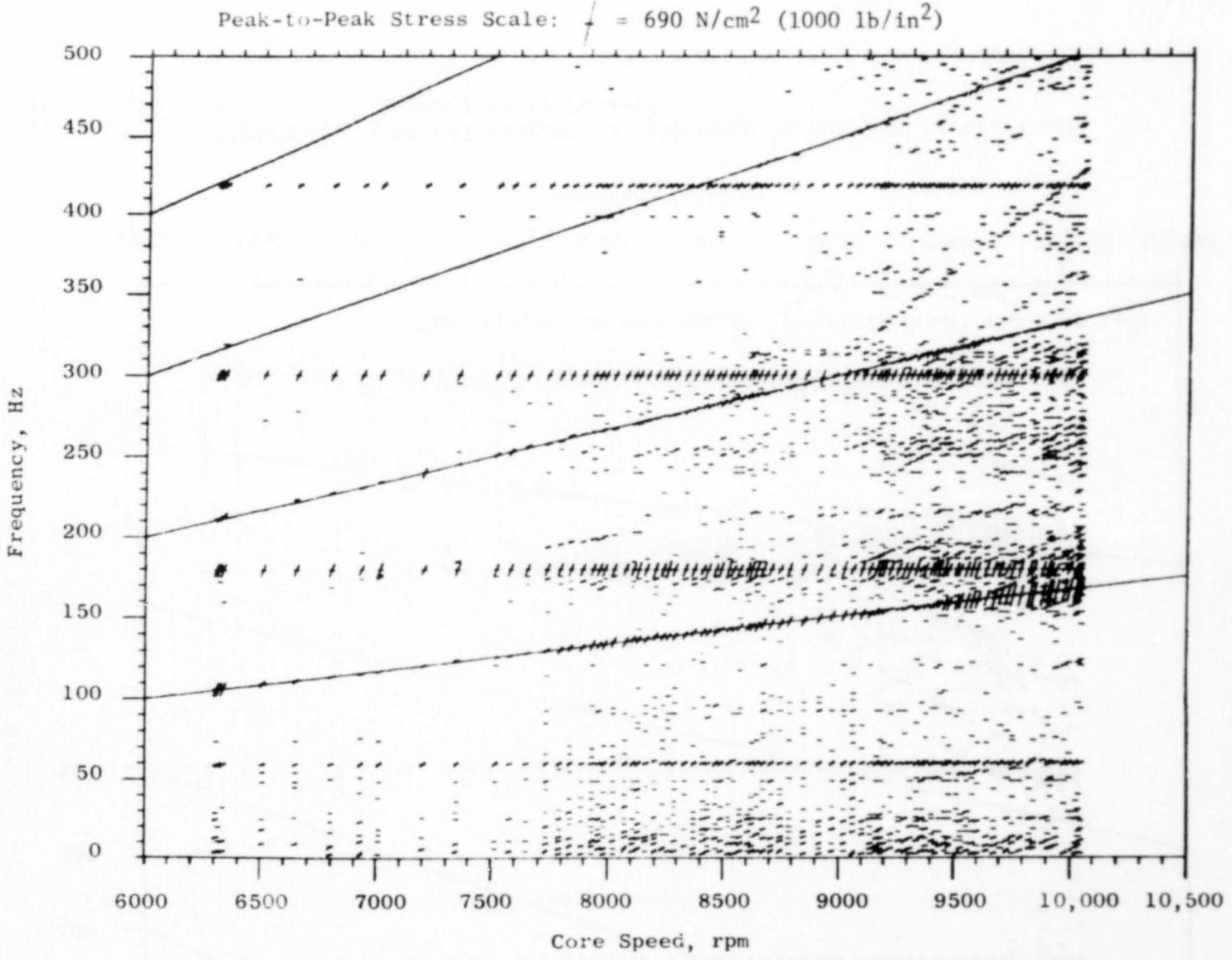

Figure 44. Campbell Diagram: Strain Gage No. 11, Two Minute Decel, Takeoff to Ground Idle.

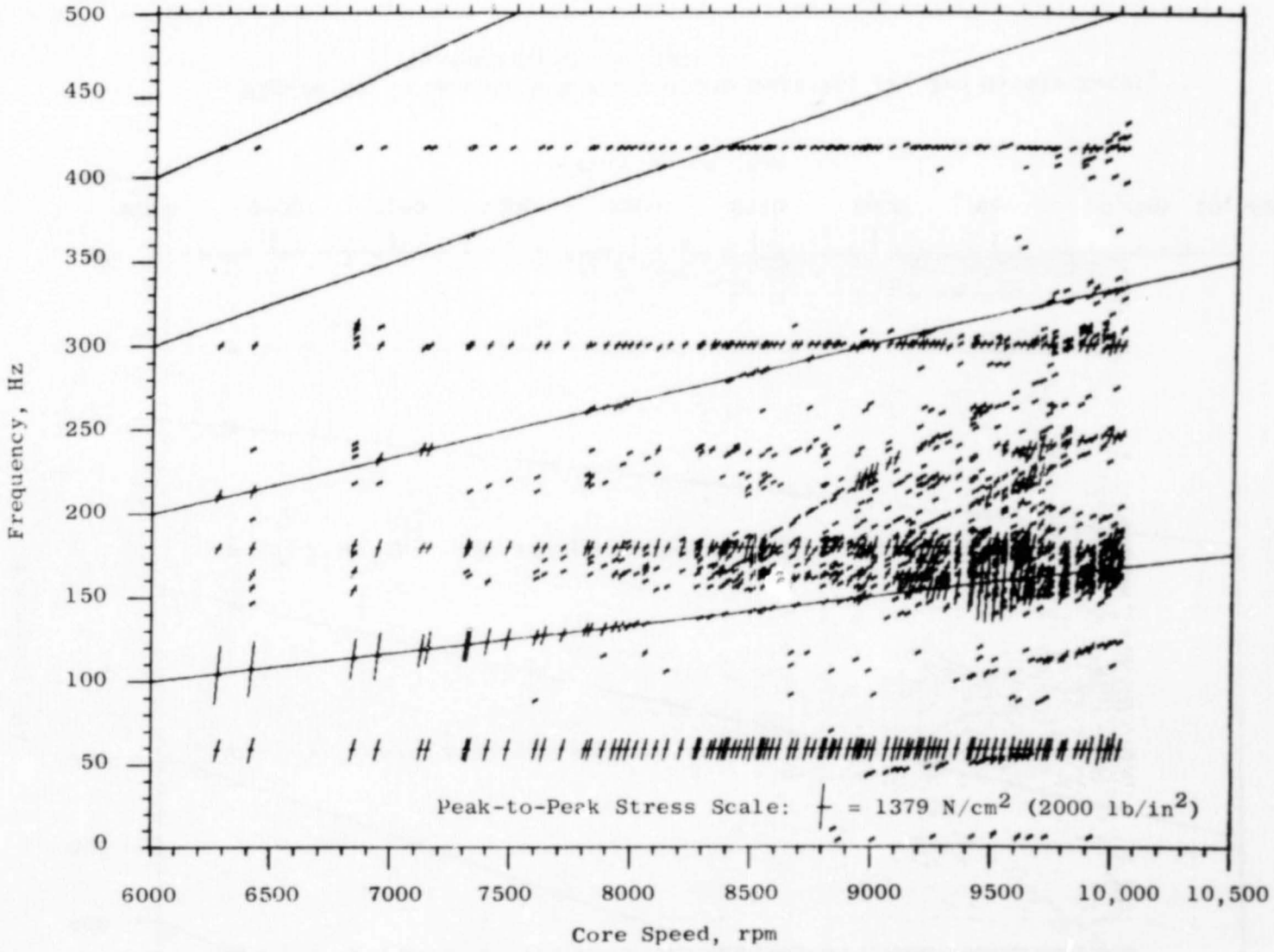

Figure 45. Campbell Diagram: Strain Gage No. 13, Two Minute Accel, Ground Idle to Takeoff.

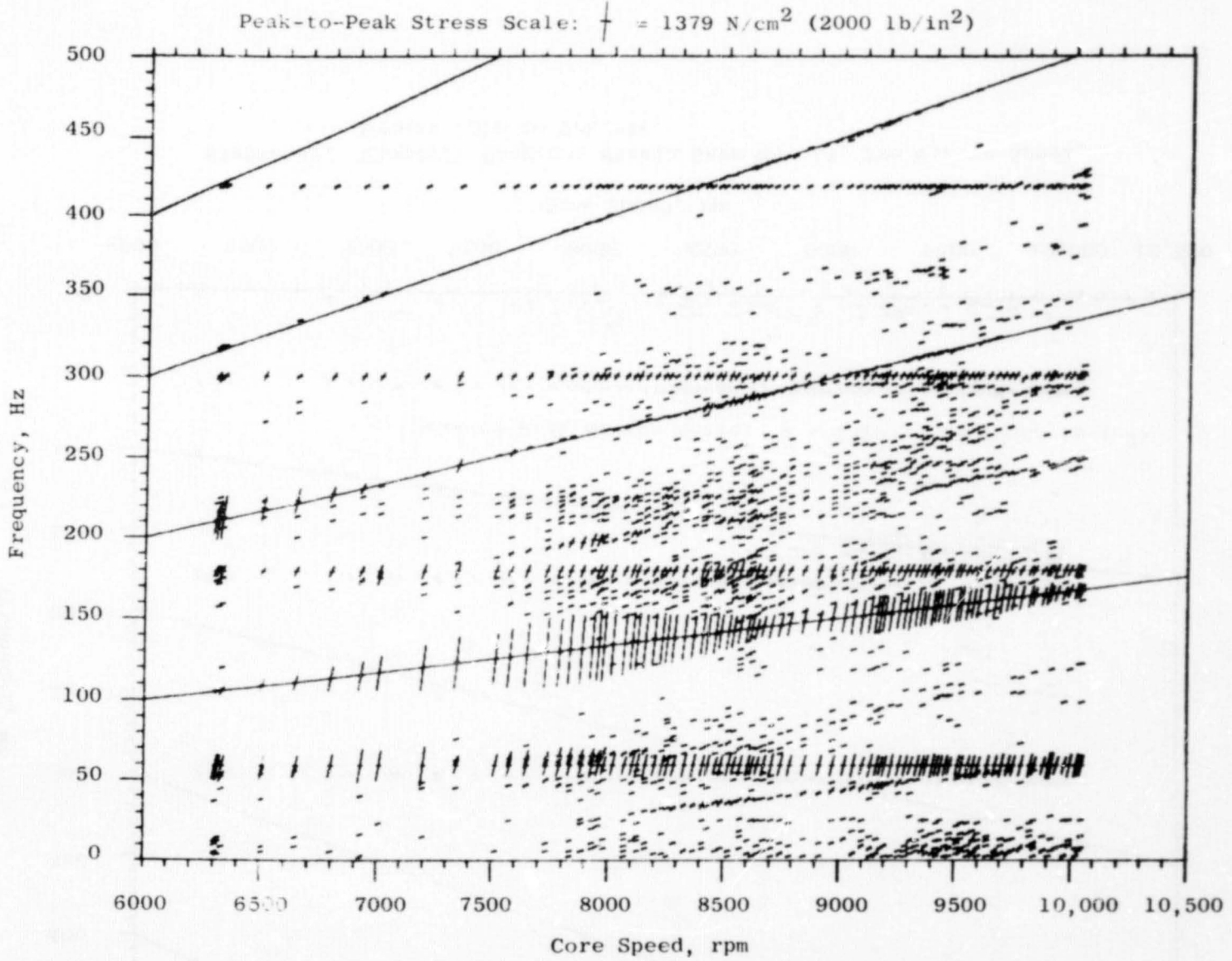

Figure 46. Campbell Diagram: Strain Gage No. 13, Two Minute Decel, Takeoff to Ground Idle.

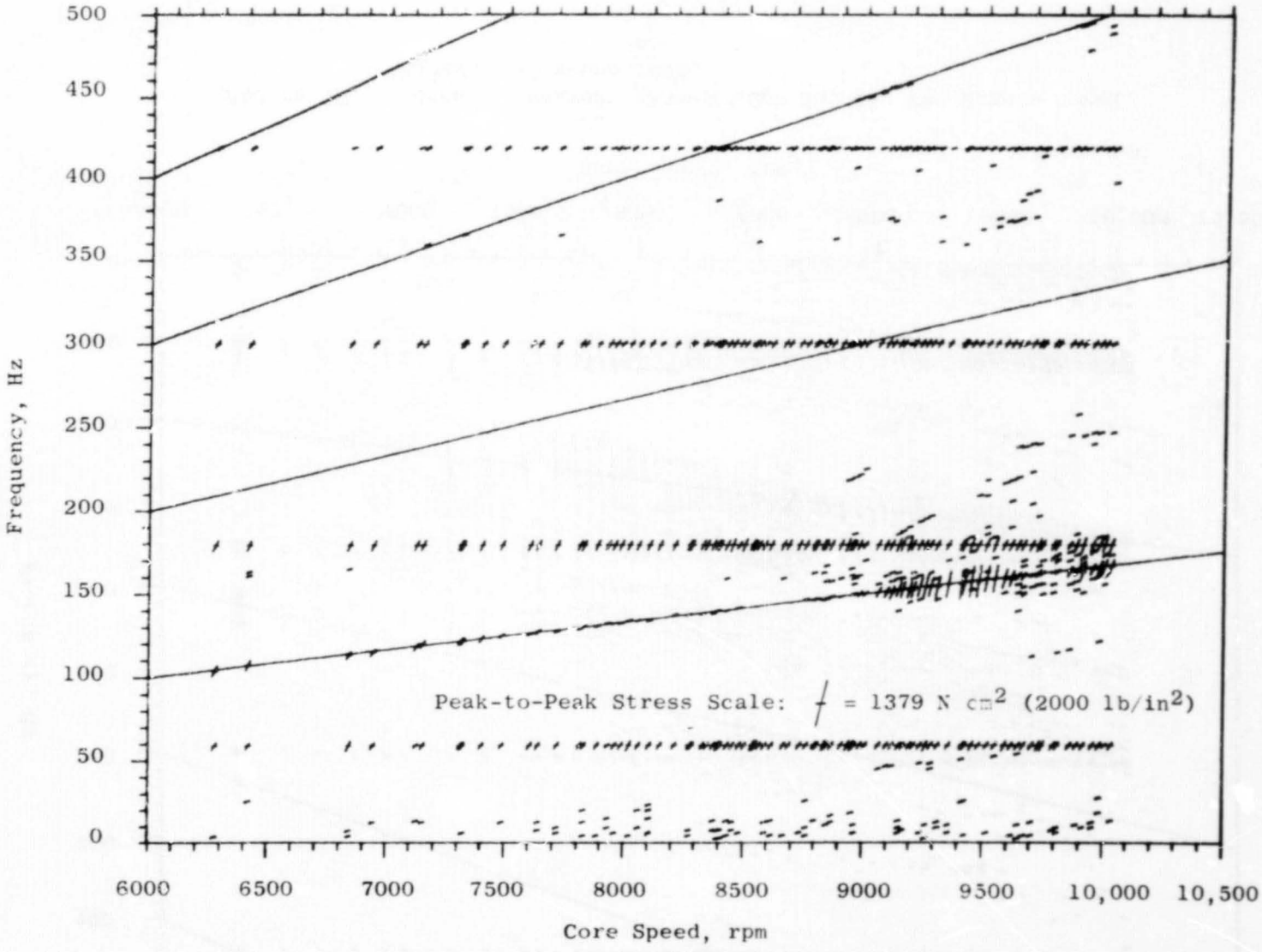

Figure 47. Campbell Diagram: Strain Gage No. 14, Two Minute Accel, Ground Idle to Takeoff.

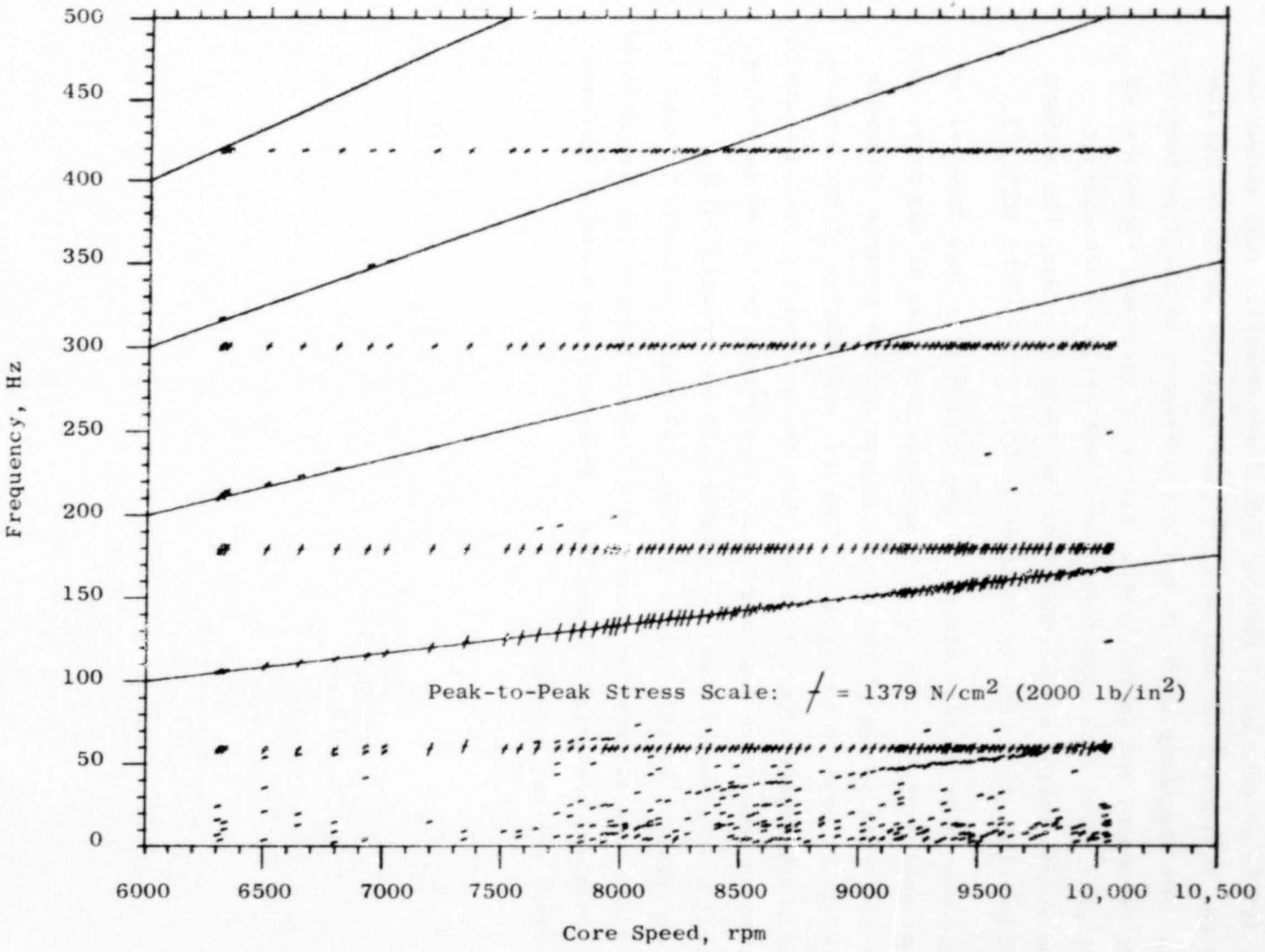

Figure 48. Campbell Diagram: Strain Gage No. 14, Two Minute Decel, Takeoff to Ground Idle.

An examination of the engine test data revealed a maximum alternating stress (for any gage) of approximately 5515 N/cm^2 (8000 $lb/in.^2$) which occurred at 145 Hz on gage No. 3 (during the 10 sec decel). This stress corresponds to the 9653 N/cm^2 (14,000 $lb/in.^2$) peak found at 165 Hz on the component test. The frequency shift is due to differences in manifold temperatures during component and engine tests. All other stresses, regardless of frequency or gage, were less than 1379 N/cm^2 (2000 $lb/in.^2$) alternating. Based on the strain ratios established from the component test, the maximum expected alternating stress at any location is 5516 N/cm^2 (8000 $lb/in.^2$).

The absolute value of mean stress, at any of the gage locations, is not known. Also, some amplification of stresses will occur due to the difference between the vibration levels of the tested engine and the maximum allowable vibration levels of production engines. However, examination of the Goodman Diagrams for the hardware materials shows that the alternating stresses are much less than the endurance limits and that significant (relative to stress rupture value) mean stresses could be present with no expected fatigue failure. This observation is illustrated in Figure 49 which presents the maximum measured manifold alternating stress on a Goodman Diagram for the manifold material and maximum operating temperature. Therefore, no manifold hardware fatigue problems are anticipated.

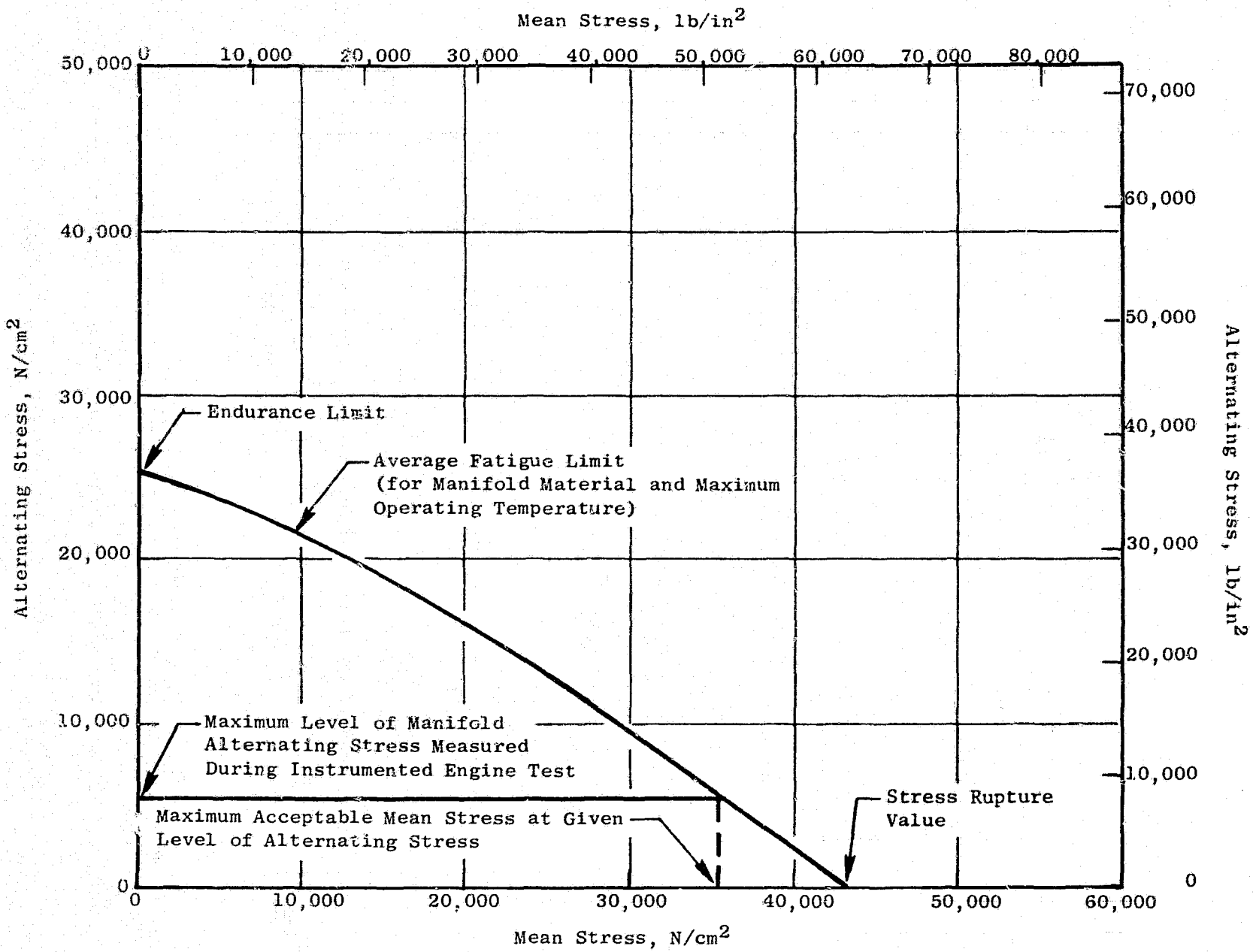

Figure 49. Goodman Diagram: Maximum Level of Measured Manifold Alternating Stress, Instrumented Engine Test.

5.0 INSTRUMENTED ENGINE TEST

The principal objectives of this test program and the analytical methodology related to these objectives are described below:

1. Obtain LPT stator operational data (including substantial quantities of data from both embedded and skin thermocouples) required to analytically define the performance improvement of the LPT ACC cooling system relative to the production LPT cooling system currently in use, for both sea level static and altitude operating conditions. The methodology employed in this analytical definition of performance was to be as follows: refine existing heat transfer (THTD) models of the LPT stator in order to match the test data obtained; incorporate THTD output into a CLASS/MASS model of the LPT stator case and generate case deflections of both the production and ACC systems, thereby defining the delta performance of the two systems (this is accomplished with the use of clearance/sfc derivatives and definition of cycle changes due to differences in airflow rates).

2. Obtain a direct measurement of the performance improvement of the ACC cooling system by measuring engine sfc during back-to-back testing of the current production and ACC cooling systems at sea level static simulated cruise test conditions. In addition to the intrinsic value of this information, it is useful in verifying the analytical definition of performance improvement, which in turn adds credence to the analytical definition of performance deltas at altitude conditions.

3. Obtain data, throughout the range of sea level static operating conditions, from several strain gages applied to the manifold at identical locations as those used in the manifold vibration component test. This data would then be correlated with component test data and used to assess the structural integrity of the manifold hardware.

5.1 TEST SETUP

The instrumented engine test was conducted in a sea level test cell. The test vehicle was a CF6-50 engine designated 455-507, Build 20. Figure 50 depicts a typical CF6-50 engine installed in a test cell and a description of the specific component configuration of engine 455-507/20 is provided below:

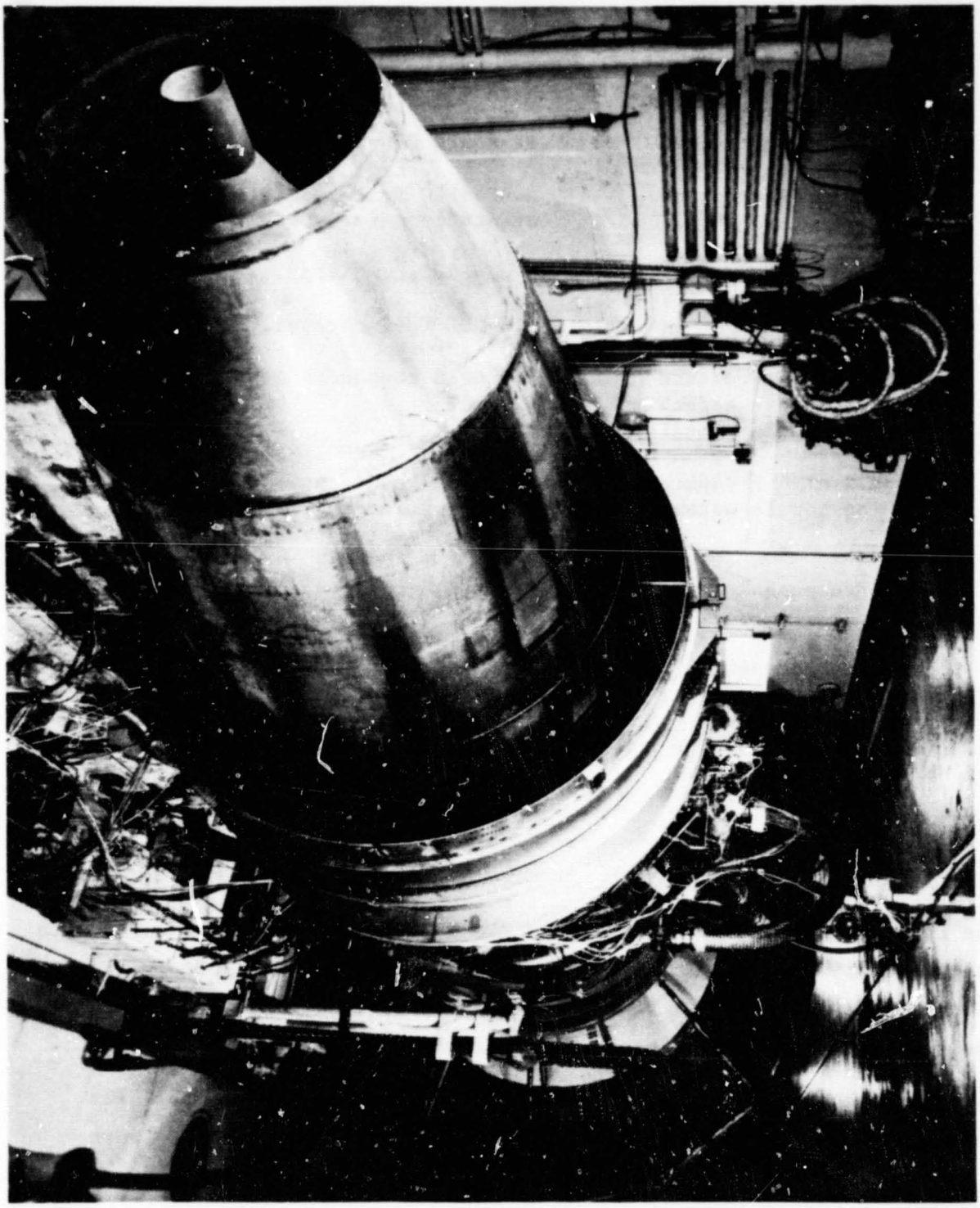

Figure 50. CF6 Engine in Test Cell.

• Front Frame	A standard CF6-50 front frame with rake pad capability to record compressor inlet characteristic, if needed.
• Compressor Stators	Standard CF6-50C compressor stator.
• Compressor Rotor	Standard CF6-50C rotor.
• Compressor Rear Frame	A CF6-50C frame modified to receive clearanceometer probes.
• Combustor	A CF6-50C combustor.
• Fuel Nozzle	CF6-50C fuel nozzles.
• Stage 1 High Pressure Turbine Nozzle Assembly (including mini-nozzle)	Improved roundness control (C2/E2 assembly)
• Stage 2 High Pressure Turbine Nozzle Assembly	Improved roundness control CF6-50C configuration modified to receive clearanceometer probes.
• High Pressure Turbine Rotor	CF6-50C Configuration
• Turbine Midframe	Improved roundness control CF6-50C Frame
• Low Pressure Turbine Module	CF6-50C - with the exception of active clearance control cooling system (manifold, supply piping, valve and scoop) for second part of test.
• Exhaust Nozzle	CF6-50C Configuration.

The test program was subdivided into two phases: (1) that conducted with a current production-type LPT cooling system, and (2) that conducted with the ACC cooling system. Table V delineates the principal components of each of these systems (brackets and mount hardware have been excluded).

Figure 51 shows the current production manifold and supply pipe. The ACC manifold and three of its supply pipes are depicted in Figure 52 (both photos were taken during airflow calibration tests).

Figures 53 through 55 show the ACC fan air scoop, ACC manifold supply pipes, and ACC manifold, respectively, in the as-installed condition on the test engine/cowling.

Table V. LPT Cooling System Hardware: Instrumented Engine Test.

A. PRODUCTION COOLING SYSTEM

Description	P/N	Quantity
Manifold, Clg., LPT Top Half	9061M13G05	1
Manifold, Clg., LPT Bottom Half	9061M14G02	1
Tube, LPT Supply	9069M70G01	1

B. ACC COOLING SYSTEM

Description	P/N	Quantity
Manifold, Clg., LPT Top Half	9224M41G01	1
Manifold, Clg., LPT Bottom Half	9224M42G02	1
Tube, Manifold Supply (Upstream of Valve)	9230M10G01	1
Tube, Manifold Supply (Y - Tube)	9230M12G01	1
Tube, Manifold Supply (Top Half)	9230M16G01	1
Tube, Manifold Supply (Bottom Half)	9230M14G02	1
Valve, Cooling Air (Variable area)	4013275-004	1
Air Scoop, Cooling Tube	4013146-853P001A	1

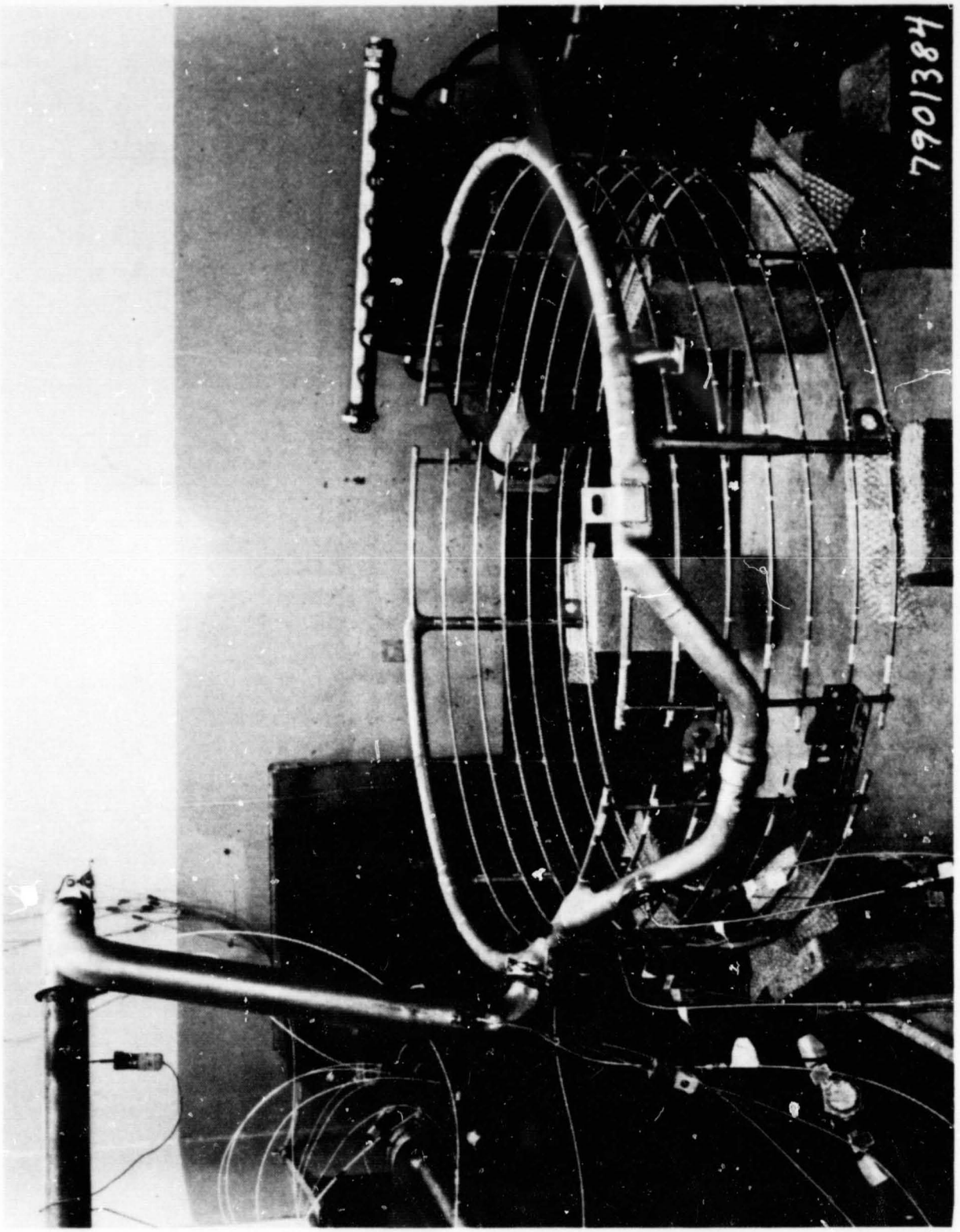

Figure 51. Current Production Manifold.

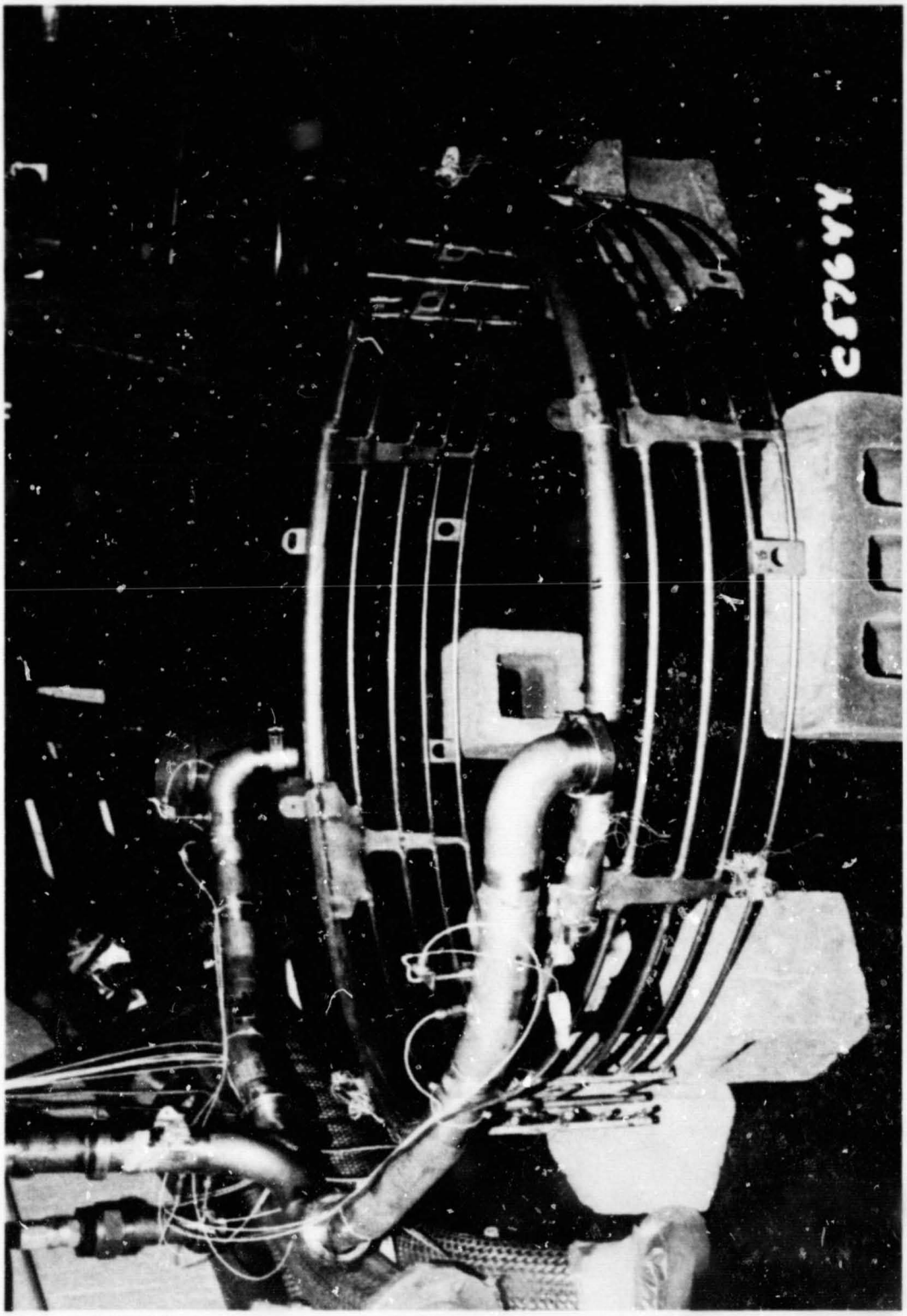

Figure 52. ACC Manifold.

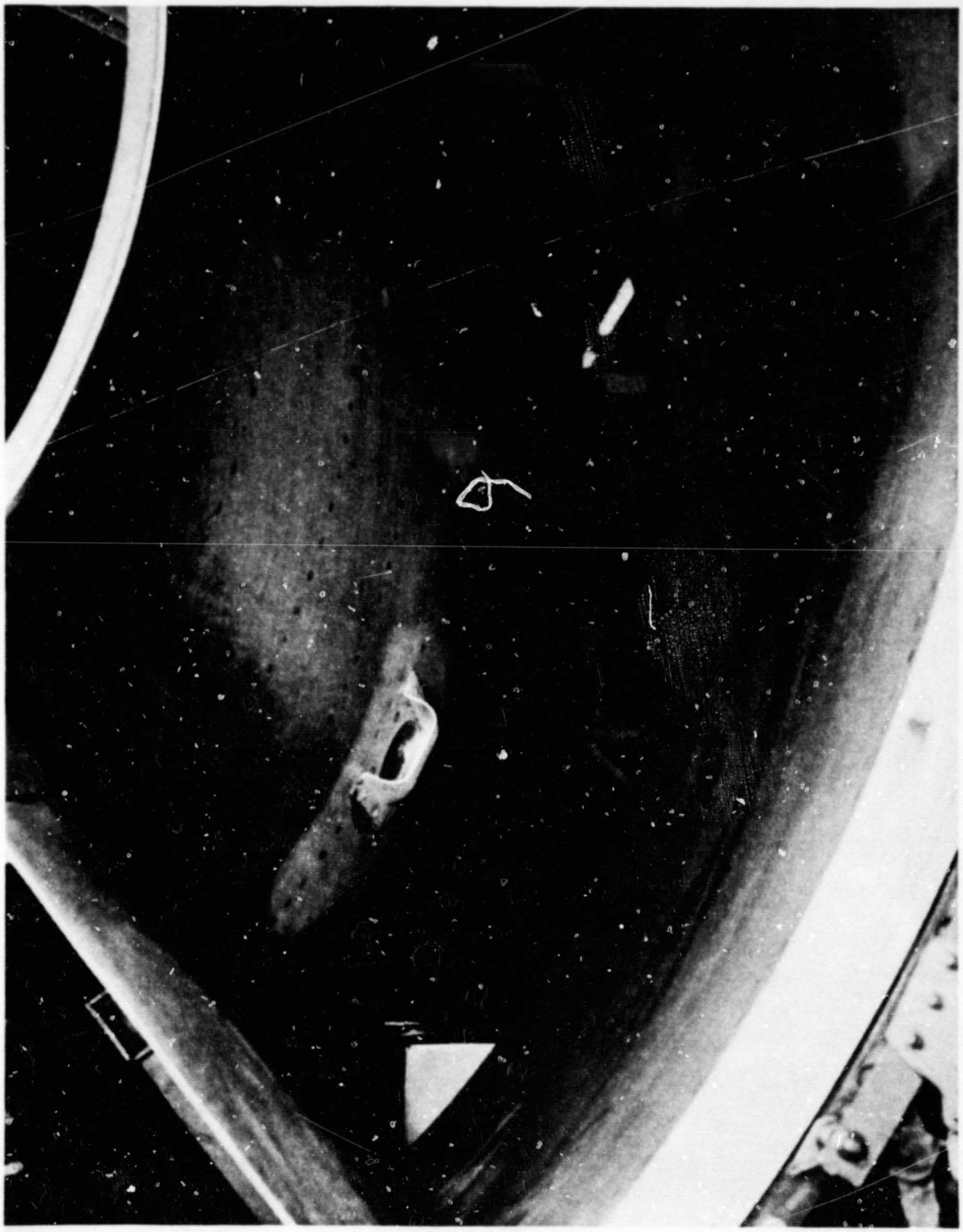

Figure 53. Fan Air Scoop: Installed.

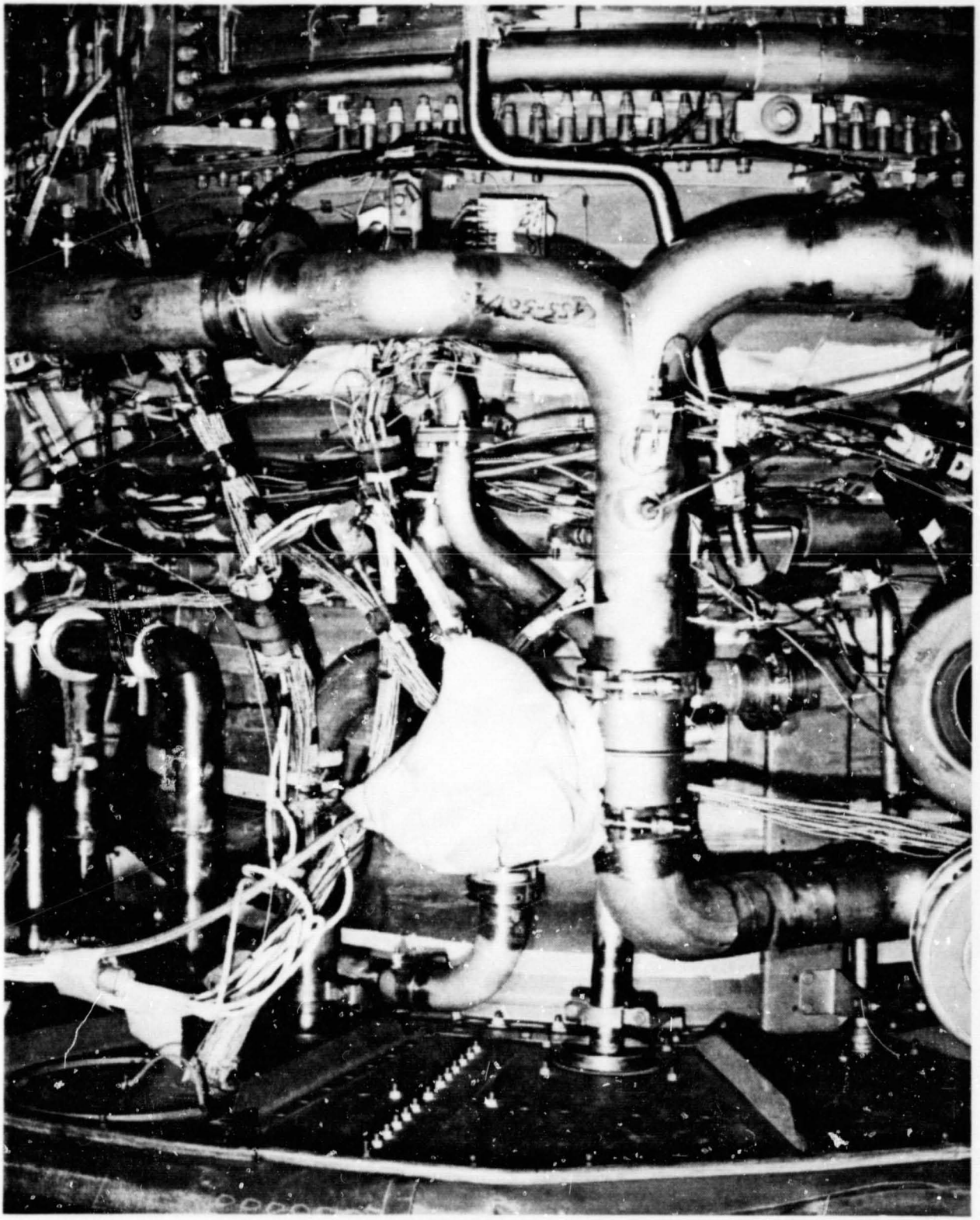

Figure 54. ACC Manifold Supply Tubes: Installed.

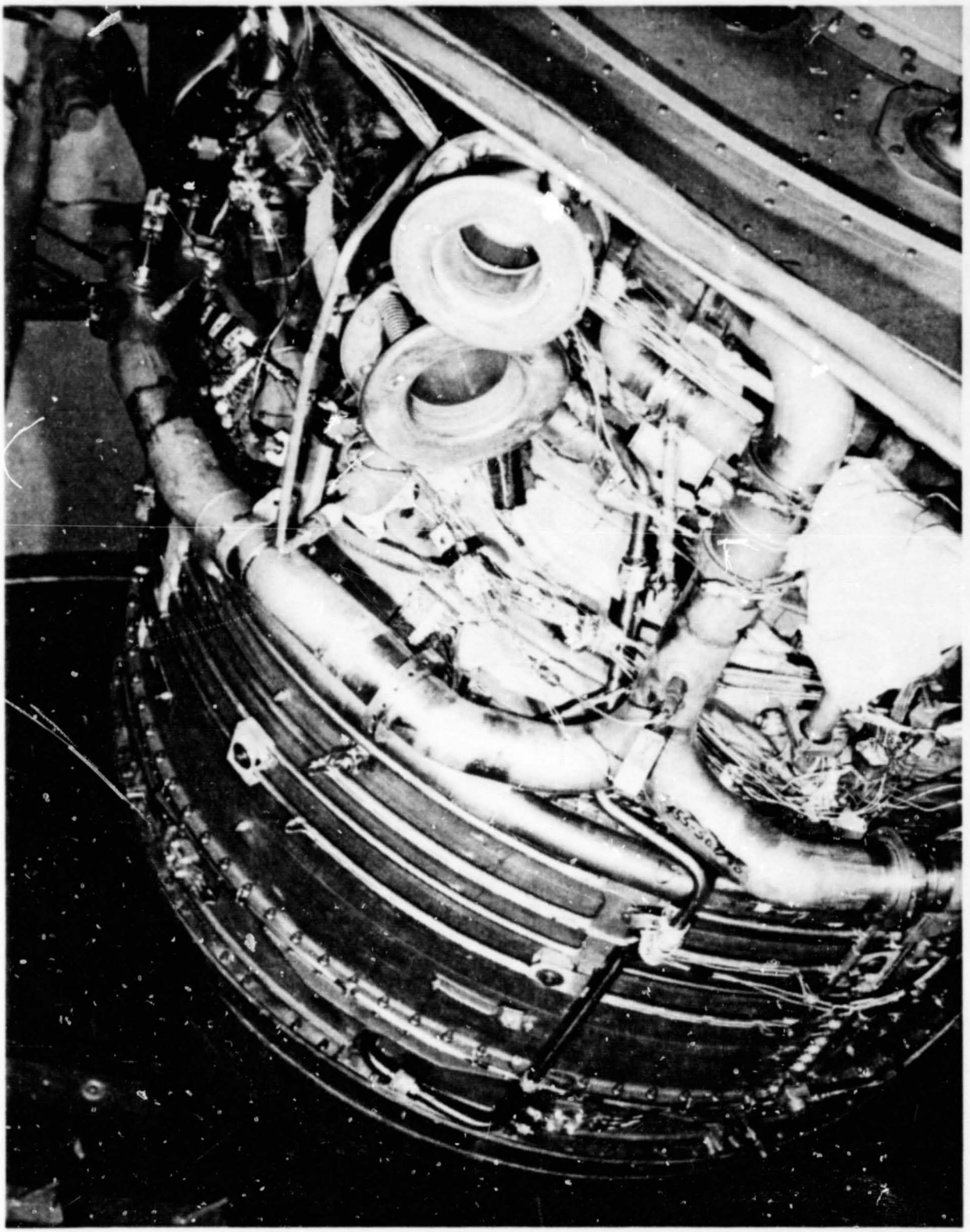

Figure 55. ACC Manifold: Installed.

5.2 INSTRUMENTATION

The engine was instrumented with the normal engine health and performance instrumentation. The LPT instrumentation used for this test consisted of the following:

80 LPT case skin thermocouples

32 LPT case embedded thermocouples

3 Stage 1 flowpath air thermocouples

3 Stage 1 flowpath static pressures

6 Stage 2 flowpath air thermocouples

6 Stage 2 flowpath static pressures

12 Stage 2 interstage seal skin thermocouples

3 Manifold supply pipe static pressures at cowling interface (common to both systems)

1 Manifold supply pipe air thermocouple at cowling interface (common to both systems)

4 Manifold/supply pipe static pressures - production system

4 Manifold/supply pipe total pressures - production system

4 Manifold/supply pipe air thermocouples - production system

3 Manifold supply pipe static pressures - ACC system

3 Manifold supply pipe total pressures - ACC system

3 Manifold supply pipe air thermocouples - ACC system

8 ACC Manifold skin thermcouples

8 ACC Manifold immersion air thermocouples

8 ACC Manifold external air thermocouples

5 ACC Manifold (and mount bracket) strain gages

4 LPT case accelerometers

3 Under-cowling air thermocouples

3 Under-cowling static pressures

Totals	168 Thermocouples
	29 Pressure Sensors
	5 Strain Gages
	4 Accelerometers
	206 Pieces of Instrumentation

Locations of the LPT case, Stage 2 interstage seal and Stage 1 and 2 flowpath instrumentation are shown in Figure 56. The ACC manifold and supply pipe instrumentation locations are given in Figures 57 and 58, while Figures 59 through 61 depict the production manifold, cowling, and under-cowling sensors.

5.3 TEST PROCEDURE

After the engine mechanical checkout, vibration survey and one transient from ground idle (G/I), to take-off (T/O) was completed, the LPT baseline testing was conducted with the production cooling system. Immediately following the baseline testing, the ACC cooling system was installed and tested. The production system was then reinstalled and the cruise and T/O setpoints were repeated for flow rate verification.

Following completion of an HPT roundness test program (Reference 2), which was also conducted on this engine, additional LPT testing was conducted with varying flow rates through the production system. The various LPT tests are discussed in the following paragraphs and Figure 62 provides a schematic representation of all test points.

Production System Baseline Test Sequence

- Power calibration
- Accel/decel - ground idle to takeoff
- Stabilization at simulated cruise for sfc definition

C-2

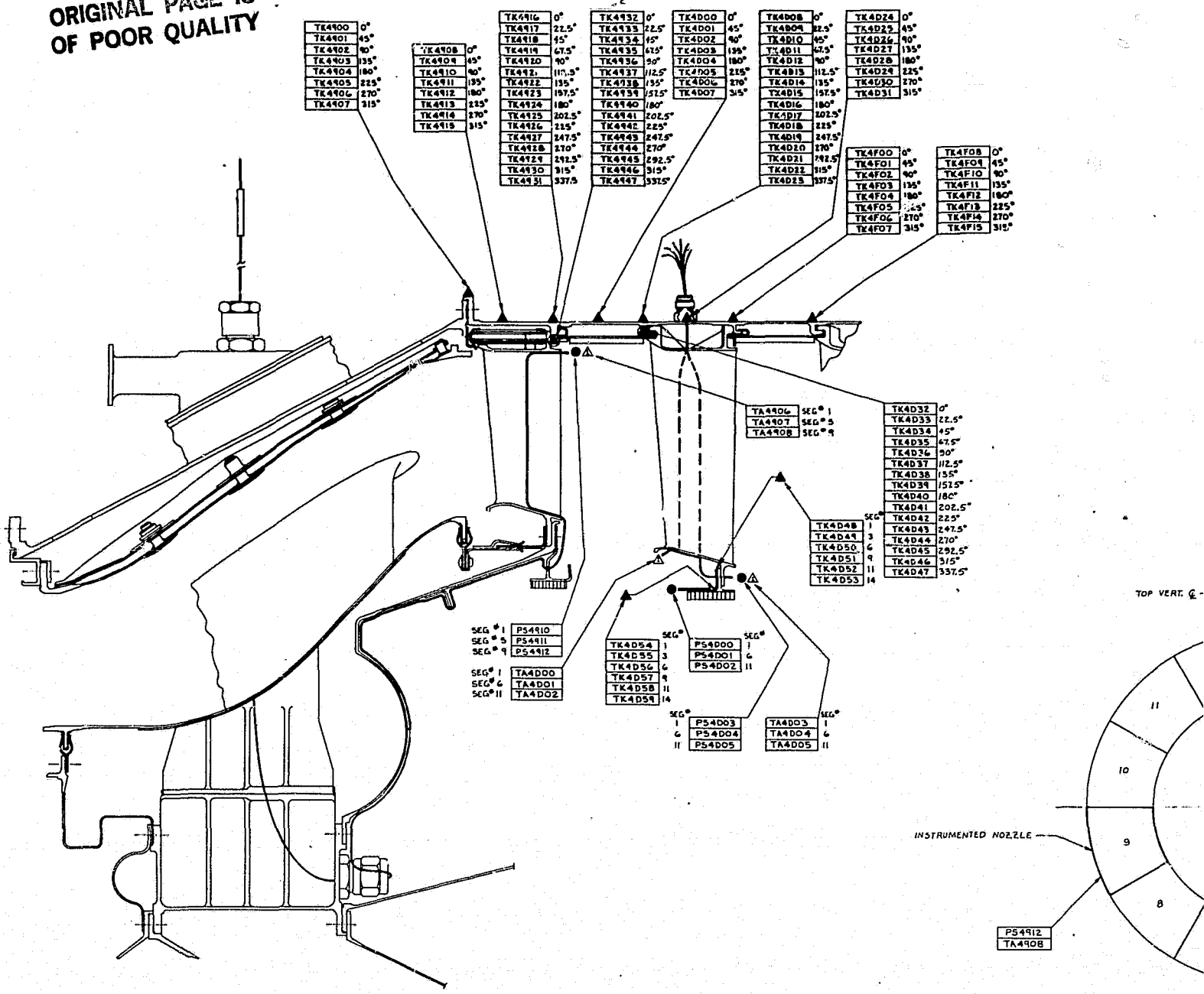

Figure 56. Instrumentation Drawing: LPT Case, Stage 2 I/S Seal and

FOLDOUT FRAME

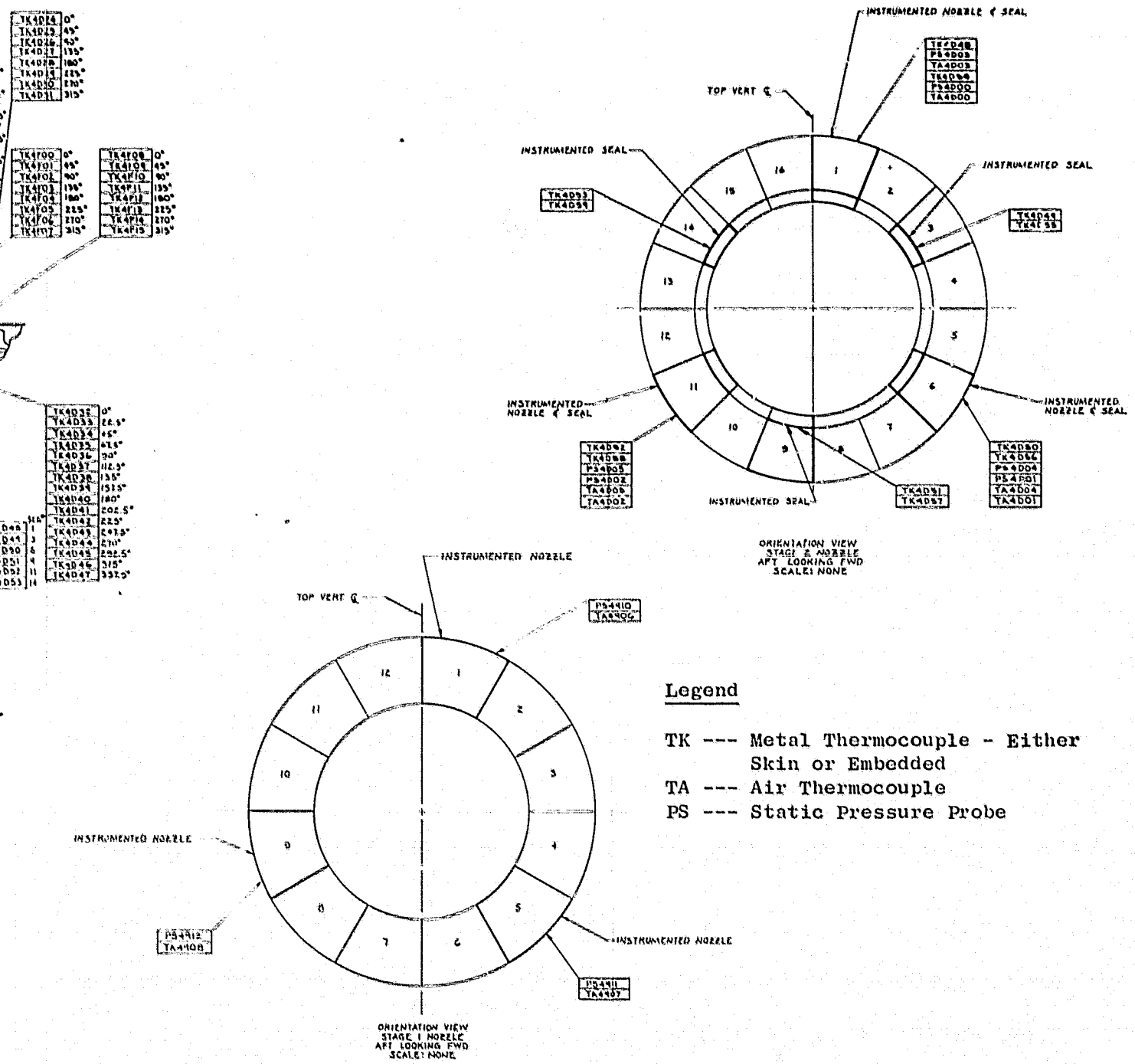

Legend

TK --- Metal Thermocouple - Either Skin or Embedded
TA --- Air Thermocouple
PS --- Static Pressure Probe

PT Case, Stage 2 I/S Seal and Stage 1 and Stage 2 Flowpath.

2 FOLDOUT FRAME

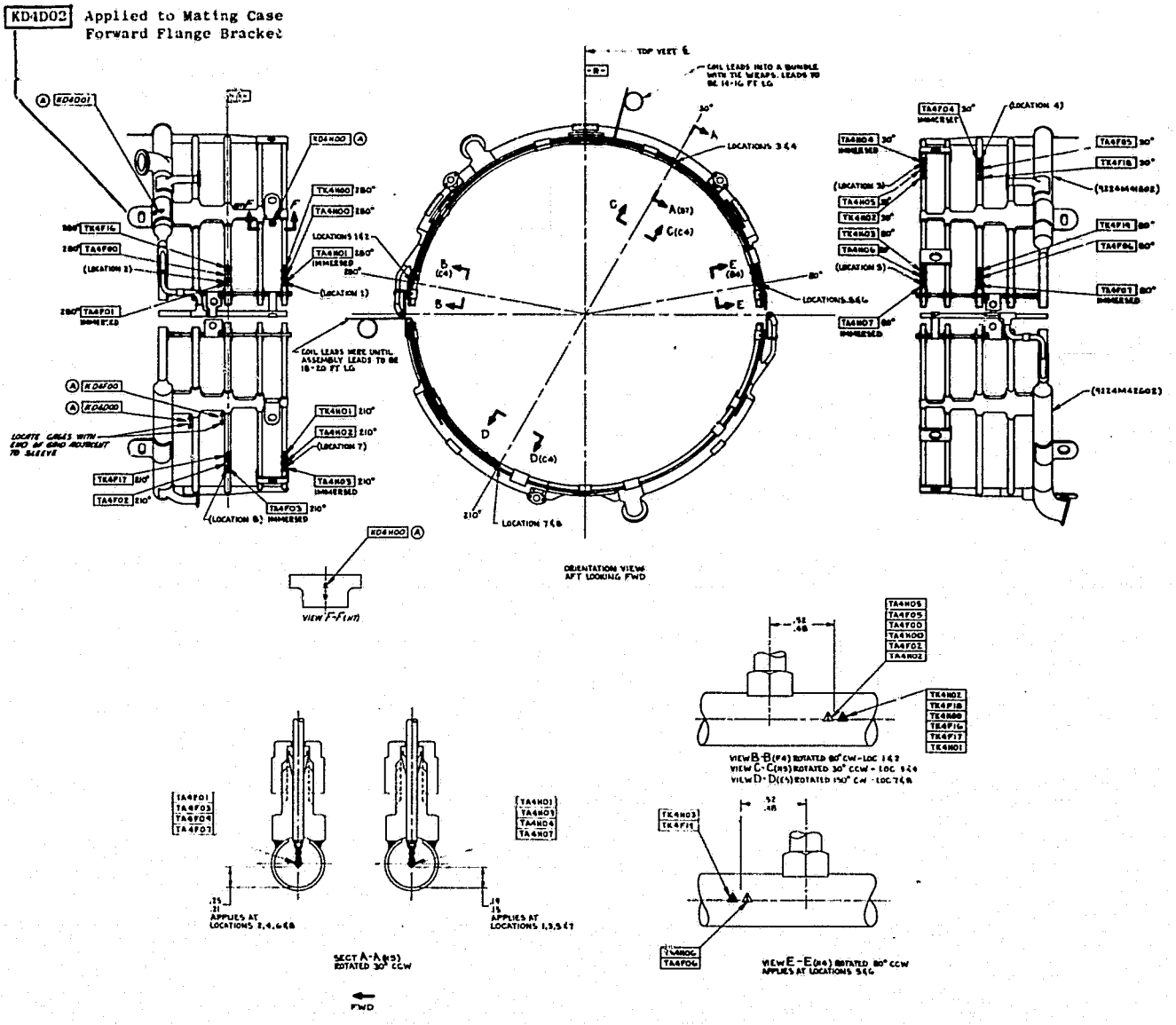

Legend

KD --- Dynamic Strain Gage
TK --- Skin Thermocouple
TA --- Air Thermocouple

Figure 57. Instrumentation Drawing: ACC Manifold.

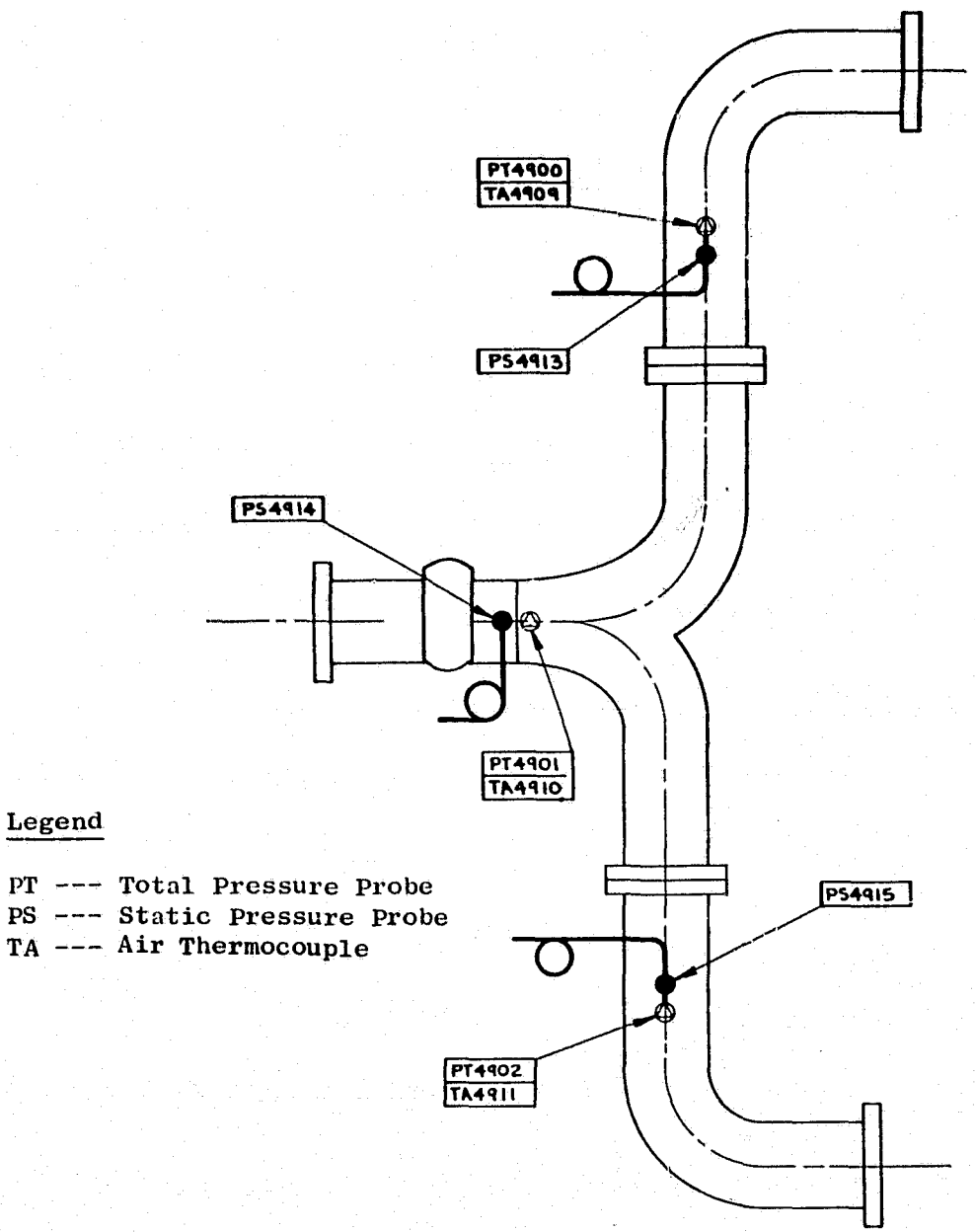

Figure 58. Instrumentation Drawing: ACC Manifold Supply Pipes.

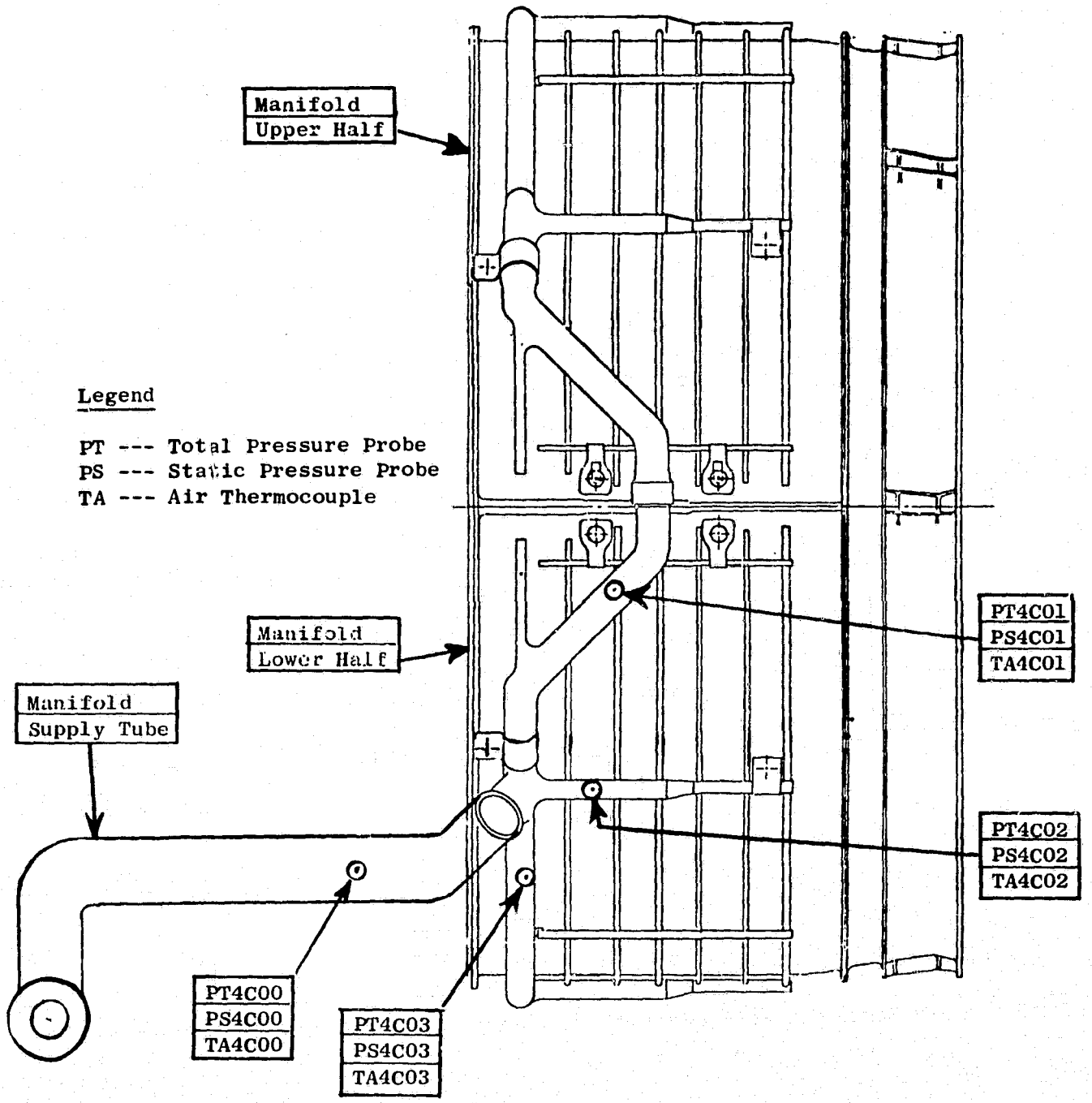

Figure 59. Instrumentation Schematic: Production Manifold.

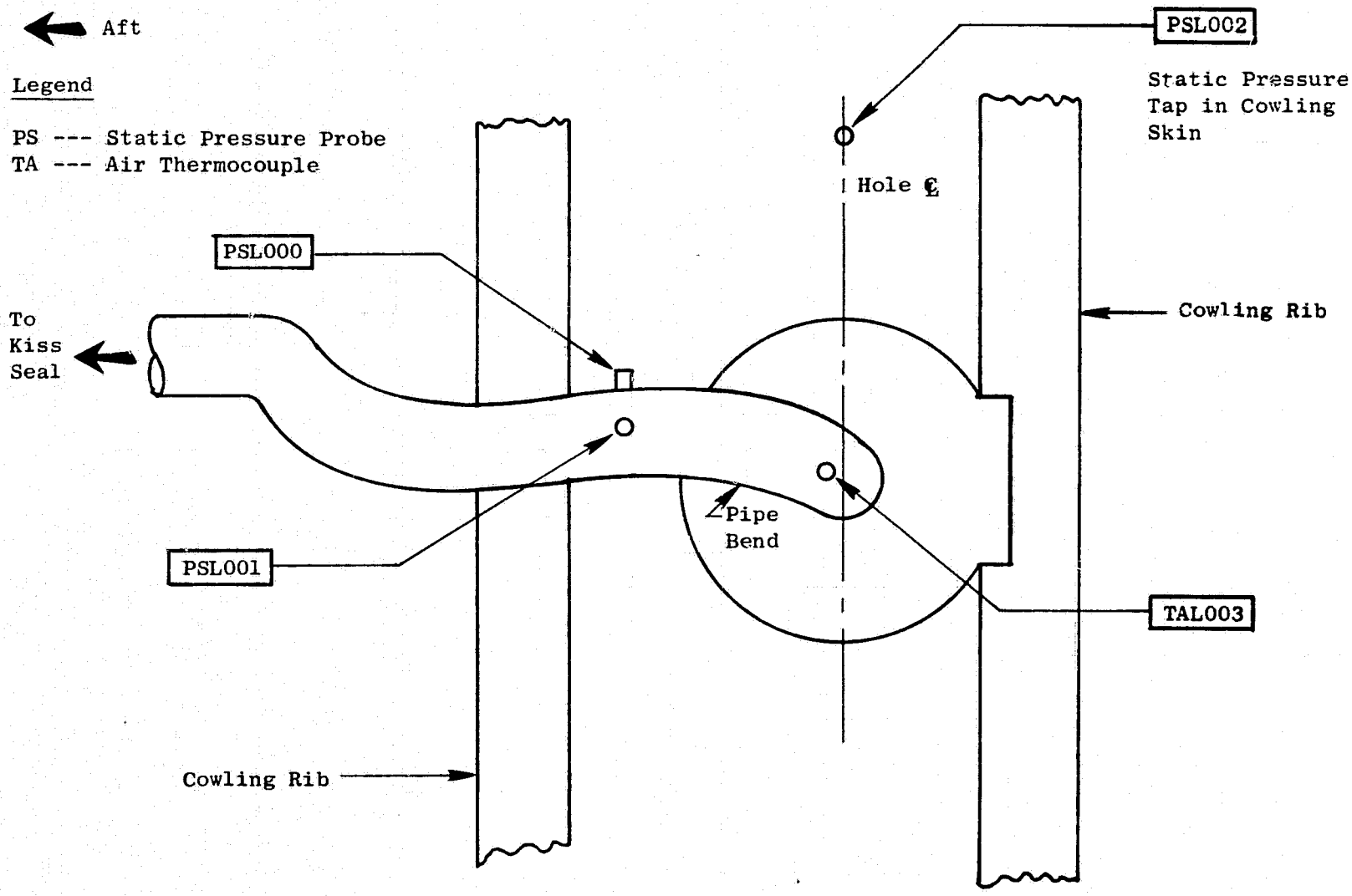

Figure 60. Instrumentation Schematic: Cowling Supply Pipe.

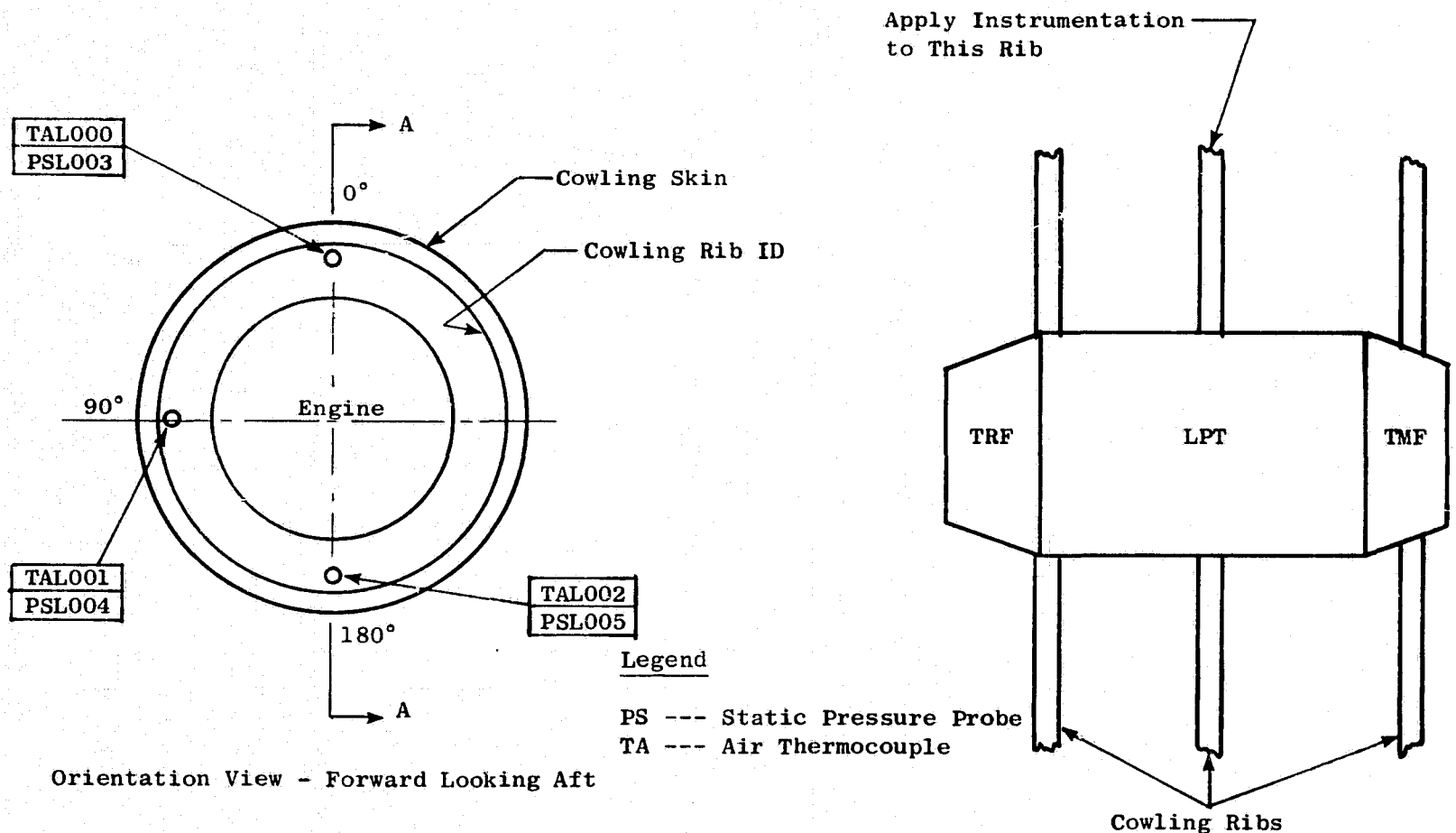

Note: 1. Apply Instrumentation (Air Thermocouples and Static Pressures) to Cowling Ribs Such That Probe Tips are Approximately Halfway Between Cowling Rib Surface and LPT Case Surface If Possible.

Figure 61. Instrumentation Schematic: Under Cowl Sensors.

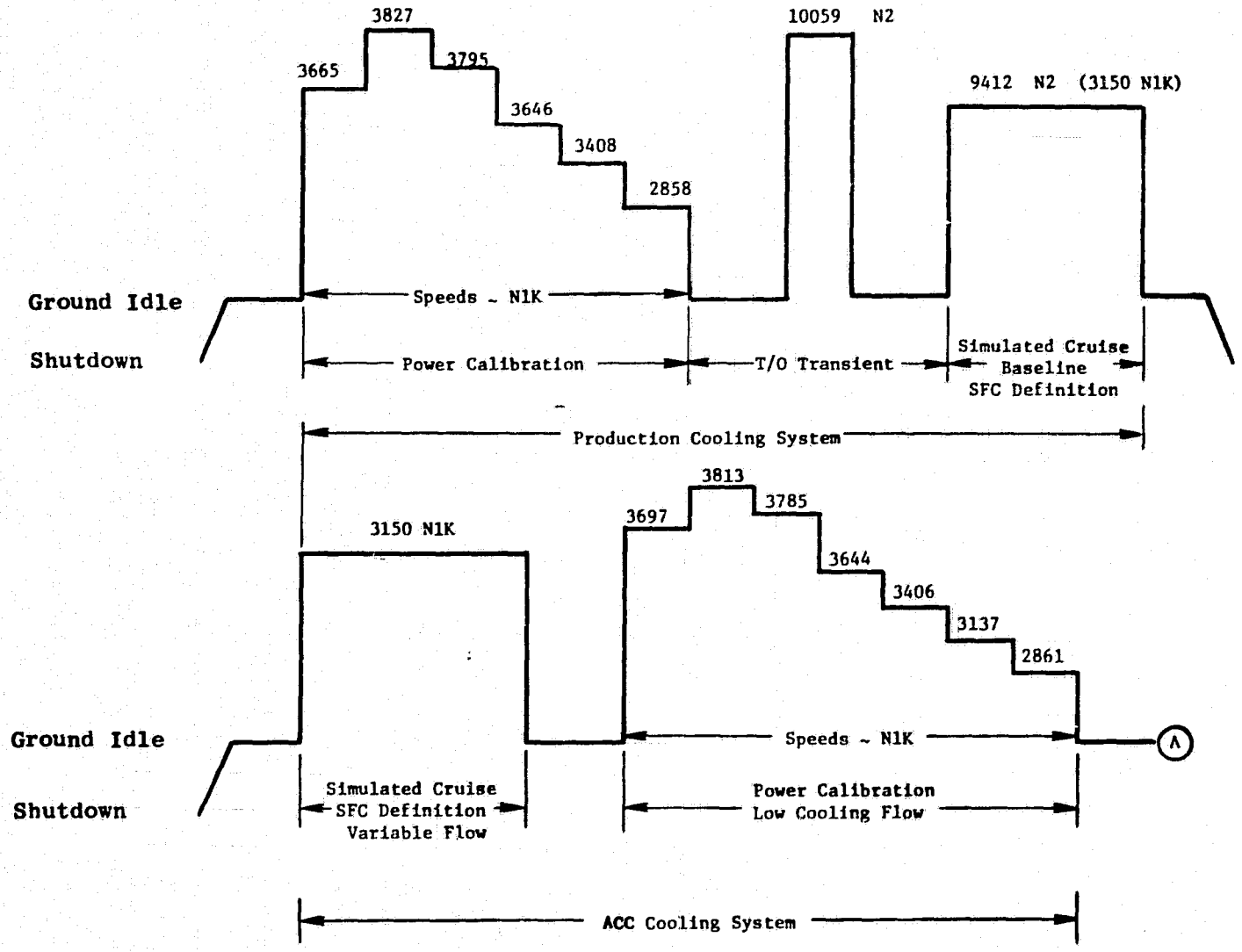

Figure 62. Test Sequence.

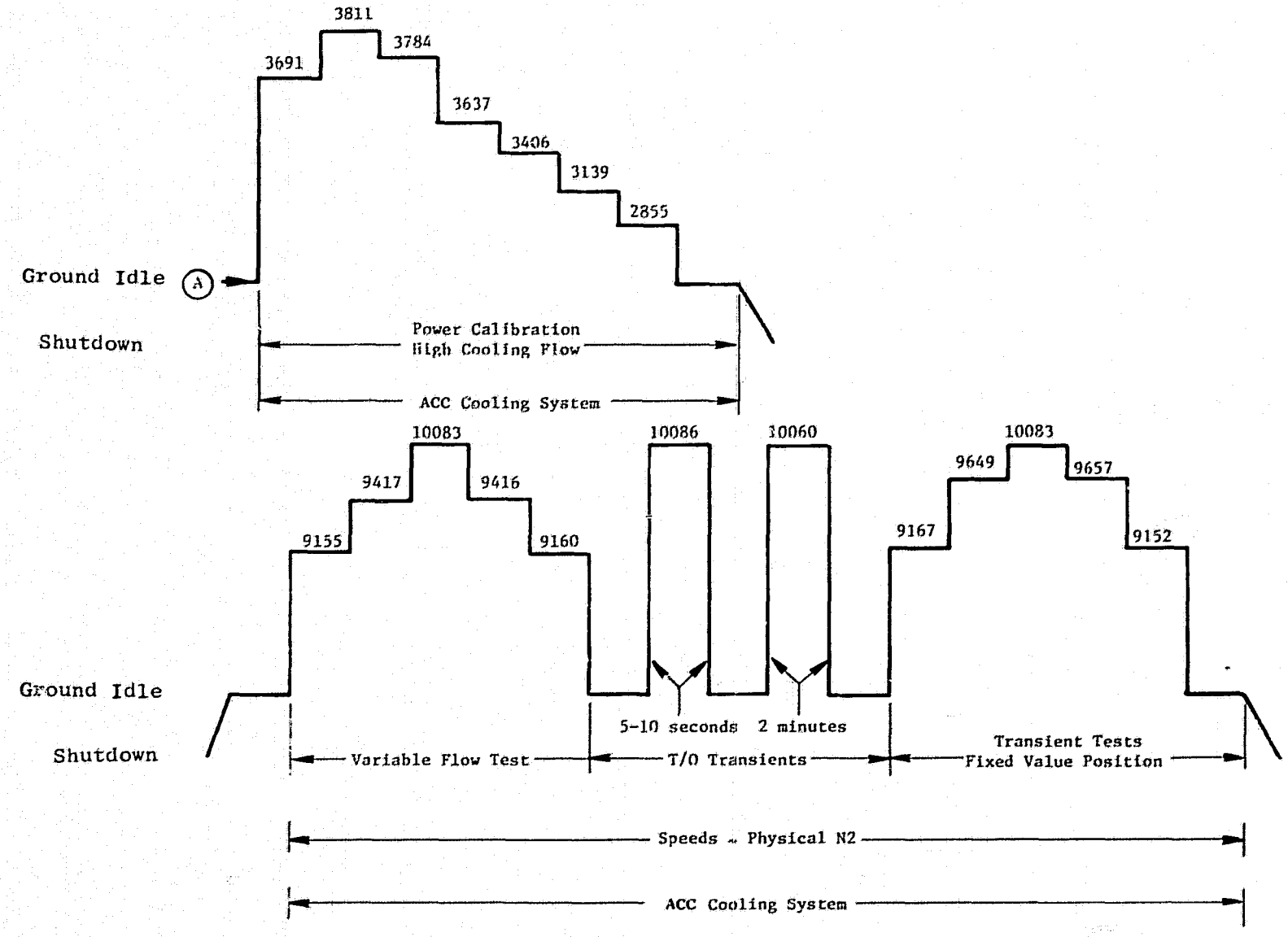

Figure 62. Test Sequence (Continued).

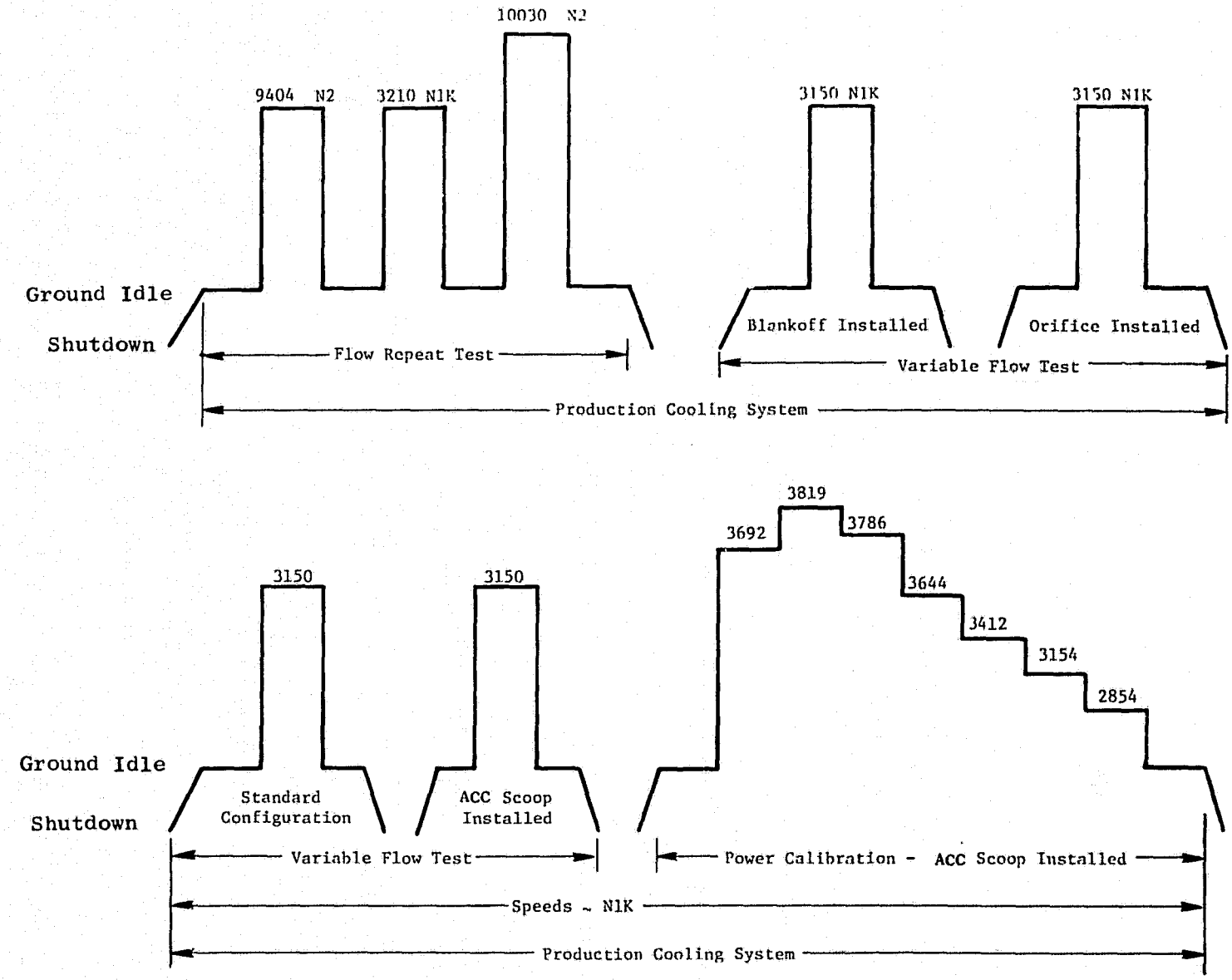

Figure 62. Test Sequence (Concluded).

ACC System Test Sequence

- Stabilization at simulated cruise and sfc definition for varying levels of cooling flow
- Power calibration - low level of cooling flow
- Power calibration - high level of cooling flow
- Shutdown transient
- Case temperature versus cooling flow definition at simulated minimum cruise, simulated average cruise and takeoff conditions.
- Accel/decel - ground idle to takeoff
- Transient testing at simulated min and max cruise and T/O settings with a fixed ACC valve setting

Production System Flow Repeat Test

- Stabilization at simulated cruise
- Stabilization at takeoff

Production System Variable Flow Test

- Stabilization at simulated cruise with no flow - blankoff plate installed
- Stabilization at simulated cruise with reduced flow - orifice installed
- Stabilization at simulated cruise with full flow
- Stabilization at simulated cruise with increased flow - ACC fan scoop installed
- Power calibration with ACC fan scoop installed

Note: The scoop was installed to increase the pressure at the manifold inlet and therefore increase the flow through the manifold.

5.4 TEST RESULTS

5.4.1 Introduction

Prior to discussing the test results and subsequent analysis within the framework of the test objectives presented previously, it is worthwhile to present a brief summary of the test results at the simulated cruise setpoints. This is important as it explains the impetus for conducting various posttest diagnostic activities which were not originally planned.

Figures 63 and 64 present delta sfc and LPT case temperatures, respectively, as a function of cooling flow for both cooling systems at the sea level static simulated cruise conditions. Figure 63 shows that at maximum flow conditions, the ACC system demonstrated some performance improvement relative to the current production system without the fan air scoop (which is the present production configuration). The temperature versus flow data, shown in Figure 64, verifies the measured performance trends shown in Figure 63. However, the level of improvement with the ACC system was less than predicted. Additionally, the flow rate of the current production system was less than anticipated. For these reasons, various posttest diagnostic investigations were conducted to verify the measured flow rates of both systems and to help explain the test results. The results of these diagnostic efforts are presented in the following section.

5.4.2 Posttest Diagnostics

5.4.2.1 Manifold Cooling Hole Sizes

The sizes of the cooling holes in each flow segment of both the production and ACC manifolds were checked with pin gages. These checks verified that the cooling holes for both manifolds were according to drawing specifications.

5.4.2.2 Flow Calibration Repeat Tests

Following completion of the instrumented engine tests both the production and ACC manifolds and their respective supply pipes were sent to the Component

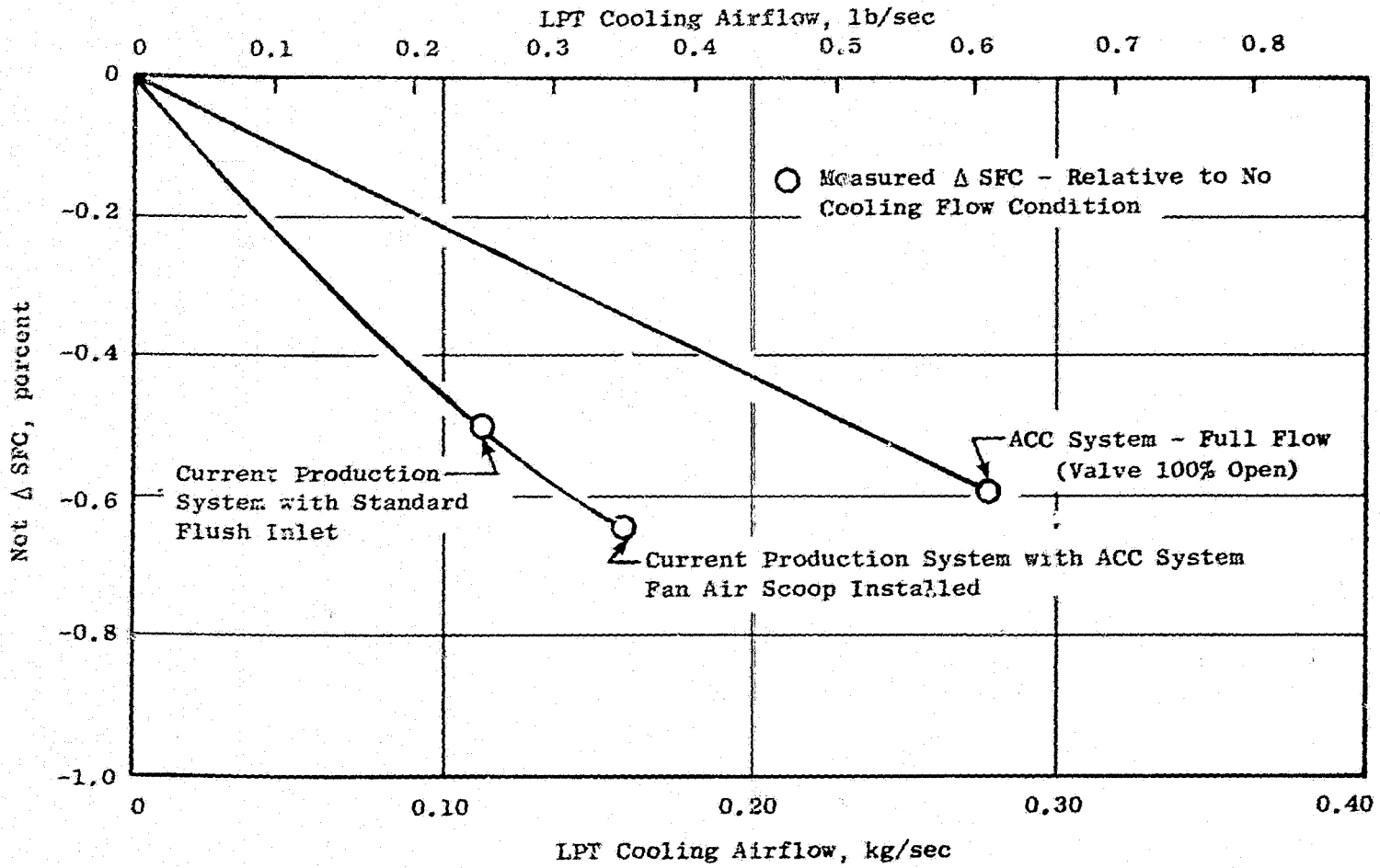

Figure 63. Demonstrated Δ SFC Versus LPT Cooling Airflow: Production and ACC Systems, SLS Simulated Cruise.

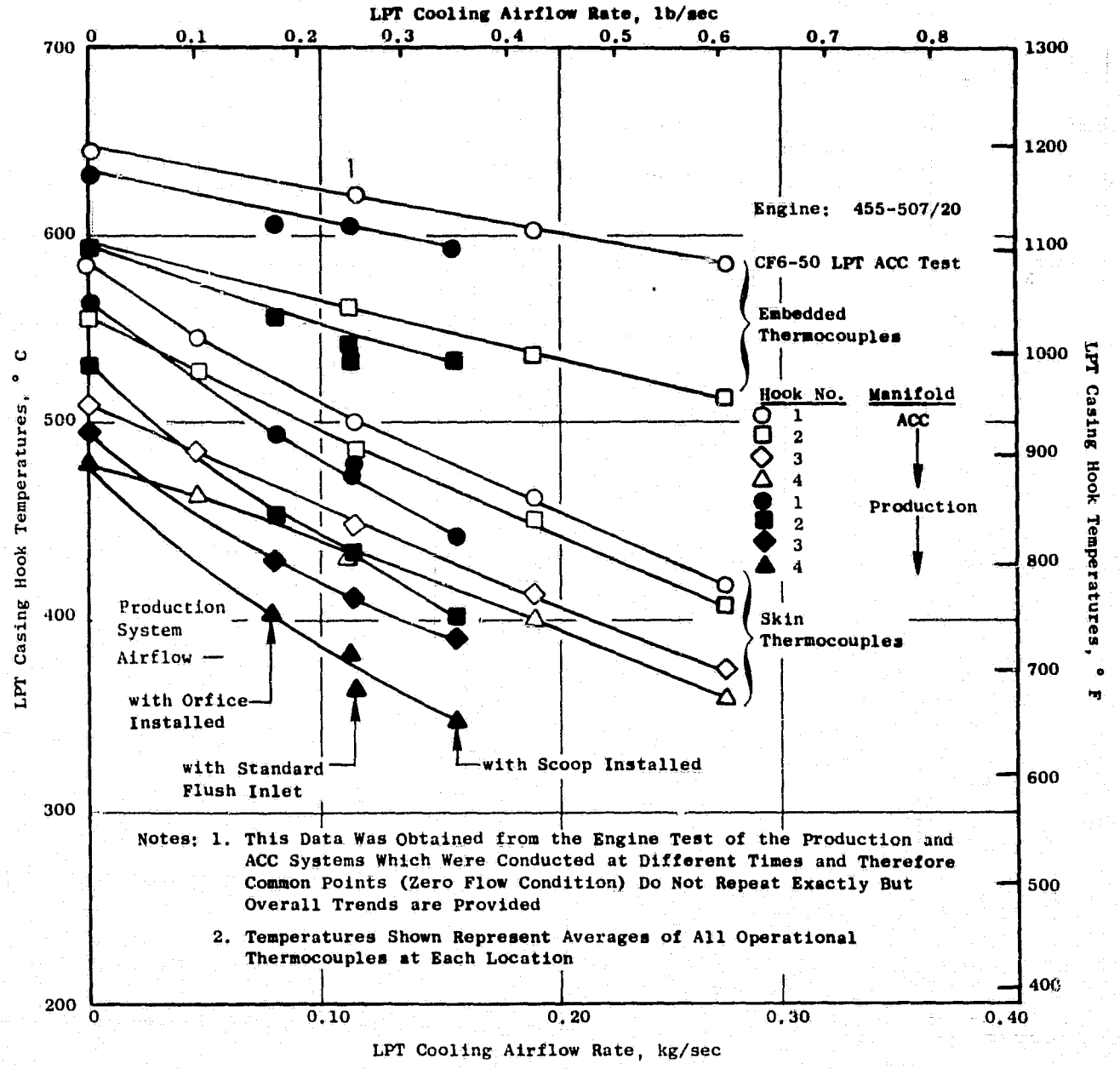

Figure 64. Measured LPT Case Hook Temperatures Versus LPT Cooling Airflow Production and ACC System, SLS Simulated Cruise.

Mechanical Laboratory for verification of flow calibration curves generated previously. The test setups were as shown previously in Figures 51 and 52.

Figures 65 and 66 compare the original and repeat flow calibrations of the production and ACC manifolds respectively. The repeat calibration data for the production system showed excellent agreement with the original calibration. Although the repeat calibration data for the ACC system was slightly lower than the original data, the agreement was still very good. The results of these tests verified the calculated flow rates from the instrumented engine test. It should also be noted that several engine test flow rates were calculated with static pressure calibration curves as well as total pressure calibration curves and excellent agreement was obtained.

5.4.2.3 Radial and Axial Dimensional Checks

Following completion of the instrumented engine test, radial and axial dimensional checks were performed on both manifolds. The radial distance between the bottom of the manifold tubes and the top of the case skin was recorded at 10 circumferential locations for each manifold tube. The axial distance from the aft side of the LPT case forward flange to the centerline of each of the manifold tubes was also recorded. Tables VI and VII show the results of the dimensional checks. These dimensional relationships are important for the following reasons: the ratio of the radial distance between the tube and the case surface to the size of the cooling hole has a direct effect on the distribution of impingement heat transfer coefficients along the case surface; the axial relationship between manifold tubes (impingement streams) and the casing hooks in conjunction with the location of the primary source of heat input to the case hooks (such as nozzle hooks) have a direct effect on cooling effectiveness. The measured dimensions recorded in these tables were incorporated in the heat transfer model of the LPT case during the test data matching process. It is worth noting that the dimensional inspections conducted on the ACC manifold indicated that the radial distance at each tube was greater (farther away from the case skin) than the drawing specification and that the axial distance to each tube was less (farther forward) than the corresponding drawing specification. The increased radial distance (spacing) decreased the cooling effectiveness of the impingement jets

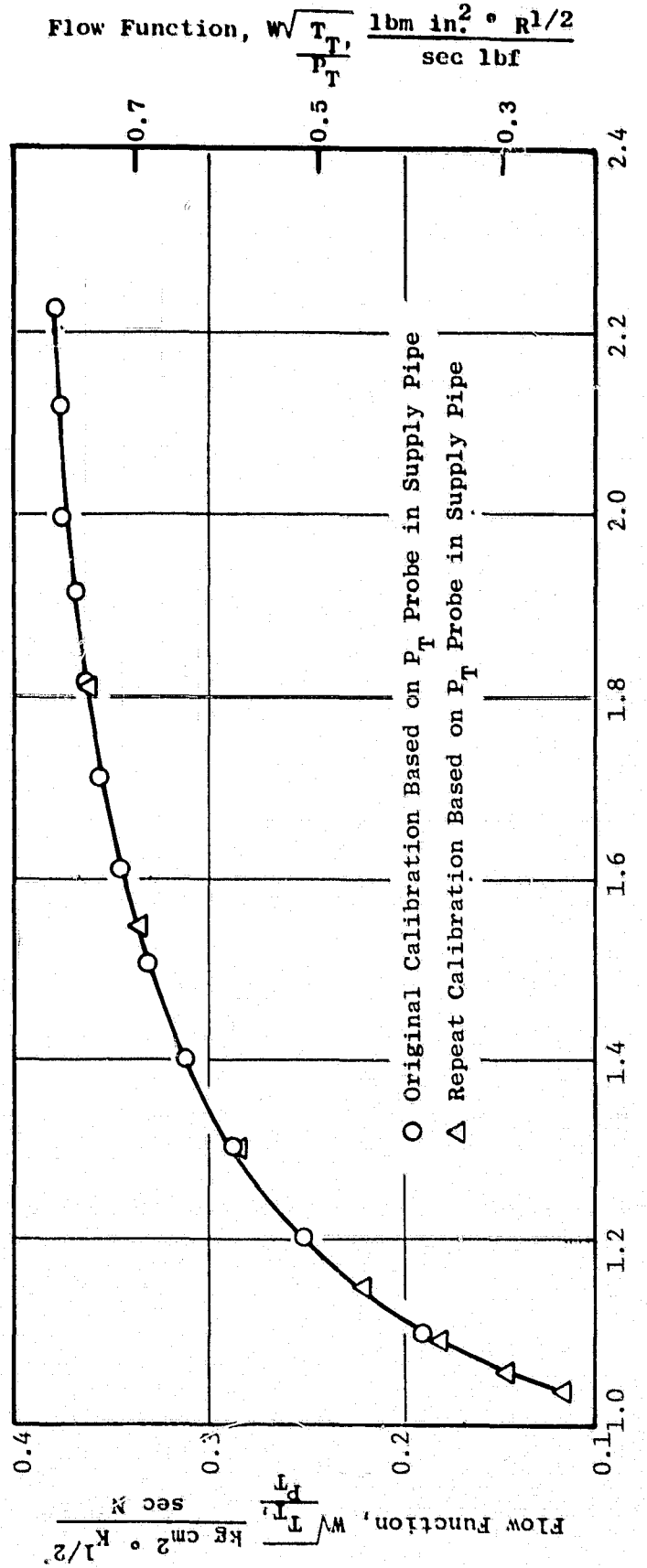

Figure 65. Comparison of Original and Repeat Flow Calibration: Production Manifold.

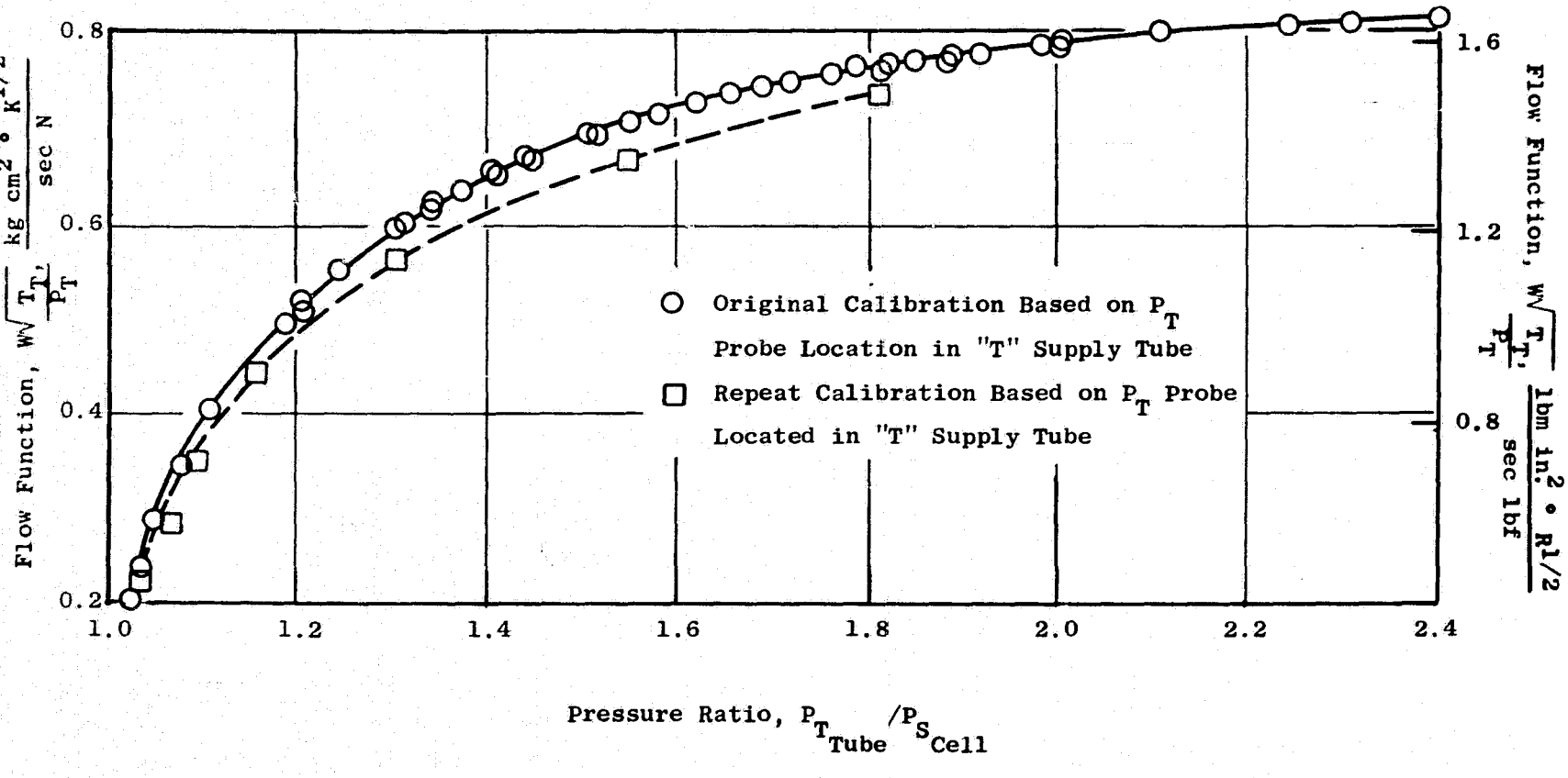

Figure 66. Comparison of Original and Repeat Flow Calibration: ACC Manifold.

Table VI. Average Radial Distance: Manifold Tube to Case Skin (mm/in.).

	Tube No. 1	Tube No. 2	Tube No. 3	Tube No. 4	Tube No. 5	Tube No. 6	Tube No. 7
Production Manifold Measured Dimension	6.48/0.255	7.49/0.295	7.16/0.282	6.53/0.257	6.43/0.253	7.09/0.279	7.24/0.285
Production Manifold Drawing Dimension	6.10/0.240	6.10/0.240	6.10/0.240	6.10/0.240	6.10/0.240	6.10/0.240	6.10/0.240
ACC Manifold Measured Dimension	6.53/0.257	7.72/0.304	7.32/0.288	7.04/0.277	7.04/0.277	N/A	N/A
ACC Manifold Drawing Dimension	4.57/0.180	4.57/0.180	4.57/0.180	4.57/0.180	4.57/0.180	N/A	N/A

Table VII. Axial Distance: Aft Side of LPT Forward Flange to Manifold Tube Centerline (mm/in.).

	Tube No. 1	Tube No. 2	Tube No. 3	Tube No. 4	Tube No. 5	Tube No. 6	Tube No. 7
Production Manifold Measured Dimension	57.10/2.248	121.26/4.774	190.04/7.482	248.54/9.785	300.30/11.823	365.46/14.408	420.10/16.539
Production Manifold Drawing Dimension	58.55/2.305	124.69/4.909	191.59/7.543	249.73/9.832	303.43/11.946	367.92/14.485	421.94/16.611
ACC Manifold Measured Dimension	60.58/2.385	121.89/4.799	192.38/7.574	247.57/9.947	302.95/11.927	N/A	N/A
ACC Manifold Drawing Dimension	61.47/2.42	124.46/4.900	194.13/7.643	249.43/9.82	305.05/12.010	N/A	N/A

from each tube. The axial shift increased the cooling effectiveness at those locations where the primary source of heat input was forward of the impingement jets and decreased the cooling effectiveness at those locations where the primary source of heat input was aft of the impingement jets. The overall effect on cooling effectiveness due to the axial shift was not as significant as that due to the radial shift.

5.4.3 Measured Performances; Sea Level Static Test

An engine core speed of 9400 rpm was chosen as the engine operating condition to simulate cruise operation during the sea level testing as it is typical of cruise operating speeds. As illustrated schematically in Figure 62, consecutive performance demonstration tests were conducted at approximately 9400 rpm core speed (3150 corrected fan speed) as the final portion of the production manifold baseline test and the intial portion of the ACC manifold test. The testing was conducted in this back-to-back fashion so that no engine deterioration would occur between the production and ACC performance demonstrations. A series of steady-state data readings were recorded during the production manifold test and multiple steady-state readings were recorded for each of several air supply valve positions (all at the same engine corrected thrust level) during the ACC tests.

Measured sfc and thrust was obtained during all readings. These data were corrected to standard day conditions: T2 = 15° C (59° F), P2 = 101.35 kPa (14.7 psi), and zero humidity. Choosing the stabilized data on an sfc versus thrust plot, the delta sfc (relative to the zero cooling flow level) was plotted versus the amount of cooling air, at a constant corrected thrust of 145,460 N (32,700 pounds). This curve was presented previously in Figure 63 which also included data from the variable flow test on the production system.

The reduction in sfc of the ACC cooling system relative to the current production system (with standard flush inlet) was approximately 0.09% at the aforementioned thrust.

5.4.4 LPT Stator Test Data and Analytical Determination of ACC System Performance Improvement

5.4.4.1 LPT Stator Test Data

A multitude of LPT stator data was obtained for a wide variety of steady-state and transient engine operating conditions. This included the acquisition of significant quantities of data from embedded and skin thermocouples which were not available prior to this program and which significantly increased the understanding of the thermal response of the LPT case. Figures 67 through 70 are plots of LPT case metal temperatures obtained during transient engine conditions (accels/decels) conducted as part of the production manifold test. Figures 71 and 72 present LPT case metal temperatures as a function of steady-state engine conditions that were obtained during the production manifold test. These data, in addition to the cooling manifold flow rates, are typical of that which were required to refine the heat transfer model of the LPT casing.

5.4.4.2 Instrumented Engine Test Data Match: LPT Case Heat Transfer Model

A detailed heat transfer computer model of the LPT case was constructed and used in conjunction with General Electric's THTD computer program. The THTD program computes transient and steady-state temperature solutions for complex problems which can include various types of heat transfer phenomena.

A portion of the THTD model corresponding to the area of the LPT case encircled on Figure 73 is depicted in Figure 74.

The methodology employed to refine the THTD model so that predicted temperatures would match measured temperatures from the engine test was as follows:

1. Various steady-state and transient operating conditions were selected for the data match. Measured LPT case temperatures corresponding to these test conditions were then plotted as a function of axial distance along the LPT case for steady-state results, and as a function of time for transient results.

2. General Electric's Turbine Design and Off-Design (TDOD) Computer Program was used to generate LPT interstage data (temperatures, pressures and velocities) corresponding to the engine conditions

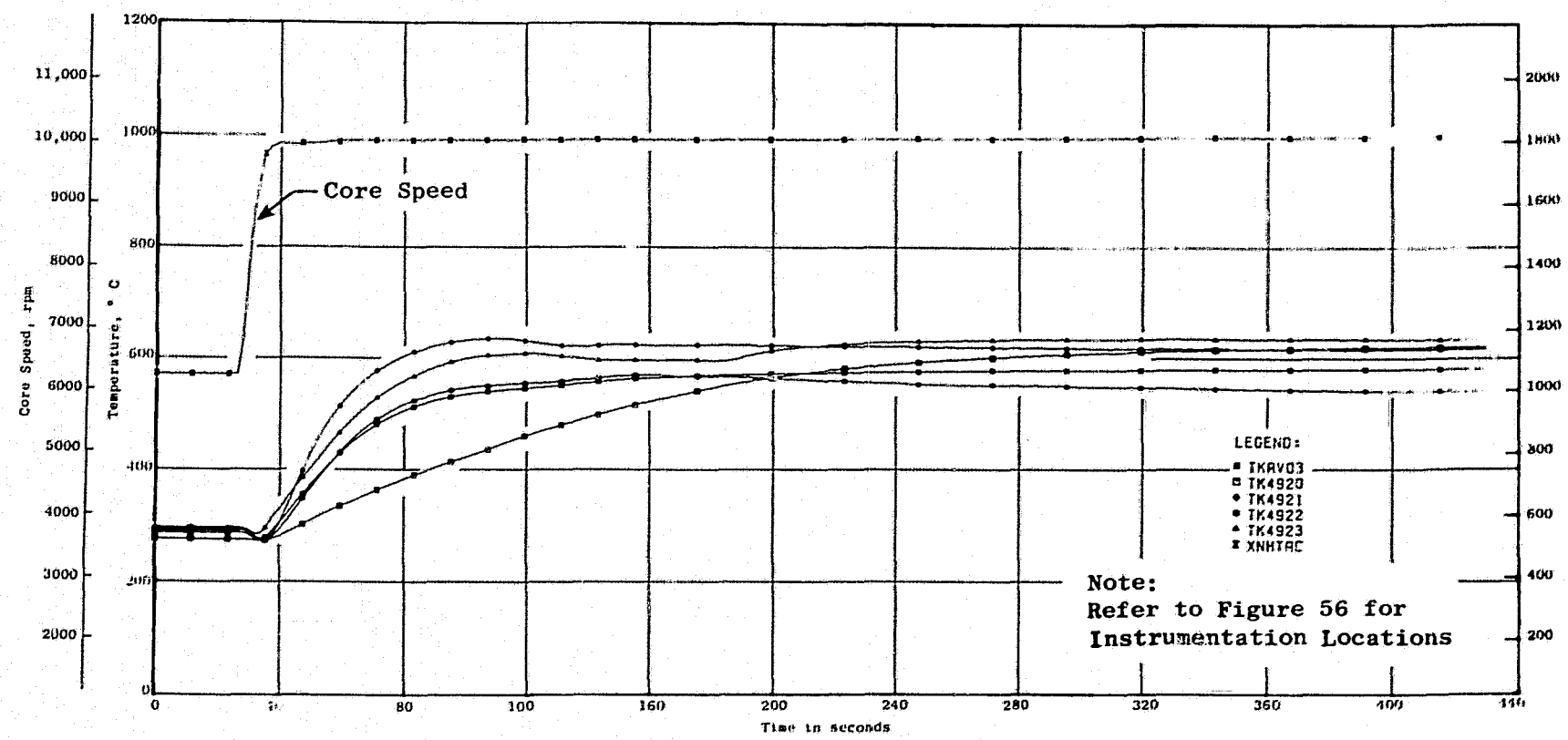

Figure 67. Measured LPT Case Surface Temperatures (Above Hook No. 1) Versus Time: Accel Ground Idle to Takeoff, Production System.

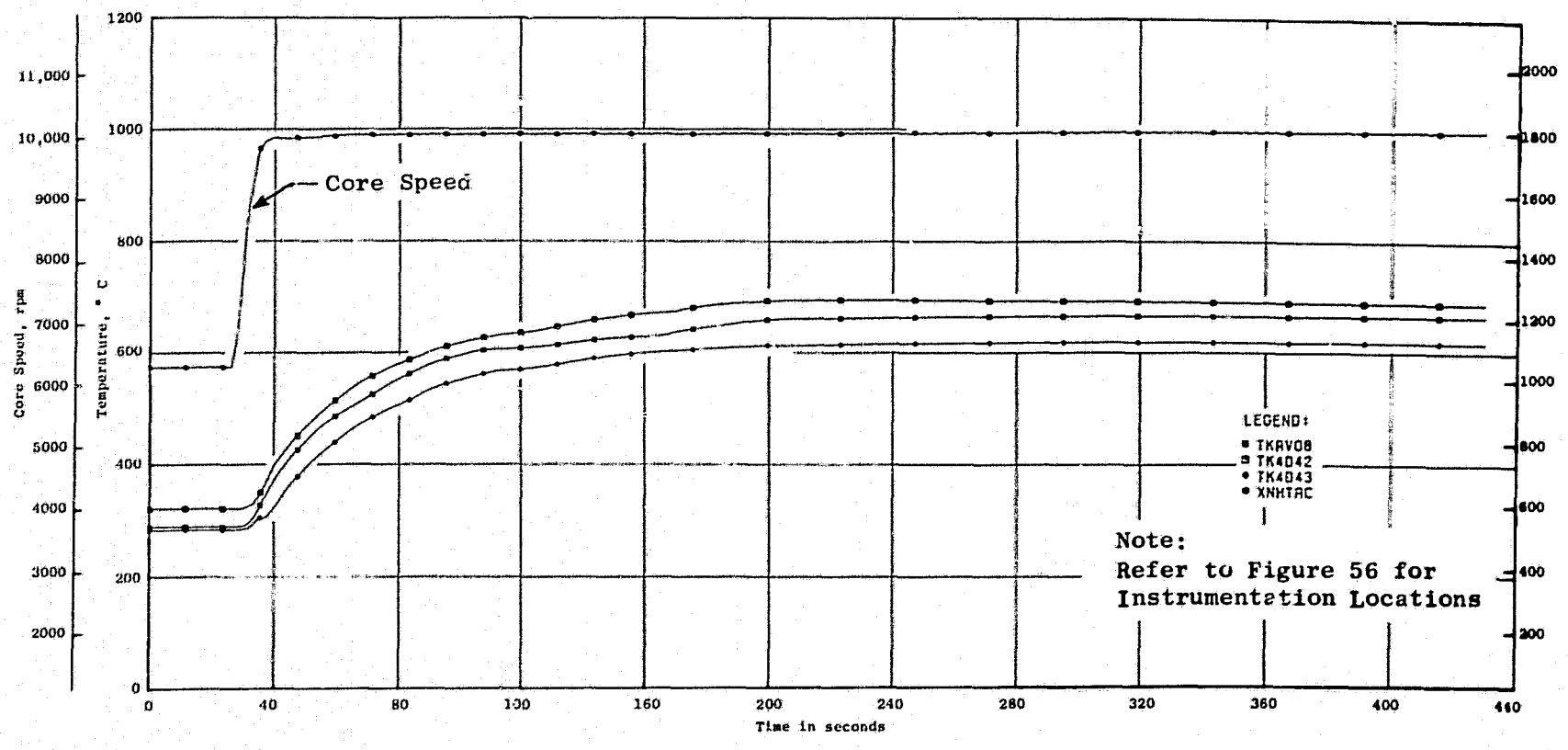

Figure 68. Measured LPT Case Temperatures (from Embedded Thermocouples in Hook No. 2) Versus Time: Accel Ground Idle to Takeoff, Production System.

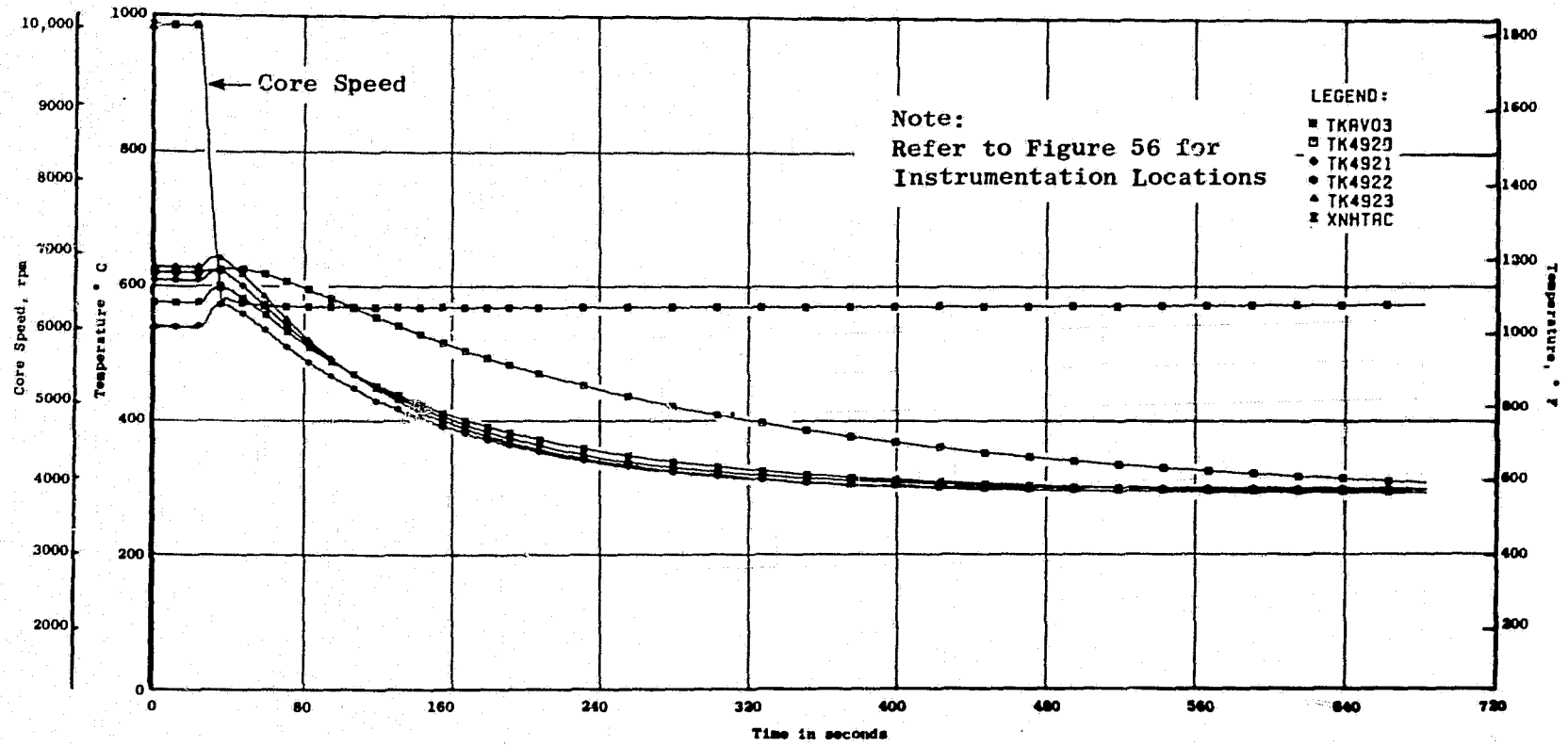

Figure 69. Measured LPT Case Surface Temperatures (Above Hook No. 1) Versus Time: Decel Takeoff to Ground Idle, Production System.

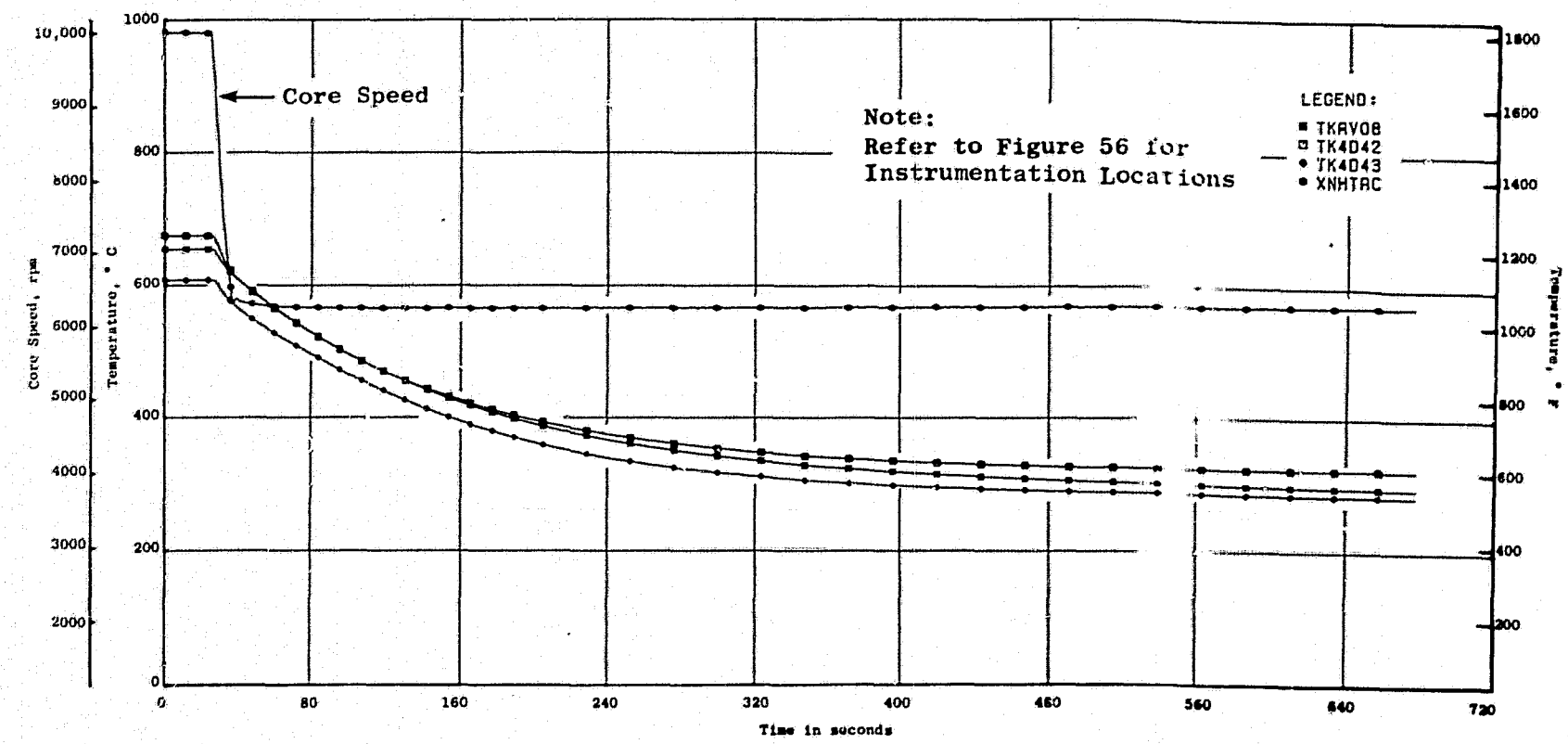

Figure 70. Measured LPT Case Temperatures (from Embedded Thermocouples in Hook No. 2) Versus Time: Decel Ground Idle to Takeoff, Production System.

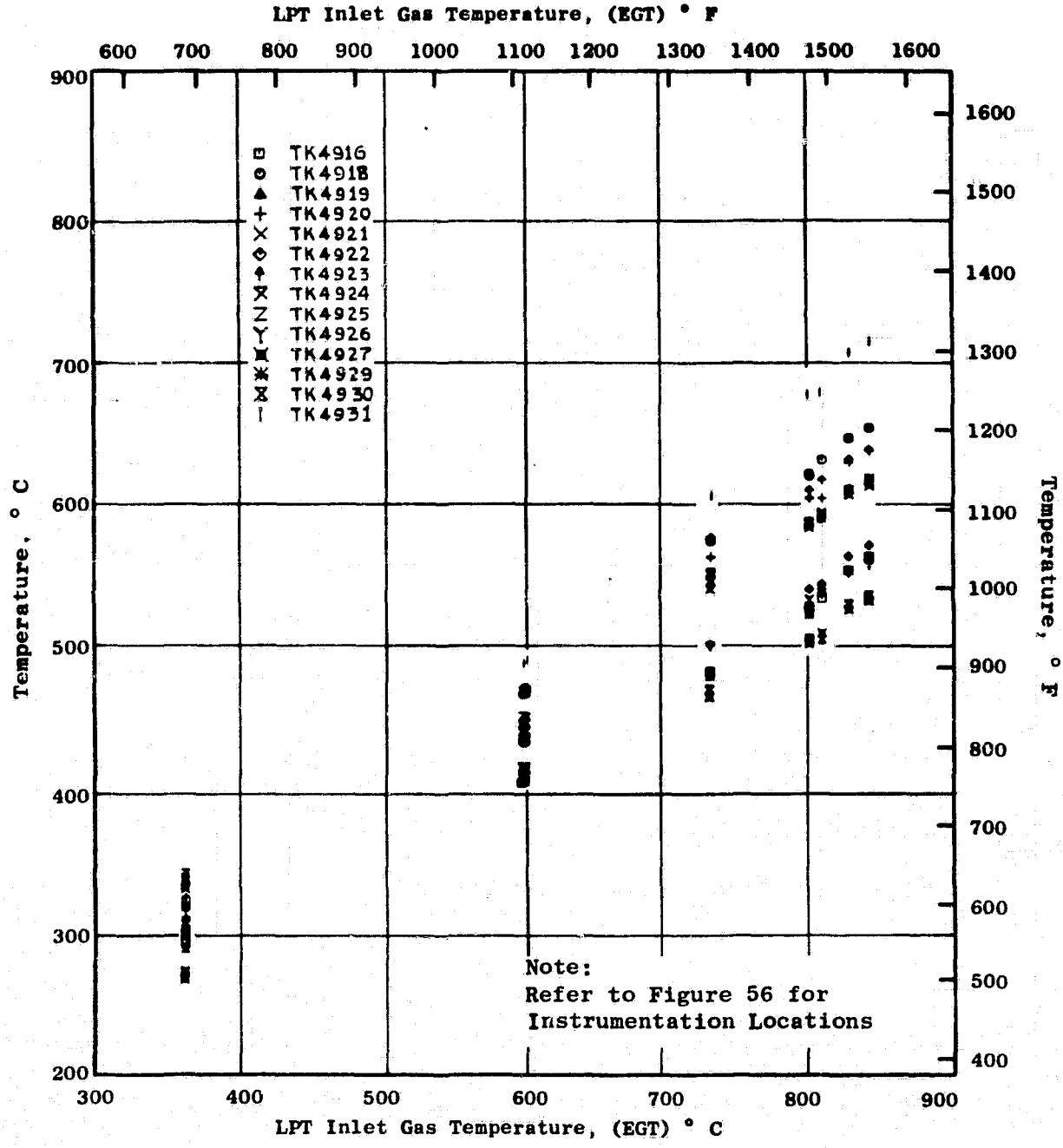

Figure 71. Measured LPT Case Surface Temperatures (Above Hook No. 1) Versus EGT: Production System.

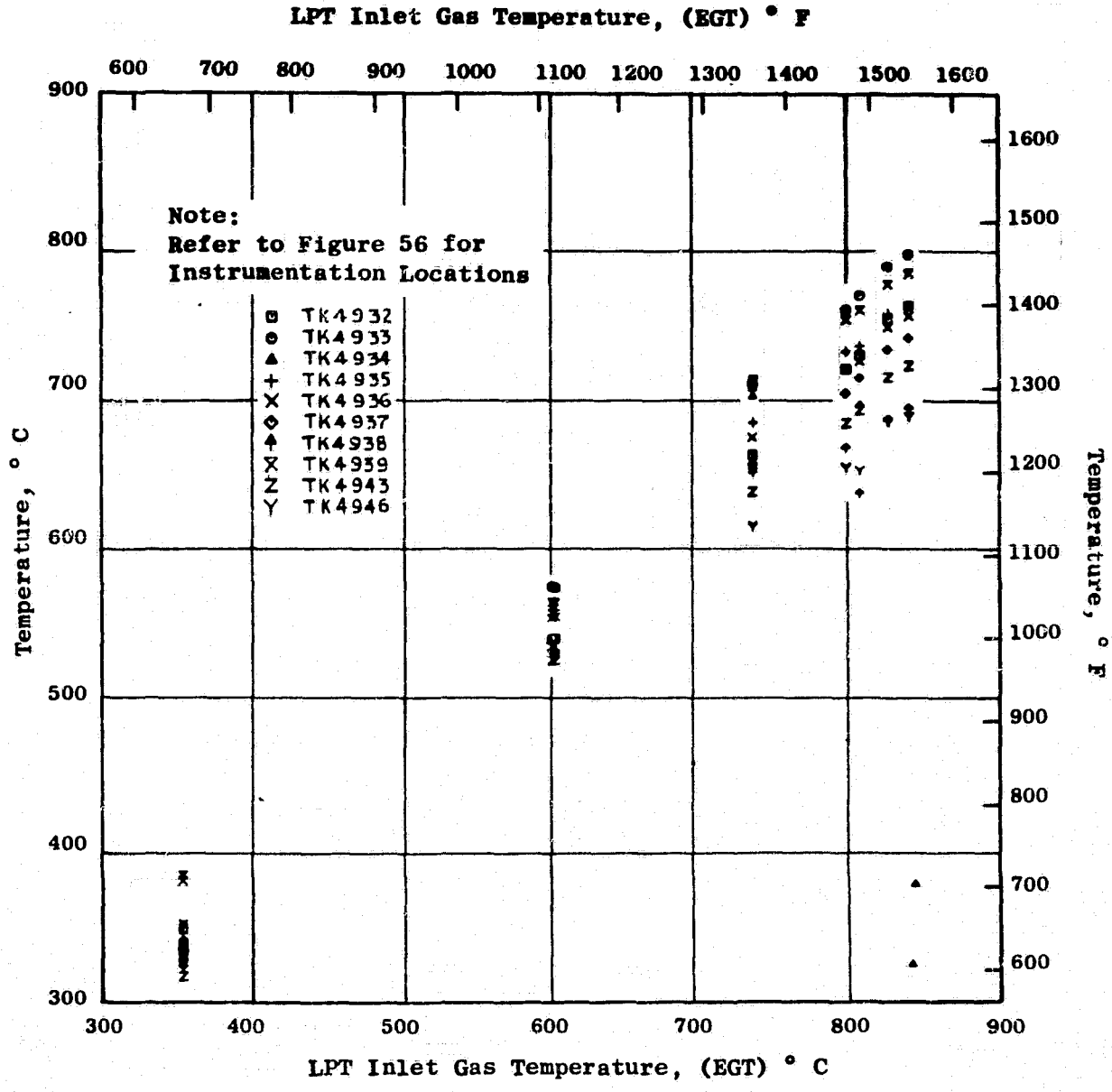

Figure 72. Measured LPT Case Temperatures (from Embedded Thermocouples in Hook No. 1) Versus EGT: Production System.

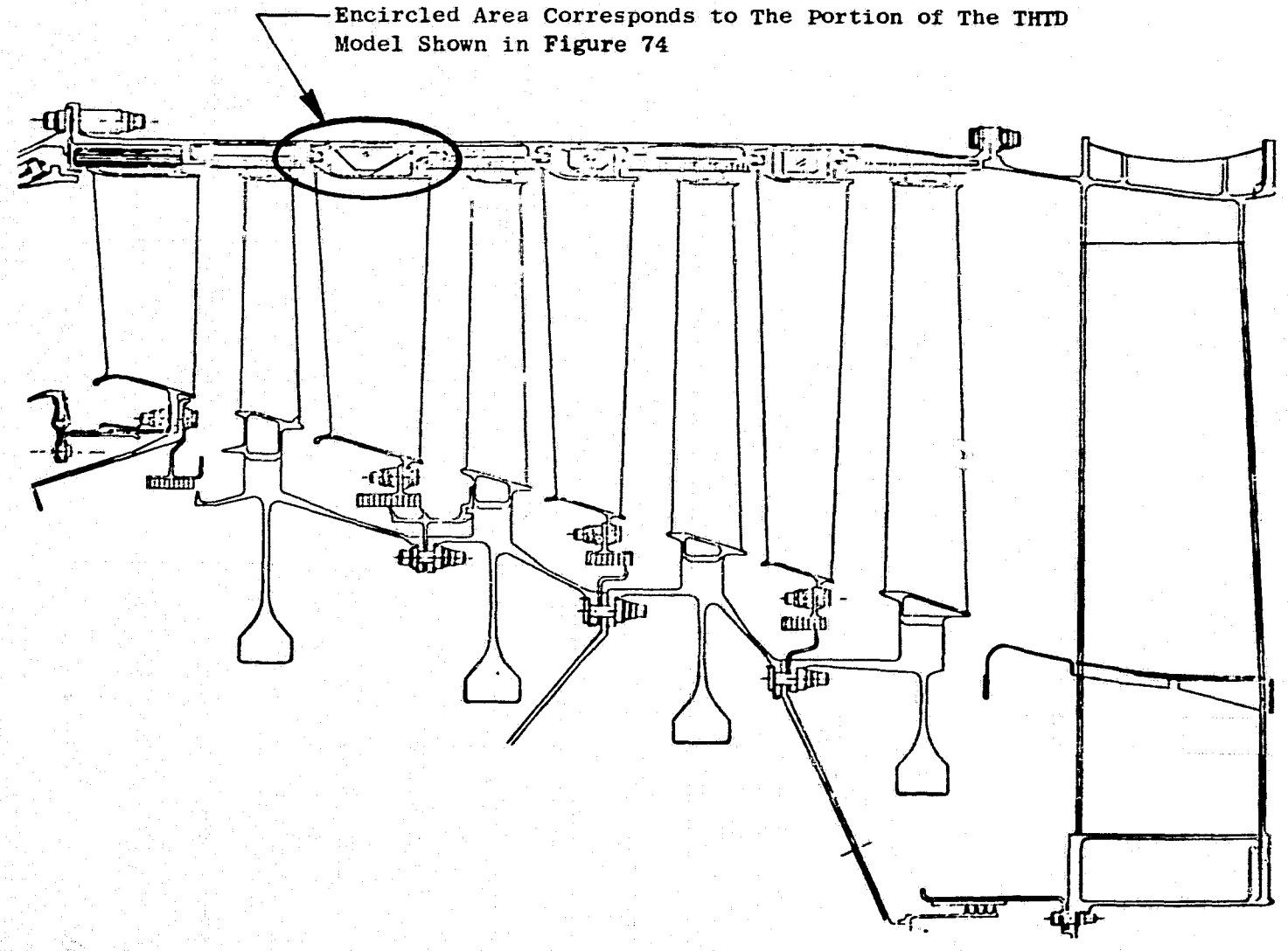

Figure 73. LPT Module Cross Section.

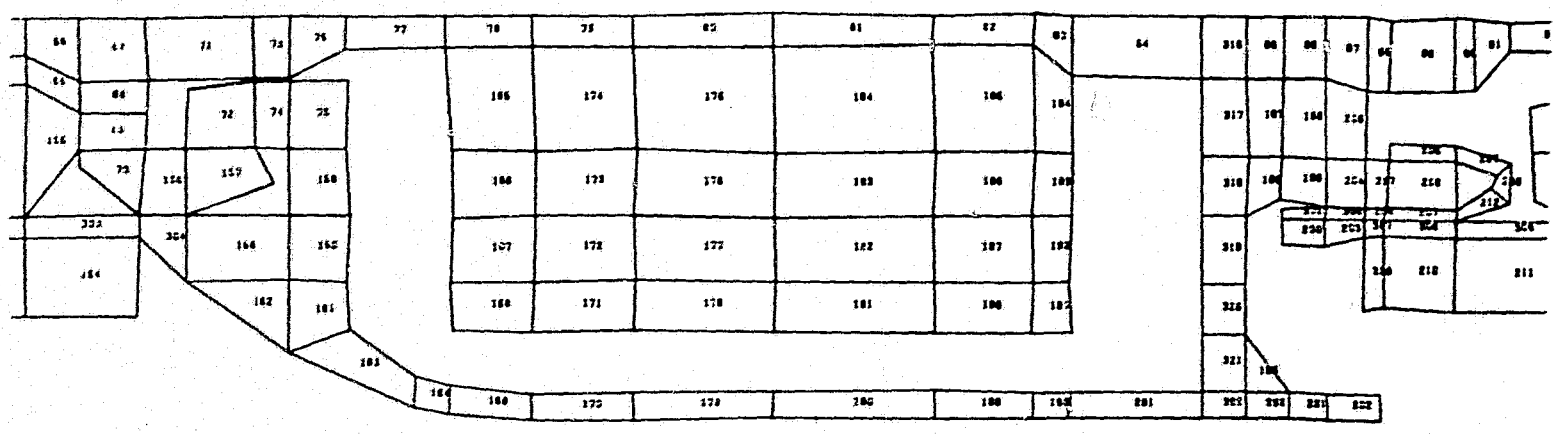

Note: This figure does not represent the entire THTD model.
Refer to Figure 73 for corresponding area of LPT stator.

Figure 74. THTD Model of LPT Case.

selected for the data match. This interstage data was used to generate input boundary conditions to the LPT case THTD computer program.

3. The external case heat transfer coefficients due to the impingement cooling air were established using an empirical relationship derived during a company-funded test program. This empirical relationship defines impingement heat transfer coefficients as a functions of Reynolds number (which includes impingement velocity effects), air temperature effects, cooling hole size and circumferential spacing, and radial distance from cooling hole to impingement surface. The results of the dimensional checks conducted on both manifolds were incorporated into the calculation of the external heat transfer coefficients. These coefficients were then incorporated into the THTD model for both systems.

4. The external heat transfer coefficients calculated for the production manifold were applied, then the internal case heat transfer coefficients (in the areas surrounding the various case hooks and inside the cavities above the shrouds and nozzles) were adjusted until the predicted temperatures matched the measured temperatures obtained during the production manifold testing. This matching was accomplished for both steady-state and transient results.

   Figures 75 and 76 illustrate the steady-state temperature data matches by comparing measured and predicted LPT case skin temperatures, as a function of axial distance along the case, for the sea level static (SLS) simulated cruise and takeoff conditions. Figures 77 through 79 depict the transient temperature data match by comparing measured and predicted skin temperatures above the first three case shroud/nozzle support hooks for an accel from SLS ground idle to takeoff. As illustrated in Figures 75 through 79, an excellent data match was obtained.

5. Next, the THTD model was revised to predict the measured case temperatures from the ACC manifold testing. The internal heat transfer coefficients obtained from the production manifold data match were held constant. The external heat transfer coefficients, corresponding to the ACC flow rates for each tube, were then applied to the model and predicted temperatures were calculated. Figure 80 compares predicted and measured temperatures at the SLS simulated cruise conditions. As shown in this figure, the data match was not good in the areas above the forward case hooks. Even after the model was adjusted to account for the measured radial and axial positions of the tubes (as opposed to positions per drawing requirements) and differences in radiation effects due to the increased size of the forwardmost tube, the data match was not satisfactory.

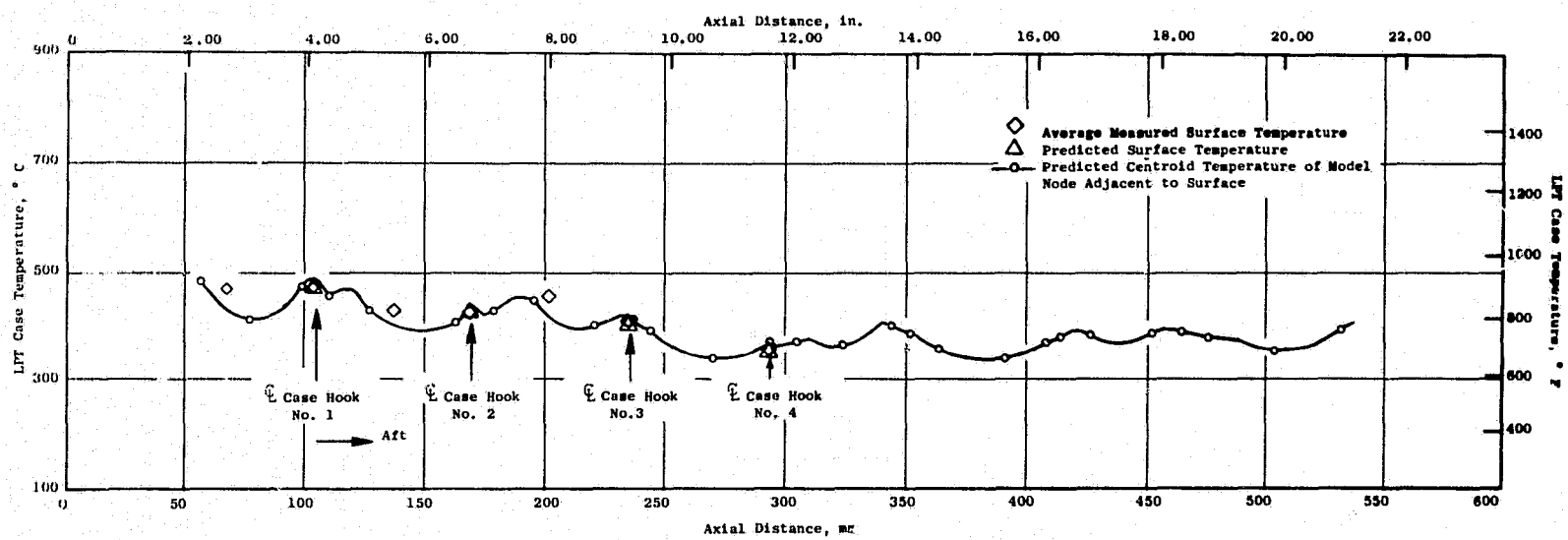

Figure 75. Steady-State Data Match: SLS Takeoff, Production System.

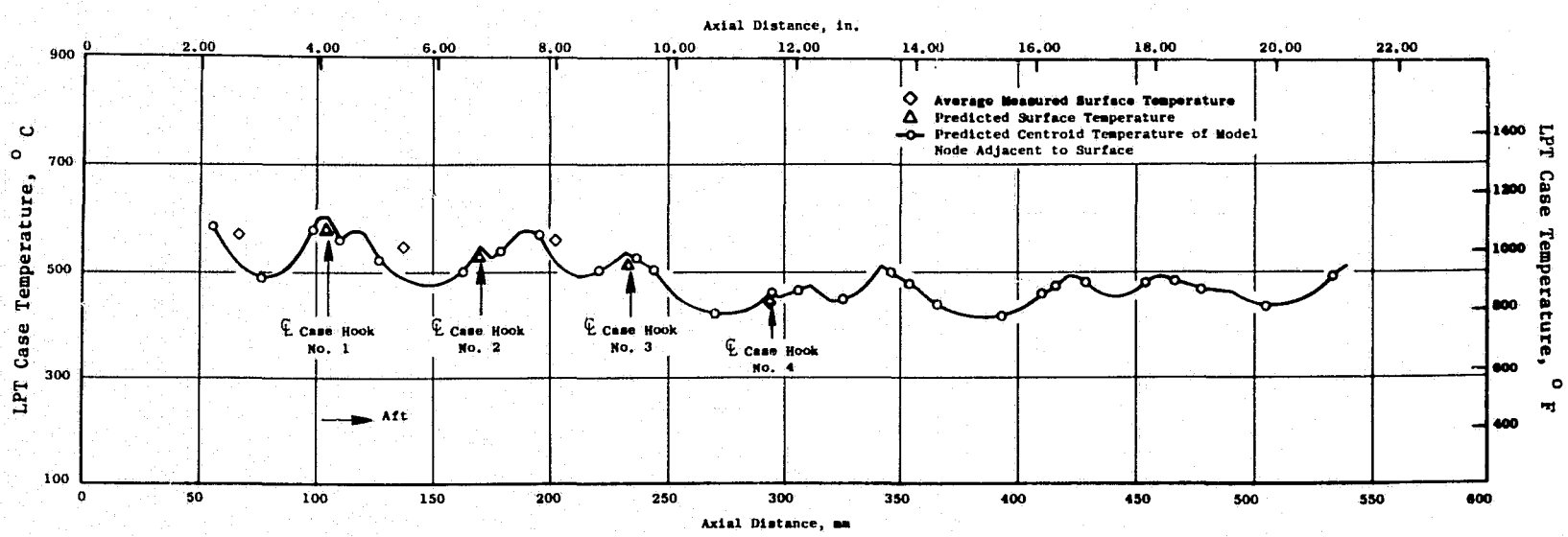

Figure 76. Steady-State Data Match: SLS Simulated Cruise, Production System.

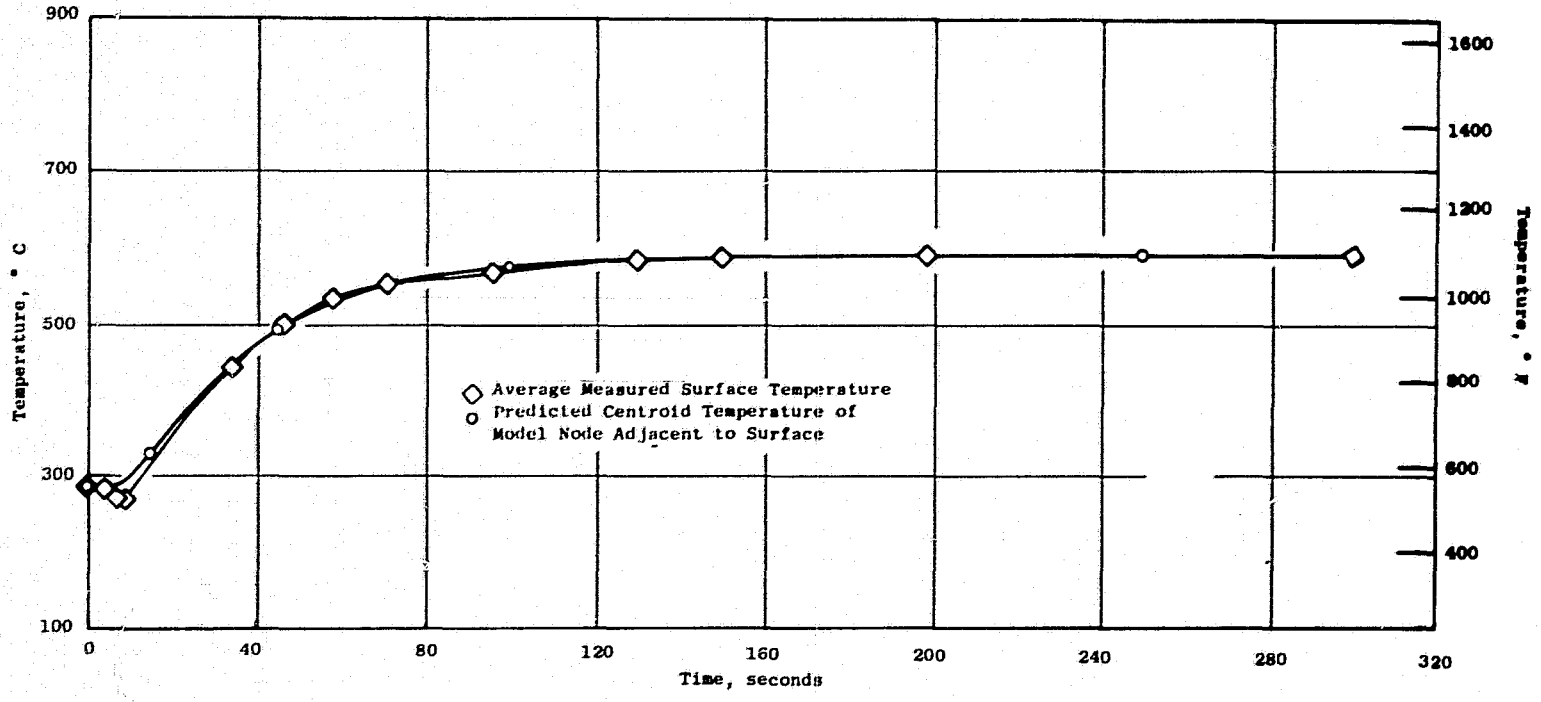

Figure 77. Transient Data Match: Accel Ground Idle to Takeoff, Hook No. 1, Production System.

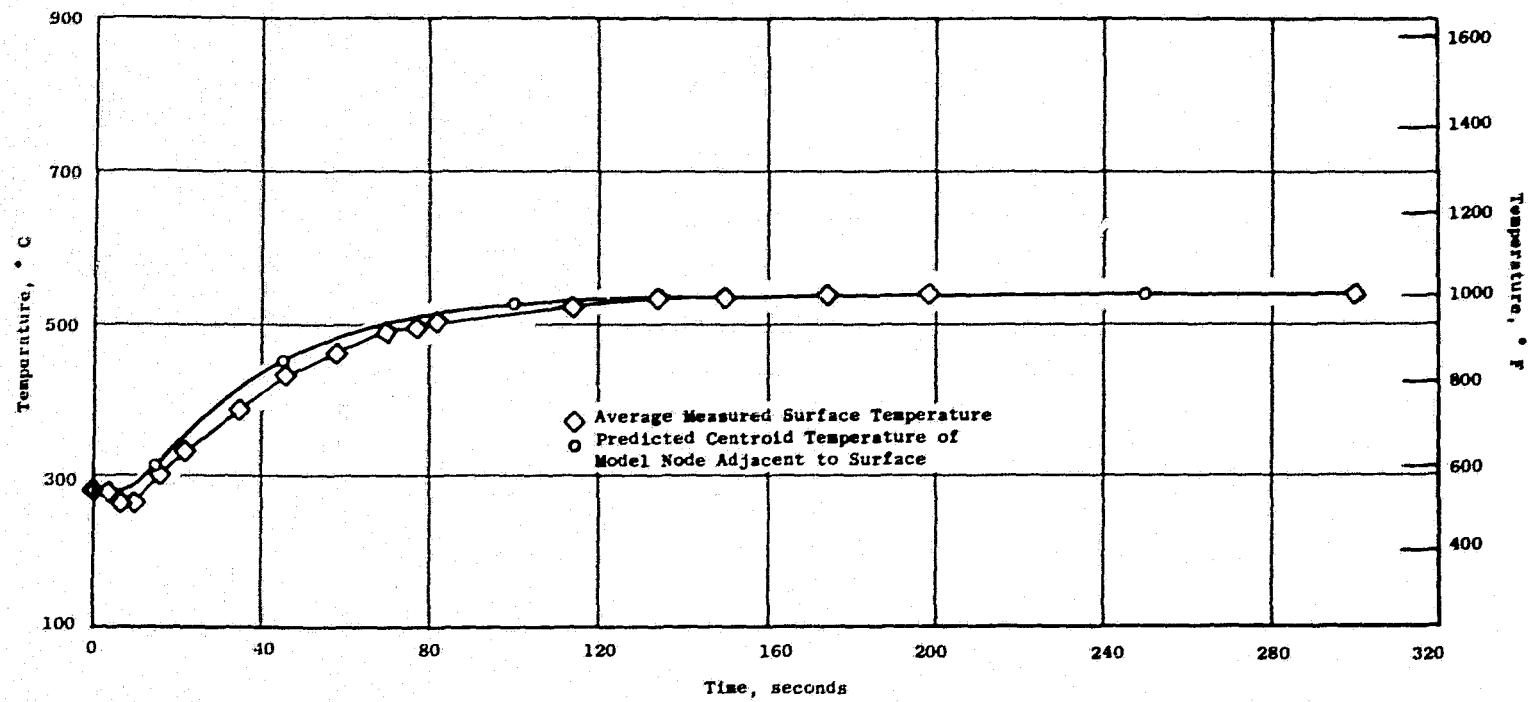

Figure 78. Transient Data Match: Accel Ground Idle to Takeoff, Hook No. 2, Production System.

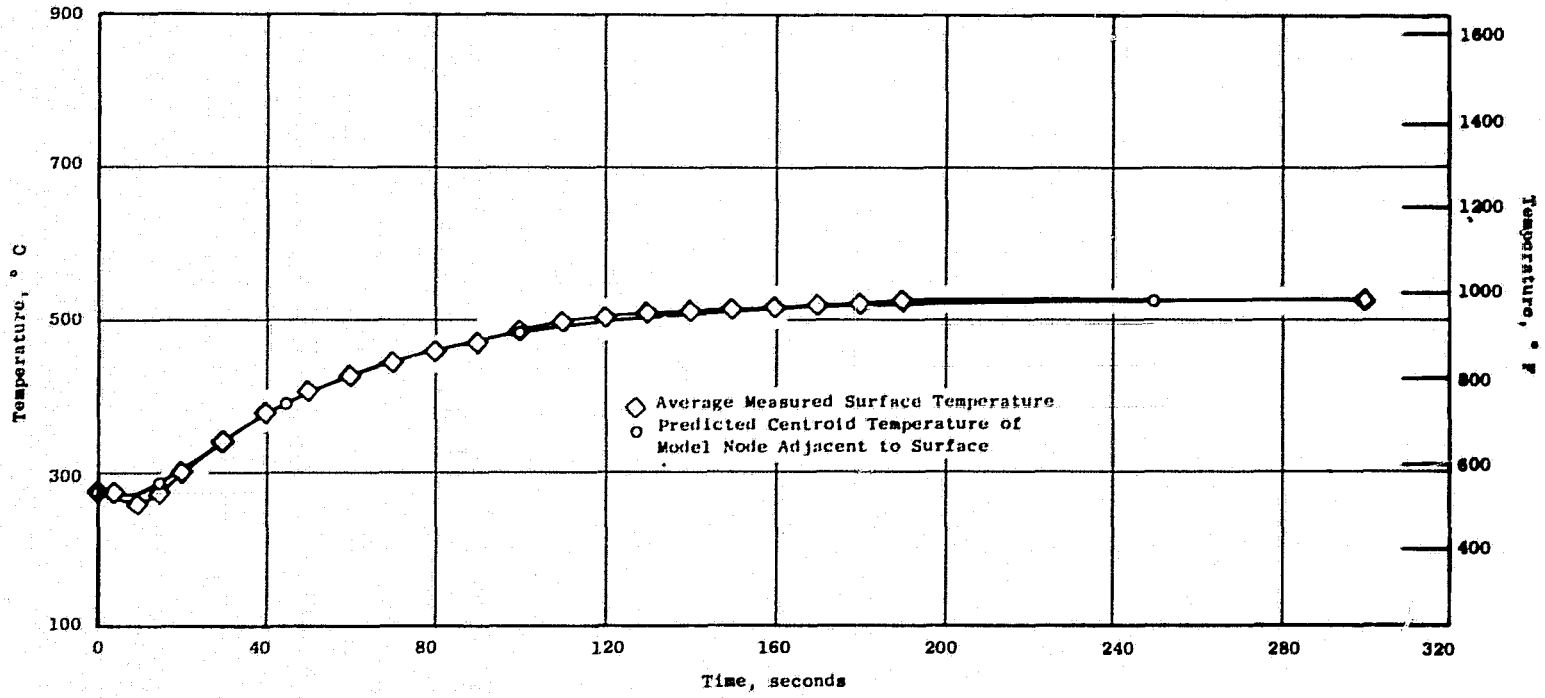

Figure 79. Transient Data Match: Accel Ground Idle to Takeoff, Hook No. 3, Production System.

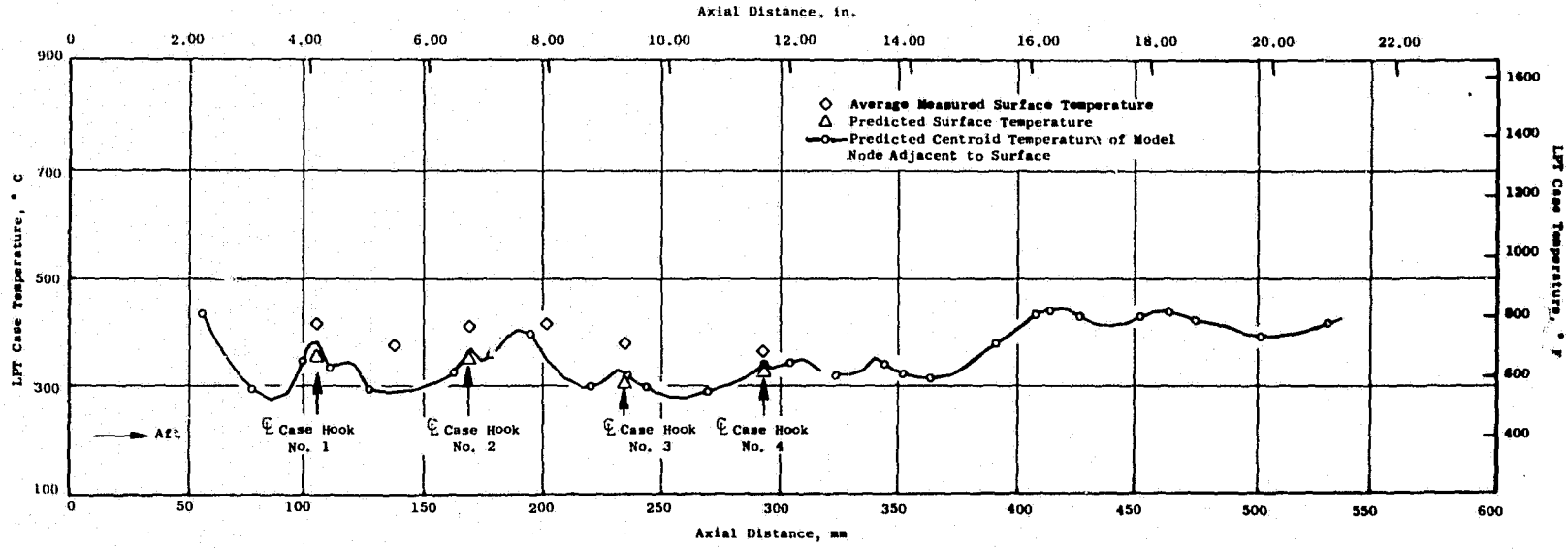

Figure 80. Steady-State Data Match: SLS Simulated Cruise, ACC System, Ideal Model.

To obtain a good data match the model was adjusted by arbitrarily changing the external heat transfer coefficients in order to force agreement with measured and predicted temperatures. Figure 81 shows the forced match at SLS simulated cruise. Subsequent sections of this report will discuss predicted temperatures, clearances, and performance deltas at altitude conditions. Any altitude predictions obtained using the ACC data matched model will be referred to as the "forced" case.

Any altitude predictions obtained with the ACC model which was not forced to match the data will be referred to as the "ideal" case. Although the differences between the forced and ideal case cannot presently be explained, it is felt that the ideal case is achievable since the same techniques for predicting the external heat transfer coefficients for the production manifold should also apply for the ACC manifold.

A significant outgrowth of this data matching process was that the internal heat transfer coefficients, at high power SLS settings and other engine power settings resulting in high cycle pressures, were significantly different than those assumed at the inception of this program.

5.4.4.3 Postdata-match Temperature Predictions

After successfully completing the instrumented engine test data match, the THTD model was used with confidence to accurately predict LPT case temperatures at various engine operating conditions of interest. One of the operating conditions selected was a 35,000 feet, 0.8 Mach number, cruise case which was chosen for definition of the delta engine performance of the ACC system relative to the production system.

Measured relationships between known engine cycle parameters (fan discharge pressure) and manifold flow governing parameters (supply pipe pressure) were used in conjunction with the manifold flow function curves to calculate the flows at altitude cruise.

Figures 82 through 84 depict predicted LPT case surface temperatures at cruise as a function of distance along the case for the production system and both the forced and ideal ACC systems. It should be noted that the ACC system predictions reflected radial distances between the tubes and case consistent with drawing requirements instead of those measured. This is justified since the desired radial spacings should be achievable with improved quality control during the manufacturing cycle.

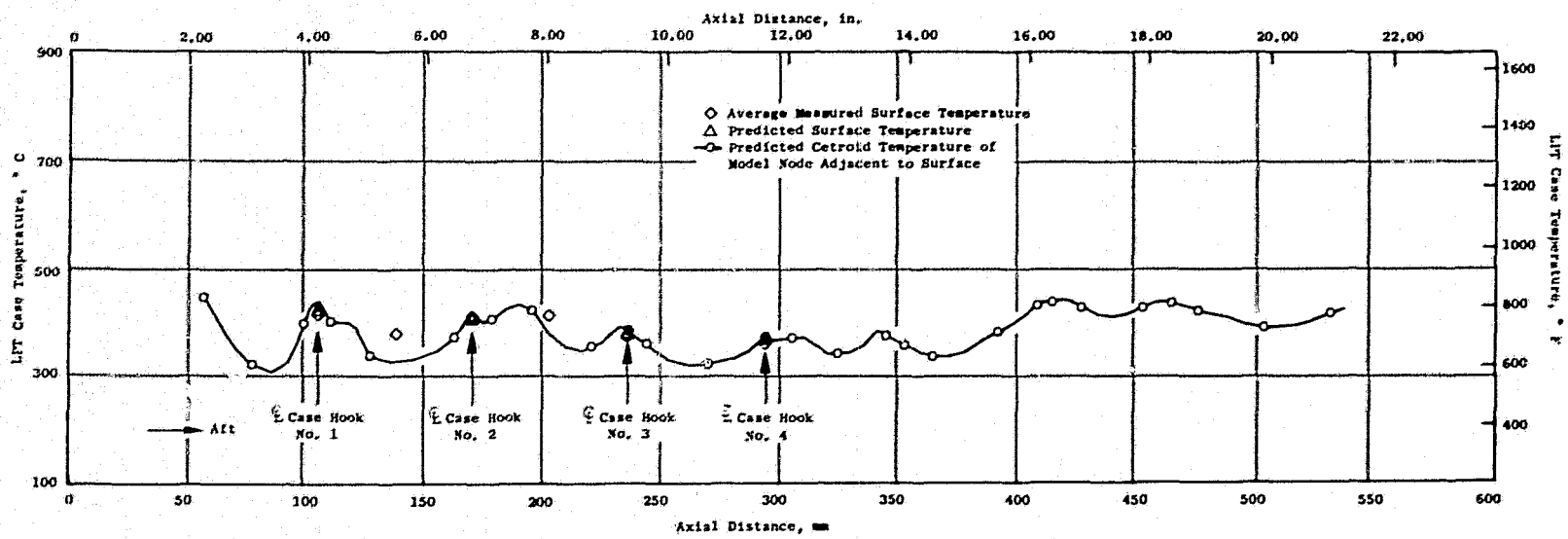

Figure 81. Steady-State Data Match: SLS Simulated Cruise, ACC System, Forced Model.

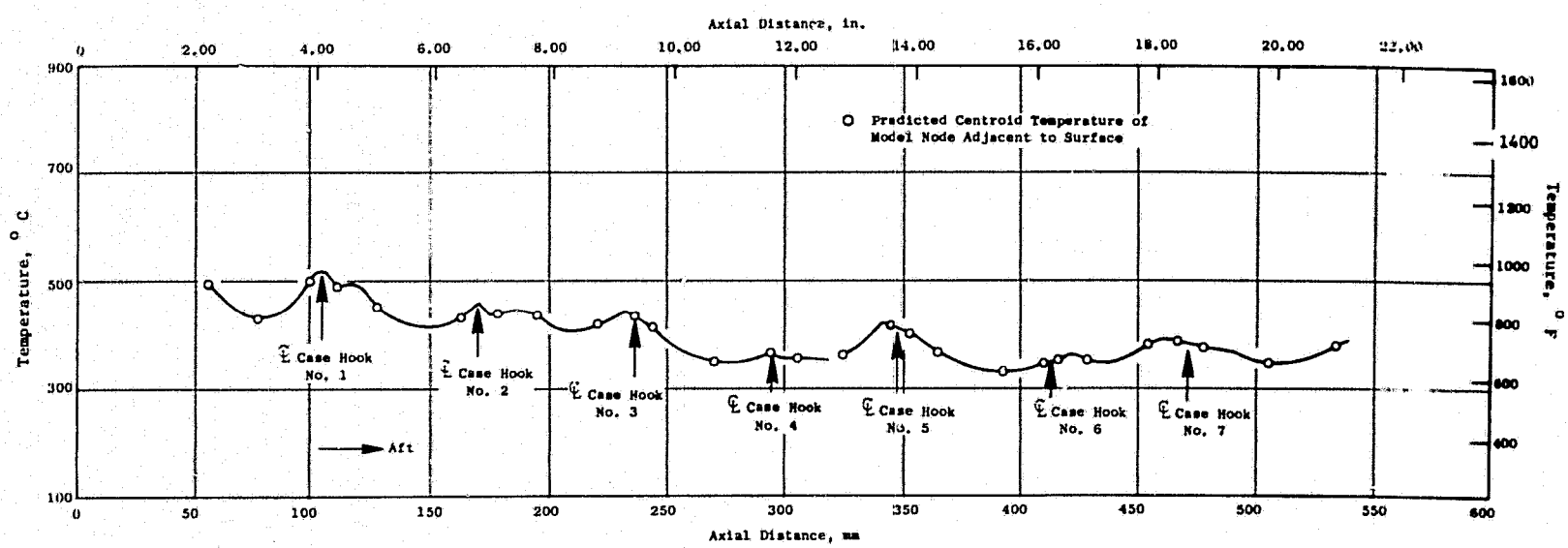

Figure 82. Predicted LPT Case Surface Temperatures: Altitude Cruise, Production System.

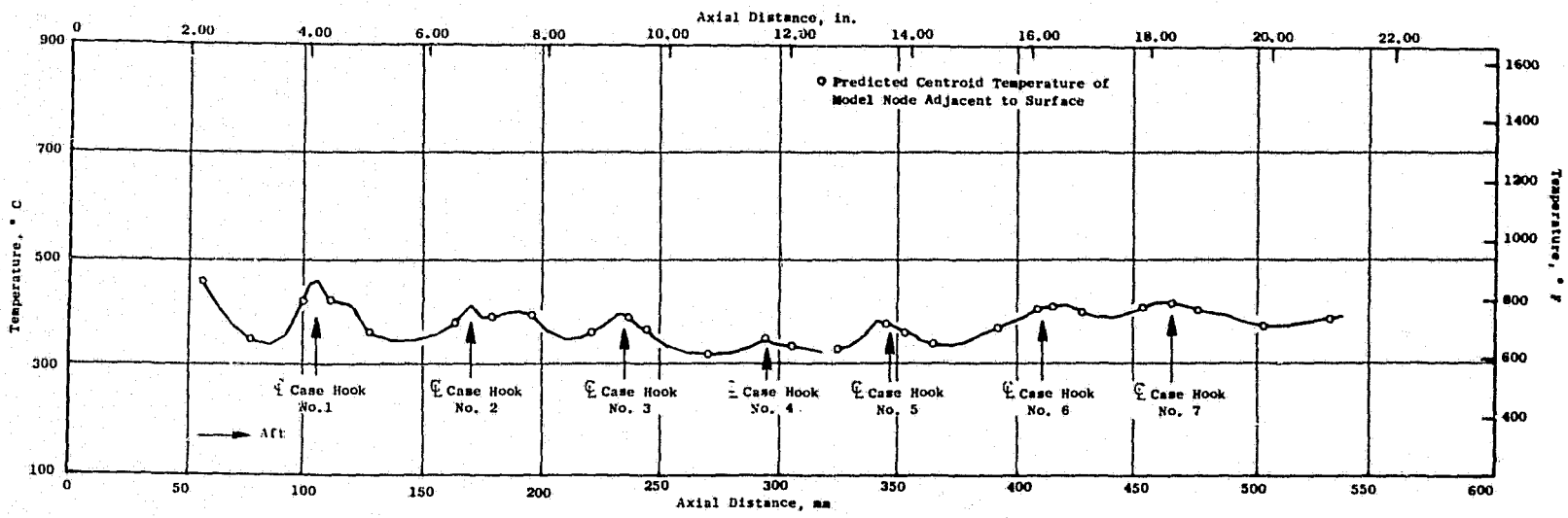

Figure 83. Predicted LPT Case Surface Temperatures: Altitude Cruise, ACC System, Forced Model.

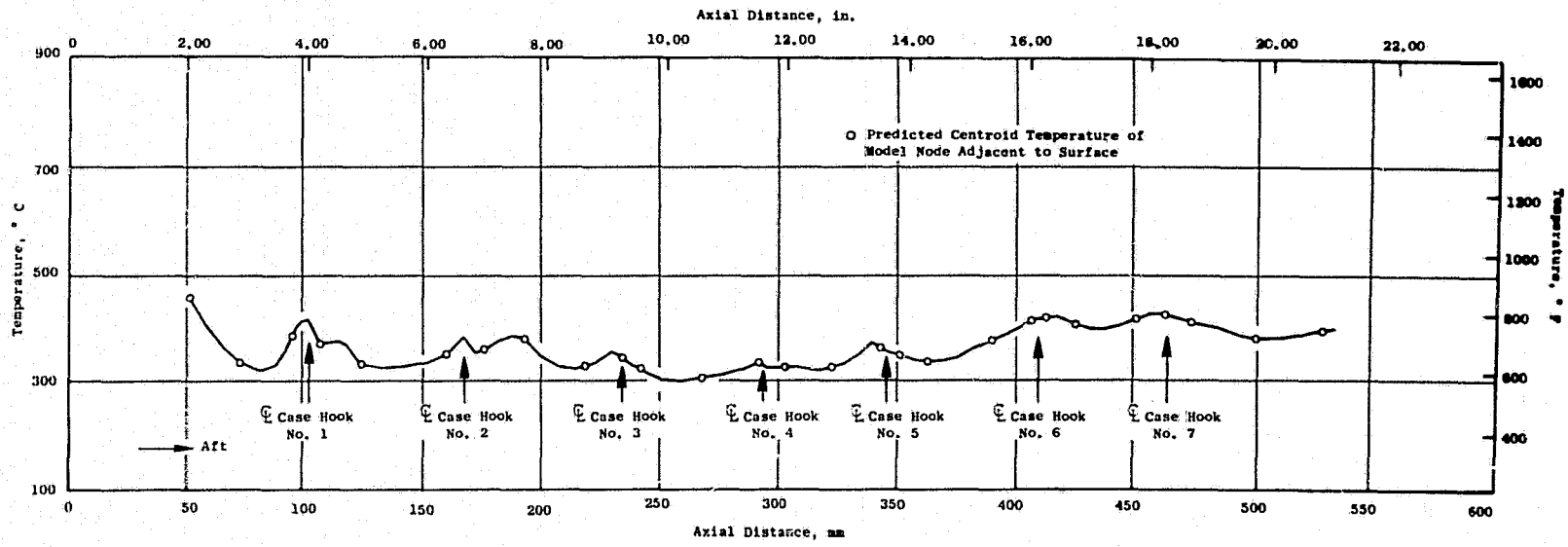

Figure 84. Predicted LPT Case Surface Temperatures: Altitude Cruise, ACC System, Ideal Model.

5.4.4.4 Analytical Definition of the Delta Clearances

A CLASS/MASS computer model of the LPT case, shown in Figure 85, was used to determine the deflections of LPT case shroud/nozzle support hooks for both the production and ACC systems. The CLASS/MASS program can be used for stress and deflection analysis of rotationally symmetric shell structures such as the LPT case.

Case temperatures, as predicted by the THTD model, and internal pressures and hook loads imparted to the case due to nozzle aerodynamic loads (obtained from the TDOD program) were used as input to the CLASS/MASS program.

The change in case deflections of the ACC system relative to the current production system are presented in Tables VIII and IX for the SLS simulated cruise and altitude cruise conditions respectively. Table VIII also provides the delta case deflections of the production system with the ACC fan air scoop installed relative to the production system with the standard flush inlet at the SLS simulated cruise condition. This comparison was included since the corresponding delta performance is used in the following section to help illustrate the match between measured and predicted performance deltas at the SLS simulated cruise condition.

For the purposes of calculating delta performance, presented in the following section, delta case deflections are assumed to be equivalent to delta clearances since the rotor position is the same for both the production and ACC systems. However, this assumption is only valid if the clearances existing with the production system are equal to or greater than the delta deflections due to the ACC system. This concept will be discussed further in Chapter 5.4.7 of this report.

5.4.5 Predicted Altitude Cruise Delta Performance

The cruise performance of the ACC system relative to the production system was assessed at a flight Mach Number of 0.8 at an altitude of 10.67 km (35,000 feet). The delta performance was obtained by using CF6-50C2 cycle partial derivatives in conjunction with previously published clearance derivatives (Reference 3) and the predicted LPT clearances presented previously in Table IX.

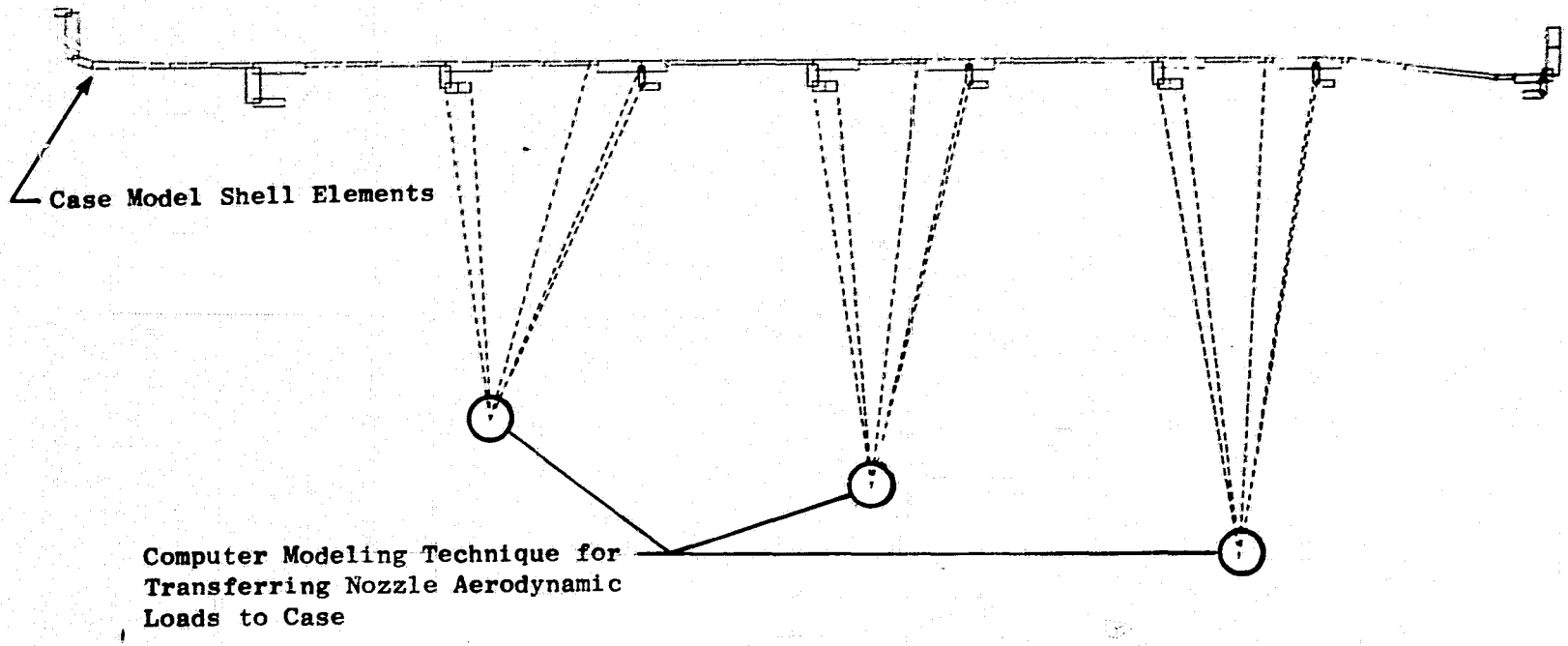

Figure 85. LPT Case CLASS/MASS Model.

Table VIII. Predicted SLS Delta Clearances and Performances Relative to the Production System with Standard Flush Inlet.

	Location[1]	Δ Clearance of ACC Forced System (mm/in.)	Δ Clearance of Production System With Scoop Installed (mm/in.)
1.	Stage 1 Rotor	-0.432/-0.017	-0.305/-0.012
	Stage 2 Seal	-0.305/-0.012	-0.330/-0.013
	Stage 2 Rotor	-0.229/-0.009	-0.330/-0.013
	Stage 3 Seal	-0.152/-0.006	-0.279/-0.011
	Stage 3 Rotor	+0.178/+0.007	-0.152/-0.006
	Stage 4 Seal	+0.356/+0.014	-0.203/-0.008
	Stage 4 Rotor	+0.178/+0.007	-0.076/-0.003
2.	System Flowrate[2] (Kg/sec/lb/sec)	0.276 0.607	0.159/0.350
3.	Net Δsfc[3] (%)	-0.079	-0.149

Notes:
1. Refer to Figure 86 for location of clearance in LPT module
2. Production system (with standard flush inlet) flow rate is 0.114 kg/sec (0.250 lb/sec)
3. Includes effects of changes in clearances, effects of additional air used and the effect of the scoop.

Table IX. Predicted Altitude Cruise Delta Clearances and Performances Relative to the Production System with Standard Flush Inlet.

	Location[1]	Δ Clearance of ACC Forced System (mm/in.)	Δ Clearance of ACC Ideal System (mm/in.)
1.	Stage 1 Rotor	-0.457/-0.018	-0.787/-0.031
	Stage 2 Seal	-0.356/-0.014	-0.711/-0.028
	Stage 2 Rotor	-0.254/-0.010	-0.533/-0.021
	Stage 3 Seal	-0.178/-0.007	-0.330/-0.013
	Stage 3 Rotor	+0.152/+0.006	+0.076/+0.003
	Stage 4 Seal	+0.457/+0.018	+0.457/+0.018
	Stage 4 Rotor	+0.203/+0.008	+0.203/+0.008
2.	System Flowrate[2] (Kg/sec/lb/sec)	0.175/0.385	0.175/0.385
3.	Net Δsfc[3] (%)	-0.019	-0.146

Notes:
1. Refer to Figure 86 for location of clearance in LPT module
2. Production system (with standard flush inlet) flow rate is 0.074 kg/sec (0.164 lb/sec)
3. Includes effects of changes in clearances, effects of additional air used and the effect of the scoop.

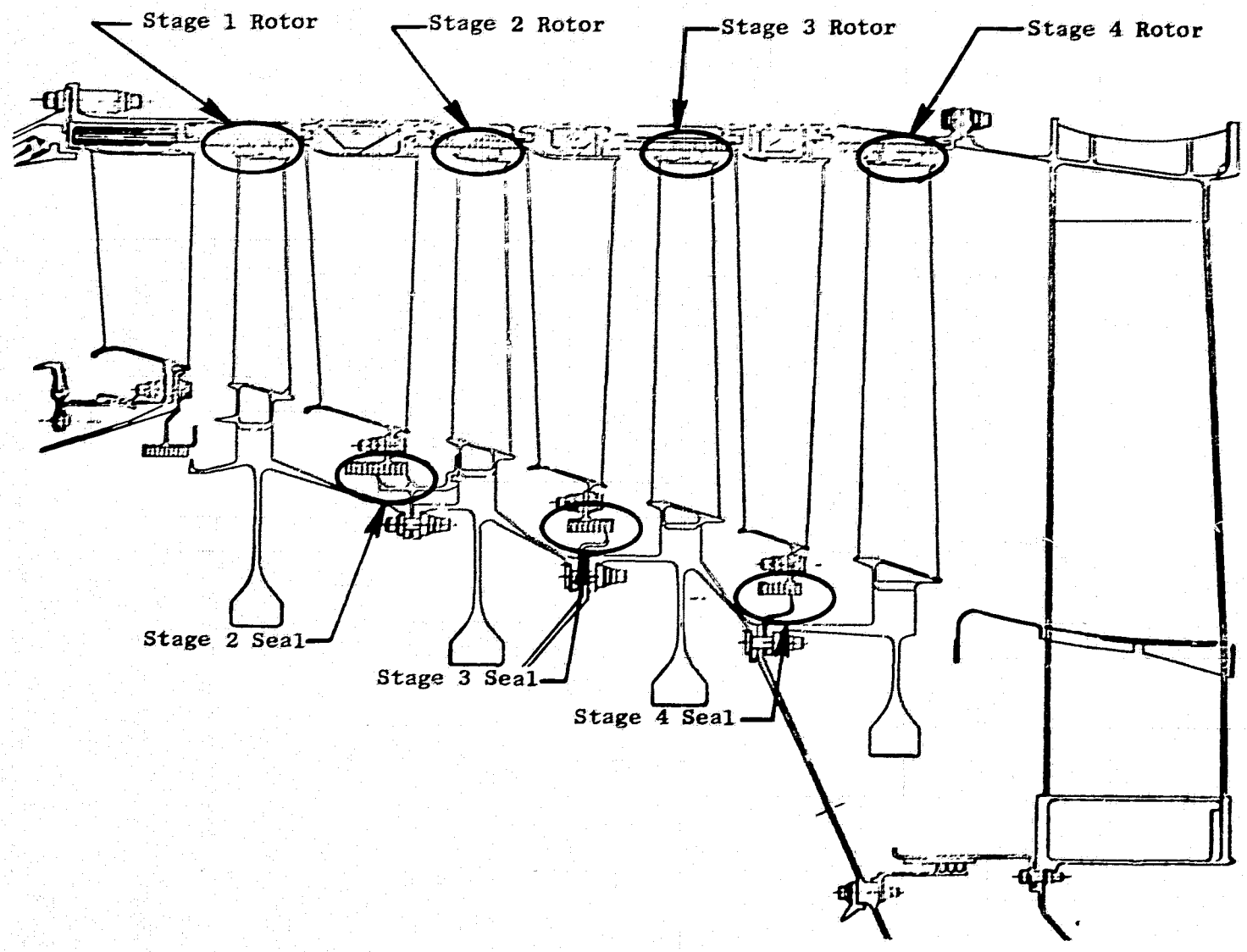

Figure 86. Location of LPT Rotor/Stator Clearances.

To confirm the accuracy of the various performance derivatives, performance stack-ups were made which included all effects on the engine cycle of the production system with standard flush inlet, the production system with the ACC system fan air scoop installed and the ACC system relative to the no-cooling-flow condition at the tested SLS simulated cruise engine operating condition. As shown in Figure 87, an excellent match was obtained between measured and predicted performance deltas. Table VIII presented the predicted SLS simulated cruise sfc reductions of the ACC system and the production system with scoop installed relative to the production system with the standard flush inlet.

The altitude cruise performance comparison of the ACC and production systems (as well as the SLS comparison) utilized cycle deck derivatives for the effects of the increased cooling flow, the fan air scoop pressure loss and the increased LPT efficiency on sfc. The air scoop pressure loss was calculated from its estimated drag coefficient. The efficiency-versus-clearance derivatives used in each stage were the same as those used in the SLS performance stackup. Table IX presented the delta sfc obtained by using predicted ACC system case temperatures (and subsequent clearances) resulting from a THTD model which was forced to match the SLS test data. Table IX also presented the delta sfc obtained by using predicted case temperatures (clearances) from the ideal (believed achievable) THTD model.

The predicted sfc reduction of 0.019 percent for the ACC forced system, as shown in Table IX, means that there is essentially no benefit from using the ACC system at altitude cruise if the forced (demonstrated) model temperatures are realized. Even though the magnitude of the clearance changes are approximately the same as those for the SLS simulated cruise conditions, the lack of any benefit is primarily due to the fact that the fan bleed-air penalty is much greater and the LPT efficiency-versus-sfc derivative is weaker at altitude as compared to the SLS condition.

Table IX also shows that if the temperature and clearance reductions of the ideal system can be achieved, an improvement of 0.146 percent Δsfc can be realized. It is important to note that the ideal case does not imply an optimized cooling system.

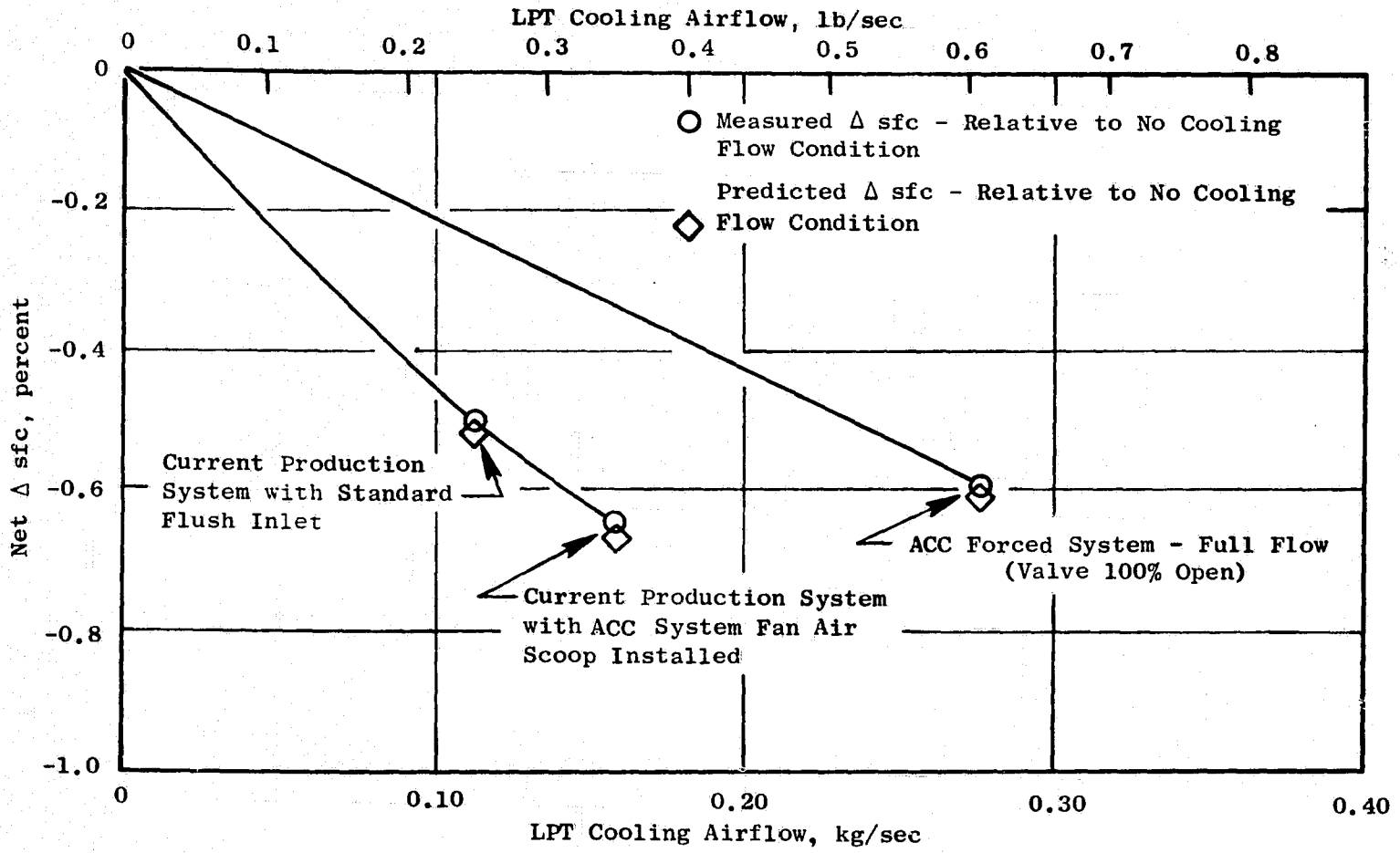

Figure 87. Comparison of Demonstrated and Predicted Δ SFC Versus LPT Cooling Airflow: Production and ACC Systems, SLS Simulated Cruise.

Finally, it must be stated that all of the delta performances shown reflect only the effects due to increases in cooling flow at cruise and that they do not account for the possible cruise performance gain due to the reduced flow during takeoff and climbout, and descent conditions. This will be discussed further in Section 5.4.7 of this report.

5.4.6 Application of Technology Developed from Instrumented Engine Test Results to Improved Manifold Designs

As part of this program, two improved manifold designs were formulated which include seven (rather than 5) circumferential tubes and reflect consideration of design parameters such as cooling hole size and circumferential and radial spacing of the tubes with respect to the case surface. The first design, referred to as the improved impingement system (Option A in the economic analysis presented in Section 6.0), retained the restriction of the current piping upstream of the kiss seal. The second design, referred to as the optimized design system (Option B in the economic analysis presented in Section 6.0), resulted from an optimization study of net Δsfc versus cooling airflow which was conducted for each of the manifold tubes/case hooks. No restrictions were placed on the size and routing of the supply piping for the optimized manifold design. The predicted performance gains, relative to the current production system, for the improved impingement system and the optimized manifold design are 0.242 percent Δsfc and 0.439 percent Δsfc respectively. Figure 88 depicts the predicted performance gain of the improved impingement system and the optimized manifold design as well as that of the ACC and production systems, relative to the no-cooling-flow conditions. As with previous predictions, these performance gains reflect only the effects of increased cooling flow at cruise and do not account for the possible cruise performance gain due to the reduced flow during takeoff, climbout, and descent conditions. This is discussed further in the next section of this report. Also, the performance predictions for both of the improved manifold designs include the assumption that a fan air scoop is used.

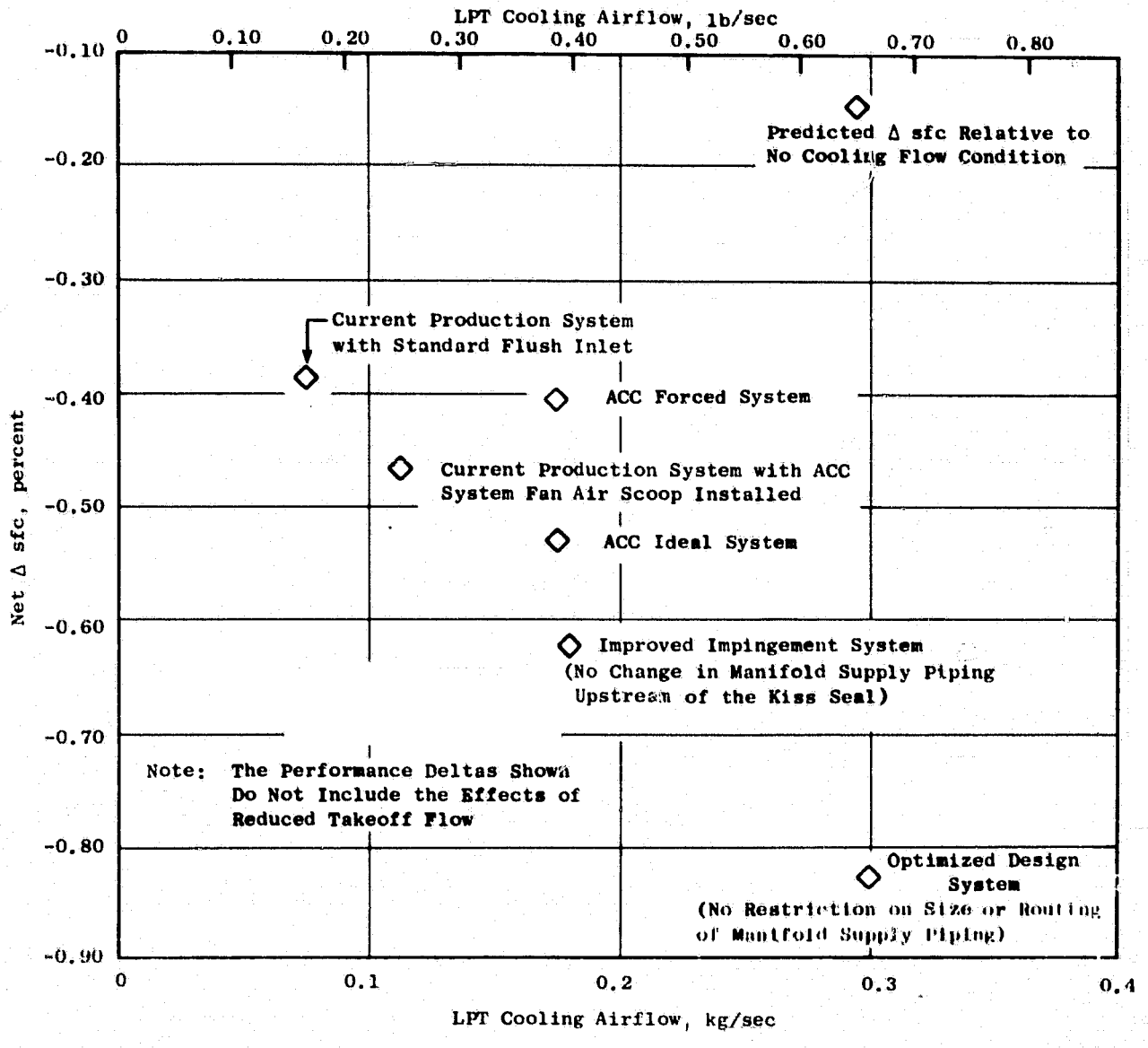

Figure 88. Predicted Δ SFC Versus Cooling Airflow: Altitude (M = 0.8, 35,000 ft) Cruise.

5.4.7 Possible Cruise Performance Gain Due to Reduced Flow During Takeoff, Climbout and Descent Conditions

All of the performance predictions presented previously have only included the effects of increased cooling at cruise conditions and they assume that the existing clearances for each stage of the production system are equal to or greater than the implied clearance reductions of the performance gains predicted. The possible benefit due to reduced flow during takeoff was not demonstrated during the engine test as an additional LPT build would have been required which was out of the scope of this program. Also, the effect of reduced takeoff flow was not assessed analytically since an analytical model of the entire engine (also ouside program scope) is required due to the sensitivity of LPT radial clearances to LPT rotor/stator relative axial position. However, it is still felt that the concept of reduced clearances due to reduced takeoff flow is possible and that a stage-by-stage reduction of 0.25 mm (0.010 inch) is achievable. This level of clearance reduction corresponds to an altitude cruise performance gain of 0.13 percent Δsfc. If this benefit is added to the increased cruise cooling flow benefits for the ACC forced system, ACC ideal system, the improved impingement system and the optimized manifold design, respective performance gains of 0.149 percent Δsfc, 0.276 percent Δsfc, 0.372 percent Δsfc and 0.569 percent Δsfc are predicted.

5.4.8 Manifold Vibration Data: Instrumented Engine Test

The engine test data acquired from the ACC manifold strain gages, as well as the correlation of this data to the vibration component test data, were presented previously in Section 4.2.4.4 for the purpose of continuity.

6.0 ECONOMIC ANALYSIS

The Low Pressure Turbine Active Clearance Control concept was previously evaluated for an estimated cruise sfc improvement of 0.3 percent under the feasibility study of this program (Reference 1). Based on the results of this investigation, the improvement for the concept has been revised and is being presented in the form of two options. The first option, referred to as Option A in the subsequent economic analysis, represents an estimated improvement of 0.25 percent in cruise sfc due to an optimized manifold system with certain restrictions imposed on the manifold supply piping (i.e., no change in the piping upstream of the kiss seal). The second option, referred to as Option B in the following economic analysis, represents an estimated improvement of 0.45 percent in cruise sfc due to an optimized manifold system with no restrictions imposed on the size or routing of the manifold supply piping. Application of these options will result in the following block fuel savings.

Block Fuel Savings

(Minimum Fuel Analysis)

Aircraft	Range		Δ Fuel, Kg		Δ Fuel, Percent	
	km	(St mi)	Option A	Option B	Option A	Option B
DC-10-30	2735	(1700)	- 64	-115	-0.25	-0.45
B747-200	3460	(2150)	-103	-185	-0.25	-0.45

The estimated annual fuel savings per aircraft for the above block fuel savings are as follows:

Estimated Annual Fuel Savings per Aircraft

(Minimum Fuel Analysis)

Aircraft	Range km	Range (St mi)	Δ Fuel Liters/AC/Year Option A	Δ Fuel Liters/AC/Year Option B	Δ Fuel Gallons/AC/Year Option A	Δ Fuel Gallons/AC/Year Option B
DC-10-30	2735	(1700)	78,500	141,000	20,740	37,252
B747-200	3460	(2150)	97,500	175,000	25,760	46,253

The medium fuel prices assumed for the study are dependent on the aircraft mission. Prices used were 14.5¢/liter (55¢gal) for the DC-10-30 (International) and 11.89 ¢/liter (45¢/gal) for the B747-200 (US Domestic). The economic assessments based on these prices are summarized in the following table:

Economic Assessment of LPT ACC Concept

(Medium Range, Medium Fuel Price, Minimum Fuel Analysis)

Aircraft	Payback, Years Option A	Payback, Years Option B	ROI, Percent Option A	ROI, Percent Option B
DC-10-30	2.7	1.5	37	67
B747-200	3.7	2.1	25	48

Because of the increase in the cost of fuel of over 100 percent since the feasibility analysis was conducted in 1978 (Reference 1), the payback and the return on investment of this concept are even more favorable now.

7.0 SUMMARY OF RESULTS AND RECOMMENDATIONS

7.1 SUMMARY OF RESULTS

A LPT ACC cooling system has been designed, manufactured, and component and engine tested.

The airflow component test demonstrated that the ACC system is capable of a significant increase in flow, relative to the current production system, and that the flow split among the various impingement tubes was very close to the design intent.

Based on the results of the vibration component test and the subsequent correlation with strain gage data from the instrumented engine test, the ACC manifold is judged to be structurally sound with no fatigue problems anticipated for a production application.

The LPT stator temperature and flow data obtained from the instrumented engine test enabled the heat transfer (THTD) model of the LPT case to be refined so that predicted temperatures matched those measured during the instrumented engine test. The development of this data matched model, made possible by this program, is significant because LPT stator case temperatures can now be accurately predicted at any operating condition. It should also be pointed out that the heat transfer coefficients, in various internal areas of the LPT case, which were developed during the data matching process, are significantly different than those assumed to be correct prior to the inception of this program. These coefficients have a significant effect on predicted LPT case temperatures.

An axisymmetric shell, stress and deflection (CLASS/MASS) model of the the LPT case was used to determine the delta clearances of the ACC system relative to the production system at various conditions including the SLS simulated cruise test condition and altitude cruise. The LPT case temperatures which were input to the model were those predicted by the THTD model which was discussed previously. In addition to the value to this program with respect to calculation of delta clearances, the CLASS/MASS

model can also be used to determine stresses and deflections of the LPT case with the current production manifold system, thereby providing a better structural capability assessment of the LPT case than was possible prior to this program.

The instrumented engine test data also established Δsfc versus cooling flow trends (for both cooling systems) and demonstrated the concept of sfc reduction due to increased cooling flow. The calculated delta performances, of both systems relative to the zero flow condition and of the ACC system relative to the production system agreed closely with the delta performances demonstrated during the instrumented engine test. This is significant since this correlation verifies the various performance derivatives used in the analytical definition of the performance of both systems.

The predicted performance gains of the ACC system (relative to the current production system) at altitude cruise, based on the effects of increased cooling flow at cruise, as derived from the forced (matched-to-test data) and ideal THTD models are 0.019 percent Δsfc and 0.146 percent Δsfc, respectively. The ACC cooling system did not develop sufficient case temperature reductions (and corresponding clearance reductions) which were required to meet the program goal of 0.2 percent Δsfc due to increased cooling flow at cruise conditions (the overall program goal also included a 0.1 percent reduction in sfc due to reduced cooling flow during takeoff, climbout and descent conditions which was not demonstrated during the test program but was discussed in Section 5.4.7). However, based on the various delta temperature (and subsequent Δsfc) versus cooling flow trends demonstrated during this program, it is felt that the required level of temperature reductions are achievable.

As part of this program, two improved manifold designs were formulated. The first design, which retained the restriction of no change in the manifold supply piping upstream of the kiss seal, resulted in a predicted performance gain of 0.242 percent Δsfc. The second design, which imposed no restriction on the size or routing of the manifold supply piping, yielded a predicted performance improvement of 0.439 percent Δsfc. (Notes: These performance gains include only the effects of increased cooling flow at cruise and they are relative to the current production system with the standard flush inlet.

Also, the performance predictions for both of the improved manifold designs included the assumption that a fan air scoop was used).

Finally, if the possible performance gain due to the reduced flow during takeoff, climbout, and descent conditions (discussed in Section 5.4.7) is added to the performance gains due to increased flow at cruise, the following performance gains are predicted:

Cooling System Identification	Predicted Performance Gain Relative to Current Production System (percent Δsfc)
ACC Forced	0.149
ACC Ideal	0.276
Improved Impingement	0.372
Optimized Design	0.569

7.2 RECOMMENDATIONS

The following items are recommended based on the data obtained and analysis conducted as part of this program:

1. The ACC manifold developed during this program should not be considered for production application unless further manifold optimization is applied.

2. An optimized manifold, which would cool all of the LPT case hooks and is capable of producing a 0.2 percent to 0.3 percent reduction in sfc, should be considered for a production application which imposes the restriction of no change in the manifold supply piping upstream of the kiss seal. A fan air scoop should be included in this LPT cooling system. A midrange performance gain of 0.25 percent Δsfc has been used in the economic analysis of this option presented in Section 6.0 of this report.

3. An optimized manifold and associated piping system, which would cool all of the LPT case hooks and is capable of producing a 0.4 percent to 0.5 percent reduction in sfc, should be considered for a production application which imposes no restriction on the size or routing of the manifold supply piping. A fan air scoop should be included in this LPT cooling system. A midrange performance gain of 0.45 percent Δsfc has been used in the economic analysis of this option presented in Section 6.0 of this report.

4. Heat transfer and structural analytical models (THTD and CLASS/MASS) should be constructed for the entire engine structure (both rotor and stator) from the forward thrust bearing through the LPT module. This must be done to accurately assess the LPT shroud and interstage seal wear patterns and the relative LPT rotor/stator axial positions at cruise conditions, which in turn would define cruise radial clearances. Finally, the models could be used to assess the benefit of reduced radial clearances at cruise due to reduced flow during the takeoff and climbout transient.

APPENDIX A - QUALITY ASSURANCE

INTRODUCTION

The quality program applied to this contract is a documented system throughout the design, manufacture, repair, overhaul, and modification cycle for gas turbine aircraft engines. The quality system has been constructed to comply with military specifications MIL-Q-9858A, MIL-I-45208, and MIL-STD-45662 and Federal Aviation Regulations FAR-145 and applicable portion of FAR-21.

The quality system and its implementation are defined by a complete set of procedures which has been coordinated with the DOD and FAA and has their concurrence. In addition, the quality system as described in the quality program meets the contractual requirements required by NASA Lewis Research Center. The following is a brief synopsis of the system.

QUALITY SYSTEM

The quality system is documented by operating procedures which coordinate the quality-related activities in the functional areas of Engineering, Manufacturing, Materials, Purchasing, and Engine Programs. The quality system is a single-standard system wherein all product lines are controlled by the common quality system. The actions and activities associated with determination of quality are recorded and documentation is available for review.

Inherent in the system is the assurance of conformance to the quality requirements. This includes the performance of required inspections and tests. In addition, the system provides change control requirements which assure that design changes are incorporated into manufacturing, procurement and quality documentation, and into the products. Material used for parts is verified for conformance to applicable engineering specifications, utilizing appropriate physical and chemical testing procedures.

Measuring devices used for product acceptance and instrumentation used to control, record, monitor, or indicate results of readings during inspection and test are initially inspected and calibrated and periodically are

reverified or recalibrated at a prescribed frequency. Such calibration is performed by technicians against standards which are traceable to the National Bureau of Standards. The gages are identified by a control number and are on a recall schedule for reverification and calibration. The calibration function maintains a record of the location of each gage and the date it requires recalibration. Instructions implement the provisions of MIL-STD-45662 and the appropriate FAR requirements.

Work sent to outside vendors is subject to quality plans which provide for control and appraisal to assure conformance to the technical requirements. Purchase orders issued to vendors contain a technical description of the work to be performed and instructions relative to quality requirements.

Engine parts are inspected to documented quality plans which define the characteristics to be inspected, the gages and tools to be used, the conditions under which the inspection is to be performed, the sampling plan, laboratory and special process testing, and the identification and record requirements.

Work instructions are issued for compliance by operators, inspectors, testers, and mechanics. Component part manufacture provides for laboratory overview of all special and critical processes, including qualification and certificaiton of personnel, equipment and processes.

When work is performed in accordance with work instructions, the operator/inspector records that the work has been performed. This is accomplished by the operator/inspector stamping or signing the operation sequence sheet to signify that the operation has been performed.

Various designs of stamps are used to indicate the inspection of status of work in process and finished items. Performance or acceptance of special processes is indicated by distinctive stamps assigned specifically to personnel performing the process or inspection. Administration of the stamp system and the issuance of stamps are functions of the Quality Operation. The stamps are applied to the paperwork identifying or denoting the items requiring control. When stamping of hardware occurs, only laboratory-approved ink is used to assure against damage.

The type and location of other part marking is specified by the design engineer on the drawing to assure effects do not compromise design requirements and part quality.

Control of part handling, storage and delivery is maintained through the entire cycle. Engines and assemblies are stored in special dollies and transportation carts. Finished assembled parts are stored so as to preclude damage and contamination; openings are covered, lines capped and protective covers applied as required.

Nonconforming hardware is controlled by a system of material review at the component source. Both a Quality representative and an Engineering representative provide the accept (use-as-is or repair) decisions. Nonconformances are documented, including the disposition and corrective action if applicable to prevent recurrence.

The system provides for storage, retention for specified periods, and retrieval of nonconformance documentation. Documentation for components is filed in the area where the component is manufactured/inspected.

APPENDIX B - SYMBOLS AND DEFINITIONS

ACC	Active Clearance Control
$\mathbb{Q}$	Centerline
CLASS/MASS	General Electric's "Classical Linear Axisymmetric Shell Structures/Mechanical Analysis of Space Structures" Computer Program
G/I	Ground Idle
HPT	High Pressure Turbine
I/S	Interstage
LPT	Low Pressure Turbine
M	Mach Number
N_1K	Corrected Fan Speed, rpm
N_2	Physical Core Speed, rpm
Ps	Static Pressure in Test Cell, N/cm^2 ($lb/in.^2$)
P_T	Total Pressure in Manifold Supply Pipe, N/cm^2 ($lb/in.^2$)
P_2	Engine Inlet Total Pressure, KPa ($lb/in.^2$)
ROI	Return on Investment, %
S/D	Shutdown
TDOD	General Electric's "Turbine Design Off Design" Computer Program
THTD	General Electric's "Transient Heat Transfer, Version D" Computer Program
TMF	Turbine Midframe
T/O	Takeoff
TRF	Turbine Rear Frame
T_T	Total Temperature in Manifold Supply Pipe, K (° R)
T_2	Engine Inlet Total Temperature, ° C (° F)
W	Manifold Airflow Rate, kg/sec (lb/sec)

APPENDIX C - REFERENCES

1. Fasching, W.A., "CF6 Jet Engine Performance Improvement Program, Task 1 - Feasibility Analysis," NASA CR-159450 (GE R79AEG295), March 1979.

2. Howard, W.D., "CF6 Jet Engine Performance Improvement - High Pressure Turbine Roundness." NASA CR - 165555, January 1982.

3. Wulf, R.H., "Engine Diagnostics Program, CF6-50 Engine Performance Deterioration," NASA CR-159867 (GE R80AEG668), November 1980.